Limited Feedback of Channel State Information in Wireless Communication Systems

Von der Fakultät für Ingenieurwissenschaften

Abteilung Elektrotechnik und Informationstechnik

der Universität Duisburg-Essen

zur Erlangung des akademischen Grades

Doktor der Ingenieurwissenschaften

genehmigte Dissertation

von

Bo Zhao

aus

Jiangsu, China

Gutachter: Prof. Dr.-Ing. Andreas Czylwik
Gutachter: Prof. Dr.-Ing. Rüdiger Kays
Tag der mündlichen Prüfung: 04. Mai 2021

Abstract

The accuracy of channel state information (CSI) available at the base station (BS) plays a very important role at increasing the overall downlink throughput of the communication systems. To facilitate this, the uplink channel must be consumed to feedback the CSI from the users, in case the channel reciprocity cannot be used. Since the uplink channel data rate is relative low, this CSI feedback should be limited. Moreover, the system throughput can be dramatically increased by BS cooperation, where the limited feedback problem becomes more complex.

This dissertation first proposes for the classic orthogonal frequency division multiplexing (OFDM) system a resource block (RB)-based feedback structure, which utilizes the frequency correlation and temporal correlation of the channel simultaneously. In each RB different feedback reduction algorithms could be implemented for different applications. This RB-based approach could achieve a better bit error rate (BER) performance by spending a few more bits for quantizing the CSI. By exploiting the temporal correlation, the feedback overhead could be reduced by a factor equal to the number of OFDM symbols, which are under similar channel condition.

In a coordinated multi-point (CoMP) coordinated beamforming (CB) system, users need to feedback the serving and interfering channels to enable BS cooperation. This dissertation introduces a bit partitioning algorithm for a two-cell system, which adaptively allocates the bits for quantizing the channel direction information (CDI) of both channels. The proposed algorithm outperforms the equal bit partitioning with the same amount of feedback overhead, especially in the high signal-to-noise ratio (SNR) regime. Also cooperative beamforming strategies are investigated, which profits from both the zero forcing (ZF) and the maximum ratio transmission (MRT) schemes. The adaptive bit allocation algorithm is then extended to a three-cell system as well as a multicell system. And the cooperative beamforming approach is generalized to a low complexity BS-specific approach for the multicell system. Simulation shows that the proposed cooperative approach increases the average user data rate, particularly for the cell-edge users.

In the CoMP joint transmission (JT) system, focus is laid on the dynamic formation of clusters to limit the amount of feedback overhead and backhaul load. By introducing the set partition problem under the assumption of non-overlapping clusters, a modified implicit enumeration algorithm is proposed, based on which the dynamic clustering method is exposed. Simulation reveals the advantage of the proposed method in comparison to the fixed clustering in terms of data rate, fairness and BS power consumption.

Acknowledgment

I would like to thank the following people, who supported and helped me throughout the writing of this dissertation.

First of all, I would like to express my sincere gratitude to my supervisor, Prof. Dr.-Ing. Andreas Czylwik, for giving me the opportunity to work on this dissertation and for his guidance, encouragement and patience throughout my work. Without his support, I could not have completed my dissertation.

I would like to offer my special thanks to Prof. Dr.-Ing. Rüdiger Kays, head of the communication technology institute of TU Dortmund University, for taking over the role of the second reviewer and for his insightful comments and suggestions.

My appreciation also goes to all members of the chair of communication systems, for the friendly and cooperative atmosphere at work and for their technical and organizational supports.

Last but not least, I would like to thank my wife and my parents. They gave me a great support and have been encouraging me in all situations.

Bo Zhao
Erlangen, July 2021

Contents

Notation

The used mathematical symbols, abbreviations and operations are listed here. These symbols and abbreviations are sorted in alphabetical order.

SYMBOLS		PAGE
$\mathbf{A}$	Characteristic matrix for the dynamic clustering in CoMP-JT system	83
$A_{\mathrm{c}}(\tau)$	Power delay profile	10
$A_{\mathrm{c}}(\tau, \Delta t)$	Autocorrelation function of the input delay-spread function with delay τ and time difference Δt	10
a_{ij}	Entries in $\mathbf{A}$ indicating whether cell i resides in cluster j in CoMP-JT system	83
B	Total number of feedback bits available at each user for quantizing the desired and interfering channels in CoMP-CB system	39
B_{c}	Coherence bandwidth	10
$\mathrm{BER}(k)$	BER on the k-th subcarrier in OFDM system	15
B_{full}	Number of bits used to quantize the complete codebook $\mathcal{C}_{\mathrm{full}}$ in OFDM system	12
$B_{i,j}$	Number of bits used for quantizing $\mathbf{h}_{i,j}$ in CoMP system	37
BS_i	Beamforming scheme used at BS i	41
B_{sub}	Number of bits used to quantize the codebook $\widetilde{\mathcal{C}}(k)$ in OFDM system with feedback compression in the recursive and trellis-based algorithms	14
B_{w}	Channel bandwidth	6
C	Total number of clusters in CoMP-JT system	80
$\mathcal{C}_{\mathrm{full}}$	Complete codebook for quantizing the beamforming vector in OFDM system	12
$\mathcal{C}_{i,j}$	Codebook used for quantizing $\mathbf{h}_{i,j}$ in CoMP system	37
c_j	Cost function of cluster j in the dynamic clustering problem in CoMP-JT system	83
$\widetilde{\mathcal{C}}(k)$	Codebook for quantizing the beamforming vector on the k-th subcarrier in OFDM system with feedback compression in the recursive and trellis-based algorithms	14

iv

vi

viii

ABBREVIATIONS		PAGE
TDD	Time Division Duplex	2
TP	Transmission Point	30
UE	User Equipment	30
UL	UpLink	32
VQ	Vector Quantization	34
WLAN	Wireless Local Area Network	7
WSSUS	Wide-Sense Stationary Uncorrelated Scattering	10
ZF	Zero Forcing	4

OPERATIONS, FUNCTIONS

$\mathbb{C}^{m \times n}$	Complex matrix with size m-by-n
$\binom{n}{k}$	Number of k-combinations from a given set of n elements
$\|\mathcal{S}\|$	Cardinality of set $\mathcal{S}$
$\bar{i}$	Complement element of i in a set
$\mathcal{S} \backslash \mathcal{A}$	Relative complement of set $\mathcal{A}$ in set $\mathcal{S}$, $\mathcal{S} \backslash \mathcal{A} := \{x \in \mathcal{S} \| x \notin \mathcal{A}\}$
$\|z\|$	Absolute value of scalar z
$\|\|\mathbf{z}\|\|$	Euclidean norm of vector $\mathbf{z}$
$\mathbf{A}^*$	Complex conjugate of matrix $\mathbf{A}$
$\mathbf{A}^{\mathrm{H}}$	Hermitian transpose of matrix $\mathbf{A}$
$\mathbf{A}^{\mathrm{T}}$	Transpose of matrix $\mathbf{A}$
$\|\|\mathbf{A}\|\|_{\mathcal{F}}$	Frobenius norm of matrix $\mathbf{A}$
χ^2_{2n}	Chi-squared distribution with 2n degrees of freedom
$\mathcal{CN}(\mu, \mathbf{C})$	Complex Gaussian distribution with mean μ and covariance matrix $\mathbf{C}$
$\mathbb{E}\{\boldsymbol{Z}\}$	Expectation of random variable $\boldsymbol{Z}$
$\beta(x, y)$	Beta function
$\lceil x \rceil$	Ceiling function at x (the smallest integer that is greater than or equal to x)
$\psi(n)$	Euler's psi function at n
$\lfloor x \rfloor$	Floor function at x (the largest integer that is less than or equal to x)
$\delta_{\mathrm{k}}[x]$	Kronecker delta function at x
$\mathrm{Q}(x)$	Q-function at x

CHAPTER 1

Introduction

1.1 Background

Recently 3GPP has approved the completion of the 5G Release 15 specifications, which operates in standalone mode using the completely new 5G radio access network and core. This is a significant step forward compared to the non-standalone mode using existing 4G Long Term Evolution (LTE) infrastructure [3]. Now the industry is in a full-blown sprint to commercialization. 5G, not only the next generation of 4G technology but a paradigm shift, satisfies the increasing demand for higher data rate, lower network latency, better energy efficiency and reliable ubiquitous network connectivity [17, 40]. It will be exploited in various scenarios and applications such as Internet of Things (IoT), big data analysis, artificial intelligence, smart cities, entertainment services, video streaming and so on.

The Next Generation Mobile Network (NGMN) has defined the requirements for the 5G standard [2], some of which are listed below:

- User experienced data rate up to 1 Gbit/s should be supported in some specific environments, like indoor offices, while at lease 50 Mbit/s should be guaranteed everywhere cost-effectively.

- Several hundred thousand simultaneous active connections per square kilometer in the wireless sensor networks.

- Significant enhancement on the spectrum efficiency compared with 4G.

- Improved coverage, particularly for the rural areas.

- More effective signaling to minimize energy consumption.

In order to provide great user experience, high system performance as well as enhanced services, some technologies have been exploited in order to increase the network capabilities, such as carrier aggregation (CA), Coordinated Multi-Point/Multiple-Input Multiple-Output (CoMP/MIMO), traffic optimization, offloading and so on. To cope with the increased number of mobile subscribers in the crowded environments and at cell edge, the heterogeneous network is included which coordinates the low power layer of small cells

and tightly integrates them with the macro cells [13, 109, 110]. Meanwhile the resource allocation problem is continuously attracting researchers' attention [15, 16, 21, 122]. Besides these, some new envisioned technologies are in the early stage of development. Some examples are (but not limited to) massive MIMO, which takes advantage of hundreds of antennas at cellular base stations to improve the effective signal-to-interference-plus-noise ratio (SINR) and to mitigate interference and suppress noise through narrow beamforming [44, 85]; millimeter waves (mmWave), which exploits the large continuous unused bandwidth over 6 GHz and fits the massive MIMO very well due to its short wavelength and narrow beamwidth [123]; full duplex, which could reduce the amount of guard bands and time and thus improve the overall spectral efficiency [2]. Despite these promising technologies, practical challenges still exist. Some well-known difficulties are the high algorithm complexity for the current hardware design, unrealistic assumptions during algorithm investigation such as zero-delay and error-free channel information at the transmitter, overestimated backhaul capability [46, 62].

1.2 Limited feedback and backhaul problem in wireless communication systems

In classic wireless communication systems, the channel state information (CSI) at the transmitter can be obtained via the feedback from the receiver as shown in Figure 1.1, such that the transmitter can adapt the forward link signal to the channel [38]. This is crucial in frequency division duplex (FDD) systems, while in a time division duplex (TDD) system, the downlink channels can be estimated from the uplink channels under the assumption of reciprocity, both of which are supported in the current 5G new radio (NR) system [139].
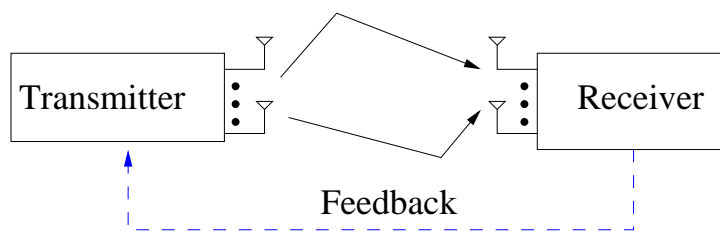
Figure 1.1: Illustration of feedback in wireless communication systems

The above-mentioned channel feedback problem allows the receiver to send a small number of information bits about the channel back to the transmitter to optimize channel adaption, and is generally referred as to limited or finite-rate feedback. An overview of limited feedback in wireless communication systems has been provided by [77]. The

limited feedback problem in single user and multiuser systems was addressed and related research results were elaborated. Channel feedback schemes in different standards were introduced as well. [77] also outlined some practical issues such as feedback delay, feedback error, quantization, etc. Furthermore, BS coordination with limited feedback was mentioned but was pointed out to be of future interest.

To facilitate the air interface technologies in 5G, the channel information should be available at the transmitter to some extent. 3GPP has defined two types of CSI feedback, namely normal and enhanced feedback [10]. In the normal feedback, which is also called implicit feedback, the precoding matrix indicator (PMI) or rank indicator (RI) or the channel quality will be fed back to the transmitter. Implicit feedback implies that the transmitter and the receiver have some assumptions in common such as a predefined codebook. It was shown that with a limited number of antenna ports the implicit feedback is the preferred feedback framework for single-user (SU) and multi-user-MIMO (MU-MIMO) [37]. The enhanced/explicit feedback is suitable for higher spatial resolution, which is one of the features of the promising massive MIMO. 3GPP defines that at least one of the following three categories should be supported for explicit feedback: precoder feedback based on linear combination of dual-stage codebooks, covariance matrix feedback and a hybrid CSI feedback of the previous two categories.

However, technical challenges arise as the number of antennas and coordinated cells increases. For instance, in 5G one vital technology that boosts the spectral and energy efficiency is massive MIMO [118]. Firstly, the performance gain of massive MIMO greatly depends on the accuracy of the CSI available at the transmitter. Secondly, traditional MIMO utilizes orthogonal pilot signals to obtain CSI, but this approach encounters huge difficulties in massive MIMO [3]. In addition, in a massive MIMO-OFDM (orthogonal frequency division multiplexing) system, the amount of CSI required by the transmitter increases linearly with the number of antennas and subcarriers [33].

CoMP transmission/reception has been adopted as the key technology to alleviate the inter-cell interference (ICI) and increase the cell-edge user performance quality. The performance of CoMP highly depends on the downlink CSI available on the BSs which must be sent back from the user equipment, consuming uplink control channel resources [38]. As the number of coordinated cells varies, the CSI matrix dimension and the amount of feedback may differ dynamically. In the meanwhile, in the CoMP system with relays CSI feedback generates even a great amount of feedback overhead that could result in significant performance degradation [41, 114, 121]. Furthermore, the CSI should be exchanged among BSs in order to perform ICI cancellation or joint processing. This burdens the backhaul link, which has already been seen as a bottleneck for the ultra-dense intercon-

nected cells with high traffic [62]. One practical solution that shrinks the number of coordinated cells is cell clustering. Clustering plays an important role in limiting the CSI feedback and backhaul. But how to dynamically form the clusters in practice requires further investigation [80, 90, 96, 97, 98].

1.3 Outline of the dissertation

Within this dissertation only **downlink** (DL) transmission is considered. In **Chapter 2** the limited feedback problem in a traditional OFDM system will be addressed. Different feedback reduction techniques from the literature will be compared and analyzed. A resource block (RB) based feedback concept combined with different feedback reduction methods will be proposed, which reduces the feedback overhead dramatically by utilizing both frequency and temporal correlation of the channel simultaneously.

In **Chapter 3** the feedback problem will be investigated in a CoMP coordinated beamforming (CB) system. Focus will be put on how to allocate the feedback bits for the serving and interfering channels. A novel bit partitioning algorithm based on zero forcing (ZF) beamforming will be proposed for a two-cell system in **Section 3.2.2** and two cooperative beamforming strategies will be proposed in **Section 3.2.3**, which select the proper beamforming scheme within ZF and eigen-beamforming. Then, the proposed bit partitioning algorithm will be extended for a three-cell system as well as a multicell system in **Section 3.3** and **Section 3.4**. Also, cooperative beamforming approaches for these two systems will be searched while not introducing high complexity to the coordinated system. These cooperative approaches select the best suitable beamforming strategy to the serving users.

The CoMP joint transmission (JT) system will be studied in **Chapter 4**. A dynamic clustering algorithm will be introduced which limits the amount of feedback and backhaul overhead of the whole system. A modified implicit enumeration algorithm will be proposed to solve this dynamic clustering problem.

Chapter 5 will summarize the results of this dissertation and show some interesting research topics in the future.

1.4 List of publications

[1] Bo Zhao and Andreas Czylwik. Cooperative Beamforming for a Two-Cell System with Limited Feedback. In *2013 IEEE 77th Vehicular Technology Conference (VTC Spring)*, pages 1-5, June 2013.

[2] B. Zhao, T. Akbudak, M. Simsek, A. Czylwik, and H. Xu. Limited feedback for MISO-OFDM systems. In *Proceedings of 17th International OFDM Workshop 2012 (In-OWo'12)*, pages 1-4, 2012.

[3] T. Tao, B. Zhao, and A. Czylwik. Beamforming design for a cooperative relay system with limited feedback. In *2013 IEEE 24th Annual International Symposium on Personal, Indoor, and Mobile Radio Communications (PIMRC)*, pages 2616-2620, Sept 2013.

[4] T. Akbudak, B. Zhao, M. Simsek, and A. Czylwik. A low-complexity resource allocation scheme for single-user MIMO transmission. In *2011 7th International Wireless Communications and Mobile Computing Conference*, pages 249-254, July 2011.

[5] M. Simsek, H. Wu, B. Zhao, T. Akbudak, and A. Czylwik. Performance of different cell selection modes in 3GPP-LTE macro-/femtocell scenarios. In *2011 Wireless Advanced*, pages 126-131, June 2011.

[6] T. Akbudak, M. Simsek, Bo Zhao, and A. Czylwik. Symmetric capacity of multi-user MIMO downlink under per-base station power constraints. In *2011 International ITG Workshop on Smart Antennas*, pages 1-4, Feb 2011.

[7] M. Simsek, T. Akbudak, B. Zhao, and A. Czylwik. An LTE-femtocell dynamic system level simulator. In *2010 International ITG Workshop on Smart Antennas (WSA)*, pages 66-71, Feb 2010.

Limited feedback for a SU-OFDM system

2.1 Introduction to the OFDM technique

Tradional single-carrier transmission suffers from frequency selectivity of the wideband channel in case of high data rate [34]. In order to overcome the drawback of single-carrier transmission, multi-carrier transmission is proposed to simplify the complexity of the equalizer in the receiver. The idea of multi-carrier transmission is to convert a high rate data stream into several low rate data streams transmitted in parallel as shown in Figure 2.1. Multi-carrier transmission greatly increases the symbol duration T_S compared with single-carrier transmission with the same data rate, which makes the transmission more robust to intersymbol interference (ISI). From the perspective on frequency domain, multi-carrier transmission analyzes the wideband signal into several narrowband signals, so that the frequency selective channel with bandwidth B_w and frequency transfer characteristic $H(f)$ can be approximated by multiple frequency flat channels [106].
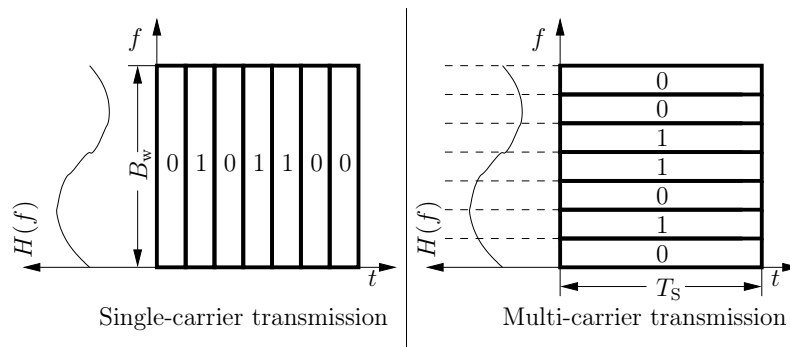
Figure 2.1: Single-carrier transmission vs. multi-carrier transmission

In a conventional multi-carrier transmission system different subchannels are spaced apart such that there is no overlapping between the spectral shapes of different subcarriers. In this way the signals can be received using conventional filters. As a special case of multi-carrier transmission, OFDM uses overlapped spectra for the subcarriers to increase the spectral efficiency as shown in Figure 2.2. Since the orthogonality between the subcarriers is maintained, the signals are still received without intercarrier interference.
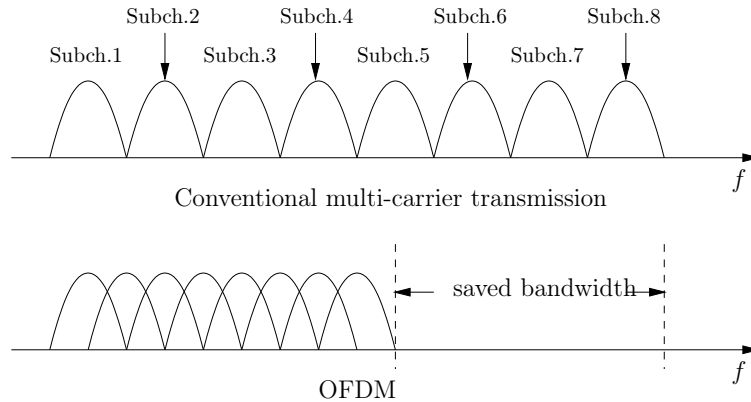
Figure 2.2: Qualitative bandwidth efficiency comparison between conventional multi-carrier transmission and OFDM [116]

The OFDM technique also has some disadvantages. For instance, it is more sensitive to frequency offset and phase noise and has a relatively large peak-to-average power ratio (PAPR). However, due to its big advantage such as low implementation complexity dealing with multipath propagation, capacity enhancement capability by adapting the data rate for each subcarrier, etc., OFDM technique has been widely used as a way for high data rate transmission for decades [116]. It has been adopted by many wireless communication standards such as the wireless local area network (WLAN) standards IEEE 802.11 a, g, n, the terrestrial TV systems Digital Video Broadcasting-Terrestrial (DVB-T) and the second generation (DVB-T2), the wireless communication standards for cellular networks Long Term Evolution and its extension LTE-Advanced (LTE-A), etc. Some wireline communication technologies such as asymmetric digital subscriber line (ADSL), power line communication (PLC), etc., also use OFDM as their key modulation technique.

2.2   Mobile radio channels

2.2.1   Fading

In wireless communications during the signal transmission via the propagation media the receiver generally does not only receive the signal from the direct link. Many replicas of the original signal are also received due to reflection, scattering or diffraction in the environment [117]. The received signal may vary with geographical position, time or frequency, which leads to nondeterministic variations in the signal amplitude. The signal fluctuations are known as *fading* [94].

Large-scale fading

The power of the electromagnetic wave degrades when the signal is transmitted between antennas. *Path loss* is used to characterize this power dissipation and generally assumed to be the same for a fixed transmit-receive distance. It is difficult to model path loss using just a single model for different environments [50]. Several path loss models were developed based on empirical measurements such as the Okumura model [89], the Hata model [53], etc. [42] introduced a simplified model for path loss as a function of the distance d between the transmit antenna and the receive antenna:

$$Path\ loss = K \left[\frac{d_0}{d} \right]^{\gamma}, \tag{2.1}$$

where d_0 is a reference distance, K is a fixed quantity that depends on the antenna characteristics and the channel attenuation and γ is the path loss exponent. This simplified path loss model will be used in Chapter 3 and 4.

Shadowing is caused by obstacles such as hills or large buildings which obscure the main signal path between the transmitter and the receiver and attenuate the signal power through absorption, reflection, scattering and diffraction. Shadowing is often modeled using a log-normal distribution [42]. Signal variation due to shadowing usually occurs over a distance of 10-100 m, and variation due to path loss occurs in the range of 100-1000 m [50]. Therefore, fading caused by path loss and shadowing is often referred to as *large-scale fading*.

Small-scale fading

The amplitudes and phases of multipath components of the received signal also experience rapid fluctuations over a short period of time or very short distances, in the order of the signal wavelength [50, 100]. These fluctuations are sometimes referred to as *small-scale fading*. Small-scale fading is caused by interference among many replicas of the original signal from multiple paths, which arrive at the receiver at slightly different time. These signal components are summed with the original signal constructively or destructively. The resultant channel models are generally nondeterministic.

For *flat fading* where the signal bandwidth is sufficiently small and all frequency components behave similarly, the delay spread of a channel is small relative to the inverse signal bandwidth B_{w}, i.e., the delay is negligible compared to the symbol duration T_{s}. The receiver will receive multiple replicas of the original signal at almost the same time. When the number of replicas becomes large, the central limit theorem applies and the in-phase and quadrature components of the channel can be seen as jointly Gaussian random processes [50]. Therefore, the most common distribution of the channel amplitude

is the Rayleigh distribution and it is also an assumption of the discussion in Chapter 3 and 4.

When the signal occupies a channel bandwidth larger than the bandwidth over which spectral components are affected in a similar way, the transmit signal at different frequencies will be distorted differently. This phenomenon is known as *frequency-selective fading*. In this case the assumption that the delay spread of the channel is negligible compared to the symbol duration is no longer valid. Different from flat fading where the received signal can be characterized by just the amplitude and phase random processes, frequency-selective fading additionally needs to take the characterization of the multipath delay and the time variation of the channel into account. Therefore, it is more difficult to model frequency-selective fading channels than flat fading channels. Usually wideband multipath measurements for different scenarios are made and the specific models are developed from these measurements [100].

2.2.2   Characterization of fading channels

The radio propagation channels can be seen as a system transforming input signals into output signals. Taking the time-varying property into consideration, one can represent the lowpass response of a channel as $c(\tau, t)$, where τ is the time delay and $c(\tau, t)$ shows the time-varying response at time t to an impulse at time $t - \tau$, which is also known as the *input delay-spread function* according to the naming convention in [28].

The channel can also be characterized in the frequency domain by the *time-variant transfer function $C(f, t)$*, which is the Fourier transform of $c(\tau, t)$ with respect to τ:

$$C(f, t) = \int_{-\infty}^{+\infty} c(\tau, t) \mathrm{e}^{-\mathrm{j}2\pi f\tau} \mathrm{d}\tau. \tag{2.2}$$

In general, $c(\tau, t)$ and $C(f, t)$ are random processes which vary with time. To characterize them precisely the infinite dimensional probability density functions are necessary. A less accurate but more practical way is to use the correlation functions [28]. Furthermore, as mentioned in Section 2.2.1, when the number of multipath becomes large, $c(\tau, t)$ and $C(f, t)$ are complex Gaussian processes. Therefore, $c(\tau, t)$ and $C(f, t)$ can be described by their means and autocorrelation functions. The autocorrelation function of $c(\tau, t)$ is defined as

$$A_\mathrm{c}(\tau_1, \tau_2, t_1, t_2) = \mathbb{E}\{c^*(\tau_1, t_1)c(\tau_2, t_2)\}. \tag{2.3}$$

Since most radio channels exhibit wide sense stationary behavior [28], $A_\mathrm{c}(\tau_1, \tau_2, t_1, t_2)$ only depends on the time difference $\Delta t = t_2 - t_1$. Moreover, practically the channel response associated with a multipath component with delay τ_1 is uncorrelated with the channel

response associated with other components with delay $\tau_2 \neq \tau_1$. This is because these components are caused by different scatterers. These channels are called the wide-sense stationary uncorrelated scattering (WSSUS) channels. The autocorrelation function of the WSSUS channels is rewritten as

$$\mathbb{E}\{c^*(\tau_1, t_1)c(\tau_2, t_2)\} = A_c(\tau_1, \Delta t)\delta_k[\tau_1 - \tau_2] \sim A_c(\tau, \Delta t), \tag{2.4}$$

with $\Delta t = t_2 - t_1$.

Then the power delay profile (PDP) $A_c(\tau)$ can be defined by setting $\Delta t = 0$ in (2.4): $A_c(\tau) \triangleq A_c(\tau, 0)$. The PDP shows the intensity of signals associated with a certain multipath delay and can be measured for different scenarios. From the PDP the root mean square (RMS) delay spread of the multipath channel σ_τ can be calculated as [50]

$$\sigma_\tau = \sqrt{\frac{\int_0^{+\infty}(\tau - \mu_\tau)^2 A_c(\tau)\mathrm{d}\tau}{\int_0^{+\infty} A_c(\tau)\mathrm{d}\tau}}, \tag{2.5}$$

where $\mu_\tau = \frac{\int_0^{+\infty}\tau A_c(\tau)\mathrm{d}\tau}{\int_0^{+\infty} A_c(\tau)\mathrm{d}\tau}$ is the average delay of the multipath channel.

Similarly, the time-variant transfer function $C(f, t)$ can also be characterized by its autocorrelation function $A_C(\Delta f, \Delta t) = \mathbb{E}\{C^*(f, t)C(f + \Delta f, t + \Delta t)\}$ which only depends on the frequency separation and time difference [50]. $A_C(\Delta f, \Delta t)$ is useful for defining the *coherence bandwidth* B_c and *coherence time* T_c of the multipath propagation channels which are important parameters for the design of the resource block (RB) based feedback structure in this chapter:

- **Coherence bandwidth**: let $A_C(\Delta f) \triangleq A_C(\Delta f, 0)$. B_c is the frequency separation which satisfies $A_C(\Delta f) \approx 0$ for $\Delta f > B_c$. [74] has also shown that over $B_c \approx \frac{1}{50\sigma_\tau}$ the channel correlation exceeds 0.9 and $B_c \approx \frac{1}{5\sigma_\tau}$ approximates the range of frequencies over which channel correlation exceeds 0.5.

- **Coherence time**: let $A_C(\Delta t) \triangleq A_C(0, \Delta t)$. When the observation time difference is larger than T_c, $A_C(\Delta t) \approx 0$. A rule of thumb is to define the coherence time as $T_c = \sqrt{\frac{9}{16\pi f_m^2}} = \frac{0.423}{f_m}$ [100], where f_m is the maximum *Doppler frequency*.

2.3   Feedback schemes for OFDM systems

The combination of multiple antennas and OFDM is keeping attractive during the last years since multiple antennas can provide high data rate or reliability for the OFDM system. In order to adapt the transmission to the time-variant radio channel some information about the channel should be available at the transmitter particularly for the

MIMO case. In MIMO-OFDM systems the amount of information is proportional to the number of subcarriers, the time duration of the transmission and the number of antennas. Therefore, the information that needs to be fed back may be huge in an FDD system. However, correlation between adjacent subcarriers and time slots can be exploited to reduce the feedback overhead drastically.

As shown in Section 2.2.2 the channel has high correlation within the coherence bandwidth which is usually much larger than the subcarrier spacing. Hence the most straightforward method with the lowest complexity to exploit the correlation among subcarriers is clustering [32, 56, 84, 120, 127, 129], i.e., to select and feedback the channel information of one subcarrier within a cluster of subcarriers. A more complex method is to feedback the channel information on some certain subcarriers and reconstruct the channel for other subcarriers by interpolation [35, 54, 56, 75]. By viewing the feedback reduction problem as a compression type of problem, [137] proposed the recursive feedback encoding and trellis-based encoding which are typical vector quantization algorithms [47]. In [71, 76] the power allocation problem for OFDM systems with a finite rate feedback channel was also addressed trying to maximize the overall system capacity. However, the power loading problem for OFDM systems is beyond the scope of this dissertation.

Although not dedicated for OFDM systems, many methods exploiting temporal correlation of the radio channel have been proposed and these methods can be applied in OFDM systems by implementation for each subcarrier. A Markov model was introduced in [58] to analyze the average feedback rate according to the temporal correlation and distribution of the channel. The average feedback rate was shown to increase linearly with Doppler frequency, i.e., the velocity of the mobile equipment. Based on this Markov model the transition probabilities that are almost zero could be discarded, hence limiting the number of Markov states that need to be known at the transmitter. Therefore, the feedback data rate can be dramatically reduced with slight performance loss [57, 59]. Similarly, due to the temporal correlation of the channel, the transition probabilities between different states of the Markov model are different. So the source coding schemes such as Huffman coding can benefit and reduce the number of bits representing the states without losing performance [108]. Moreover, by modeling the time evolution of the channel as a first-order Gauss-Markov process, [68, 69, 70] analytically discussed the problem of how to select a feedback update period to achieve a certain performance such as average effective signal-to-noise ratio (SNR). Also prediction is a straightforward method to make use of the temporal correlation in case that the statistics of the channel are known. In [60] a geodesic prediction on the Grassmann manifold as well as a codebook design algorithm was proposed. Although codebook design is important for systems with limited feedback,

this problem is not the focus of this dissertation.

2.3.1   System model

In this chapter the downlink transmission of a SU multiple-input single-output (MISO) OFDM system with N_{t} transmit antennas and a single receive antenna as shown in Figure 2.3 is considered. At the transmitter the bit stream is first modulated by 4-quadrature amplitude modulation (QAM). The normalized beamforming vector $\mathbf{w}(k)$ $(||\mathbf{w}(k)|| = 1)$ on the k-th subcarrier is used to facilitate the transmission. The corresponding $1 \times N_{\mathrm{t}}$ channel gain vector in the frequency domain is $\mathbf{h}(k)$. Thus the received frequency-domain signal on the k-th subcarrier $y(k)$ can be written as

$$y(k) = \mathbf{h}(k)\mathbf{w}(k)s(k) + n(k), \tag{2.6}$$

where $s(k)$ is the transmitted 4-QAM symbol and $n(k)$ represents the additive white Gaussian noise with entries distributed according to $\mathcal{CN}(0, N_0)$. In this chapter the transmit power is equally allocated across the subcarriers and $\mathbb{E}\{|s(k)|^2\} = E_{\mathrm{s}}$. Also a zero-delay error-free feedback channel is assumed.
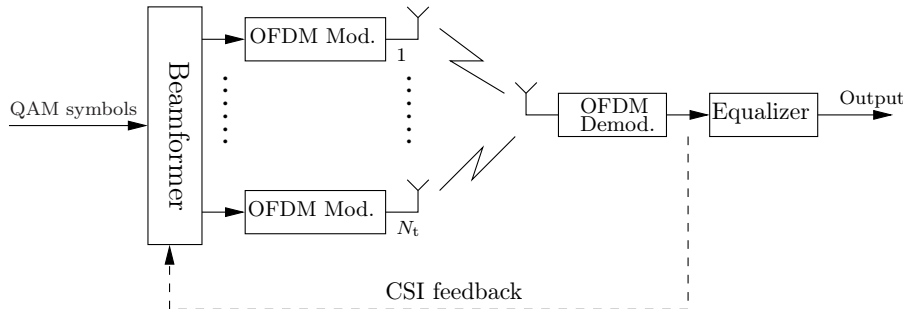
Figure 2.3: MISO-OFDM beamforming system with N_{t} transmit antennas and a single receive antenna using feedback

In the MISO-OFDM system the beamforming vector $\mathbf{w}(k)$ is designed subcarrier-wise. Generally, the channel gain is a matrix $\mathbf{H}(k)$ $(N_{\mathrm{r}} \times N_{\mathrm{t}})$ in case of MIMO transmission. In order to maximize the received SNR on subcarrier k

$$\gamma(k) = \frac{E_{\mathrm{s}}}{N_0}||\mathbf{H}(k)\mathbf{w}(k)||^2, \tag{2.7}$$

$\mathbf{w}(k)$ is chosen as the right singular vector of $\mathbf{H}(k)$ corresponding to the largest singular value of $\mathbf{H}(k)$ [84]. In reality a quantized version of $\mathbf{w}(k)$ is conveyed from the receiver to the transmitter using a finite rate feedback channel. Without a feedback compression technique, usually a codebook $\mathcal{C}_{\mathrm{full}}$ which contains $N = 2^{B_{\mathrm{full}}}$ codewords (quantized

beamforming vectors) $\mathcal{C}_{\text{full}} = \{\mathbf{c}_1, \mathbf{c}_2, \cdots, \mathbf{c}_N\}$ is used. The receiver selects the codeword which maximizes the received SNR, i.e.,

$$\mathbf{c}_{\text{opt}}(k) = \arg \max_{\mathbf{c}_i \in \mathcal{C}_{\text{full}}} \frac{E_{\text{s}}}{N_0} ||\mathbf{H}(k)\mathbf{c}_i||^2, \tag{2.8}$$

and just sends back the index of the optimal codeword using B_{full} bits. Therefore, a total number of $B_{\text{full}}N_{\text{c}}$ bits are necessary for all the subcarriers of one OFDM symbol, where N_{c} denotes the number of subcarriers. If multiple OFDM symbols are to be transmitted, the required bits are also proportional to the number of OFDM symbols.

2.3.2   Feedback reduction techniques

As mentioned before the high correlation among the subcarriers or time slots can be exploited to reduce the amount of feedback information. In this chapter we focus on the clustering, interpolation, recursive and trellis-based feedback algorithms and the frequency-domain algorithms will be combined with the time-domain methods to build up the RB-based structure in the following sections.

Frequency-domain clustering

The simplest method to utilize the correlation of neighboring subcarriers or beamforming vectors is to combine adjacent subcarriers into a cluster and just use one beamforming vector for the whole cluster. Different metrics can be used for each cluster. A simple method is to select the beamforming vector on the central subcarrier in the cluster, i.e., the beamforming vector in the $(m + 1)$-th cluster can be calculated as

$$\mathbf{w}(mK_{\text{c}} + l) = \arg \max_{\mathbf{c}_i \in \mathcal{C}_{\text{full}}} |\mathbf{h}(mK_{\text{c}} + \lceil \tfrac{K_{\text{c}}}{2} \rceil)\mathbf{c}_i|^2, \quad \text{for } l = 1, \cdots, K_{\text{c}}, \tag{2.9}$$

where K_{c} is the cluster size and the cluster index m ranges from 0 to $\frac{N_{\text{c}}}{K_{\text{c}}} - 1$. Clustering can reduce the number of feedback bits required by one OFDM symbol by a factor of the cluster size K_{c}, i.e., $\frac{B_{\text{full}}N_{\text{c}}}{K_{\text{c}}}$.

Interpolation

Instead of using the beamforming vector on one subcarrier for a whole cluster, interpolation uses several beamforming vectors on certain subcarriers to estimate for other subcarriers. Since the beamforming vectors have a unit norm, some spherical interpolation algorithms can be implemented. As can be seen from (2.7), the optimal beamforming vector has phase invariance property, i.e., when $\mathbf{w}(k)$ is optimal for maximizing the received SNR, $e^{j\theta}\mathbf{w}(k)$ is also optimal. Based on this property [35] proposed to divide the subcarriers into several interpolation intervals with size K_{in} and evaluate the beamforming vectors by linear interpolation using the first subcarrier of the adjacent intervals. The

interpolator computes for subcarrier $mK_{\text{in}} + l$ $(1 \leq l \leq K_{\text{in}})$

$$\mathbf{w}(mK_{\text{in}} + l; \theta_m) = \frac{(1 - c_l)\mathbf{w}(mK_{\text{in}} + 1) + c_l e^{j\theta_m}\mathbf{w}((m+1)K_{\text{in}} + 1)}{||(1 - c_l)\mathbf{w}(mK_{\text{in}} + 1) + c_l e^{j\theta_m}\mathbf{w}((m+1)K_{\text{in}} + 1)||}, \quad (2.10)$$

where m is the interpolation interval index $(0 \leq m \leq \frac{N_c}{K_{\text{in}}} - 1)$, $c_l = \frac{l-1}{K_{\text{in}}}$ is the linear weight value and θ_m is a parameter for phase rotation which takes into account the phase invariance property of the beamforming vector. Due to the fast Fourier transform (FFT) processing at the receiver the channel gain in frequency domain is expressed as a periodic waveform. Therefore, the beamforming vectors in the last interpolation interval can be obtained from $\mathbf{w}(N_c - K_{\text{in}} + 1)$ and $\mathbf{w}(1)$, i.e., $\mathbf{w}(N_c + 1) = \mathbf{w}(1)$.

For practical implementation firstly the beamforming vector on the first subcarrier of each interval should be quantized

$$\mathbf{w}(mK_{\text{in}} + 1) = \arg \max_{\mathbf{c}_i \in \mathcal{C}_{\text{full}}} |\mathbf{h}(mK_{\text{in}} + 1)\mathbf{c}_i|^2, \quad \text{for } 0 \leq m \leq \frac{N_c}{K_{\text{in}}} - 1. \quad (2.11)$$

Then with the help of (2.10) grid search with respect to the phase parameter can be used to find the optimal θ_m. Here the optimal θ_m is determined to maximize the minimum channel gain

$$\theta_m = \arg \max_{\theta \in \Theta} \min_{1 \leq p \leq K_{\text{in}}} |\mathbf{h}(mK_{\text{in}} + p)\mathbf{w}(mK_{\text{in}} + p; \theta)|^2, \quad \text{for } 0 \leq m \leq \frac{N_c}{K_{\text{in}}} - 1, \quad (2.12)$$

where Θ is the codebook for the phase parameter which may contain equally distributed quantization levels in $[0, 2\pi]$. After the optimal θ_m for each interval is determined at the receiver, it is conveyed back to the transmitter together with the quantized beamforming vector on the first subcarrier of each interpolation interval. The total required number of bits for one OFDM symbol using interpolation feedback scheme is $\frac{N_c}{K_{\text{in}}}(B_{\text{full}} + \log_2 |\Theta|)$, where $|\Theta|$ stands for the cardinality of Θ.

Recursive feedback algorithm

In [137] the recursive algorithm for feedback reduction was proposed. Due to frequency correlation the channel vector $\mathbf{h}(k)$ or the optimal beamformer $\mathbf{w}(k)$ on subcarrier k lies in the "neighborhood" of the previous ones $\mathbf{h}(k-1)$ and $\mathbf{w}(k-1)$ with a high probability. Therefore, given $\mathbf{h}(k-1)$ or $\mathbf{w}(k-1)$ it is not necessary to quantize $\mathbf{h}(k)$ and $\mathbf{w}(k)$ using the complete codebook $\mathcal{C}_{\text{full}}$. The recursive encoding proposes to use $\mathcal{C}_{\text{full}}$ only for the first subcarrier and a subset $\widetilde{\mathcal{C}}(k)$ of $\mathcal{C}_{\text{full}}$ as the codebook for subcarrier k $(k = 2, 3, \cdots N_c)$. $\widetilde{\mathcal{C}}(k)$ differs for different subcarriers and depends on the optimal codeword $\mathbf{c}_{\text{opt}}(k-1)$ on subcarrier $k-1$. The $2^{B_{\text{sub}}}$ elements in $\widetilde{\mathcal{C}}(k)$ can be chosen as $2^{B_{\text{sub}}}$ nearest codewords of $\mathbf{c}_{\text{opt}}(k-1)$ including $\mathbf{c}_{\text{opt}}(k-1)$ itself, where $B_{\text{sub}} < B_{\text{full}}$. An example for $B_{\text{sub}} = 2$ is shown in Figure 2.4. Here the chordal distance $d_c(\mathbf{c}_i, \mathbf{c}_j) = \frac{1}{\sqrt{2}}||\mathbf{c}_i\mathbf{c}_i^H - \mathbf{c}_j\mathbf{c}_j^H||_{\mathcal{F}}$ is considered

as the distance measure. After $\widetilde{\mathcal{C}}(k)$ is determined for subcarrier k, the optimal codeword $\mathbf{c}_{\mathrm{opt}}(k)$ can be found out using (2.8) by replacing $\mathcal{C}_{\mathrm{full}}$ with $\widetilde{\mathcal{C}}(k)$ and sent back with B_{sub} bits. In this way the total number of feedback bits for one OFDM symbol is reduced to $B_{\mathrm{full}} + (N_{\mathrm{c}} - 1)B_{\mathrm{sub}}$. However, when the channel between adjacent subcarriers varies abruptly, the recursive encoding may lose track of the channel and cause performance degradation.

Codebook $\widetilde{\mathcal{C}}(k)$ of size 4 for subcarrier k

Optimal codeword $\mathbf{c}_{\mathrm{opt}}(k-1)$ on subcarrier $k-1$
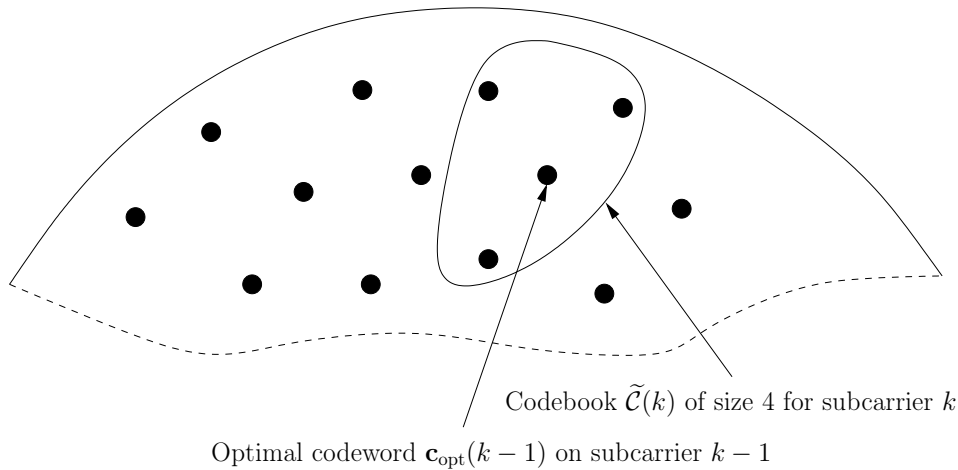
Figure 2.4:   4 neighboring codewords of the codeword $\mathbf{c}_{\mathrm{opt}}(k-1)$ including itself

Trellis-based algorithm

To overcome the drawback of the recursive algorithm [137] introduces a trellis-based feedback encoding. Similar to the recursive algorithm the trellis-based encoding also uses $\mathcal{C}_{\mathrm{full}}$ for the first subcarrier and $\widetilde{\mathcal{C}}(k)$ for other subcarriers. However, the optimal codeword is not determined for each subcarrier separately. A metric is defined for each subcarrier and here the bit error rate (BER) is used. For 4-QAM symbols the BER on the k-th subcarrier is calculated as [136]

$$\mathrm{BER}(k) = \mathrm{Q}(\sqrt{\gamma(k)}). \tag{2.13}$$

The trellis-based encoding utilizes the Viterbi algorithm to calculate the cumulative metrics for different possible paths (**a path is the selection of one codeword for each subcarrier throughout the whole bandwidth**) and the final decision is made for all the subcarriers simultaneously. The algorithm is explained as following:

- The Viterbi algorithm is implemented subcarrier-wise. Firstly, the BER metric for all the codewords in $\mathcal{C}_{\mathrm{full}}$ on the **first** subcarrier

$$\mathrm{Metric} = \mathrm{Q}\left(\sqrt{\frac{E_{\mathrm{s}}}{N_0}|\mathbf{h}(1)\mathbf{c}_i|^2}\right), \quad \text{for } i = 1, \cdots, N, \tag{2.14}$$

will be calculated. So there are in total $\mathcal{C}_{\text{full}}$ paths initiated, i.e., there are $\mathcal{C}_{\text{full}}$ codeword candidates for the first subcarrier.

- For subcarrier k ($k = 2, \cdots, N_{\text{c}}$) depending on the codeword candidates used for subcarrier $k - 1$, each path is extended and selects $2^{B_{\text{sub}}}$ neighboring codewords (codeword candidates for subcarrier k) and calculates the metrics for subcarrier k. The metric is then accumulated with the previous metrics of each path. As a result, for each codeword on subcarrier k, there could be multiple paths passing through. The path with minimum accumulated metric will be further considered for this codeword and the other paths are discarded. Hence, the number of paths can only be equal to or less than $\mathcal{C}_{\text{full}}$.

- After the selection of the codewords for all subcarriers is finished, the cumulative metrics of all paths are compared and the one with the minimum cumulative metric is the optimal path. The codewords associated with the optimal path are the quantized beamforming vectors for each subcarrier.

The trellis-based algorithm also reduces the number of feedback bits for one OFDM symbol to $B_{\text{full}} + (N_{\text{c}} - 1)B_{\text{sub}}$. Although trellis-based encoding partially solves the losing track problem of the recursive encoding, the Viterbi algorithm increases the complexity and required memory size at the receiver. Also both approaches still have the tracking problem when the feedback link is not error-free.

Time-domain clustering

Within this dissertation we only consider the clustering scheme for time-domain techniques due to its low implementation complexity. Different from the clustering in frequency domain, the beamforming vector designed for the current time slot can only be used for the current or subsequent time slots if a zero-delay feedback channel is assumed. For each time interval, the beamforming vectors on the subcarriers of the first OFDM symbol are also used for several consequent OFDM symbols. Hence the required number of feedback bits is reduced by a factor equal to the number of OFDM symbols in each time interval compared with the scheme which does not exploit the temporal correlation.

2.3.3 RB-based feedback structure

In the aforementioned references the frequency and temporal correlation are usually not considered simultaneously. Taking both correlations into account we propose to use a RB-based feedback structure [132]. Similar terminology is also used in the 3GPP standard [4]. A RB is a frequency-time resource consisting of N_{sub} adjacent subcarrier of N_{sym} consecutive OFDM symbols (time slots) as illustrated in Figure 2.5. Generally, a

feedback algorithm in each RB can be designed independently and adaptively according to the actual channel properties.
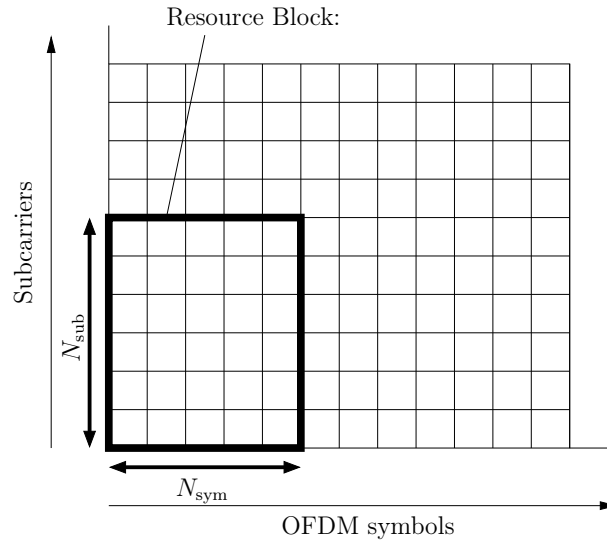
Figure 2.5:   Frequency-time resource grid for one RB

In this dissertation the following *RB-based feedback algorithm* is used:

- The feedback information is created independently for each RB.

- In the first time slot of each RB, frequency-domain feedback schemes are implemented for the design of the feedback information and beamforming vectors for all subcarriers.

- Since only clustering is considered as the time-domain scheme, the transmit beamforming vectors for other time slots within the same RB choose the same ones as for the first time slot.

In [35] it was mentioned that when the SNR is high the performance using the interpolation scheme is getting worse compared with the scheme using optimal beamforming vectors, where full channel knowledge is available at the transmitter. This phenomenon is called by [35] **diversity loss**. In order to show this phenomenon we generate the channel using the HIPERLAN/2 channel model B [83], whose PDP is defined in Appendix A. HIPERLAN/2 channel model B models a typical large open space environment with non-line-of-sight (NLOS) conditions or an office environment with large delay spread where the transmitter and the receiver are usually immobile or at very low speed. Hence we only compare different frequency-domain feedback schemes.

For the simulations we use the parameters listed in Table 2.1. It is assumed that no spatial correlation exists between antennas. For the codebook design the Grassmannian codebook is used which is derived from the Grassmannian line packing problem [78]. This problem tries to maximize the minimum distance between any two vectors in the codebook and the distance between $\mathbf{w}_i$ and $\mathbf{w}_j$ is defined as the sine of the angle $\theta_{i,j}$ between these two vectors

$$d(\mathbf{w}_i, \mathbf{w}_j) = \sin(\theta_{i,j}) = \sqrt{1 - |\mathbf{w}_i^{\mathrm{H}} \mathbf{w}_j|^2}, \quad i \neq j. \tag{2.15}$$

In this simulation $B_{\mathrm{full}} = 6$ and $B_{\mathrm{sub}} = 2$ for the recursive and trellis-based schemes and the RB structure is firstly not considered (or $N_{\mathrm{sub}} = N_{\mathrm{c}}$). The complete Grassmannian codebook consisting of 64 4×1 unit-norm vectors is given in Table B.2. The clustering scheme uses a cluster size of $K_{\mathrm{c}} = 3$ and within each cluster 6 bits are used to quantize the optimal beamforming vector employing the same Grassmannian codebook. The interpolation interval $K_{\mathrm{in}} = 6$ and the number of bits for quantization of the beamforming vector on the first subcarrier of each interval is 6. We also use 6 bits to quantize the phase parameter, i.e., the codebook Θ for the phase parameter is $\{0, \frac{2\pi \cdot 1}{64}, \frac{2\pi \cdot 2}{64}, \frac{2\pi \cdot 3}{64}, \cdots, \frac{2\pi \cdot 63}{64}\}$. In total each scheme uses 132 feedback bits for one OFDM symbol. Note that in case of 4-QAM the number of information bits in one OFDM symbol is 128 bits, which means the feedback bits used for channel quantization are huge for one OFDM symbol. Thanks to the time-domain clustering, the channel information can be reused for several consequent OFDM symbols.

Table 2.1: Simulation parameters for HIPERLAN/2 channel model B

Number of transmit antennas N_{t}	4
Number of receive antennas N_{r}	1
Number of subcarriers N_{c}	64
Guard interval length N_{g}	16
Sampling rate	20 MHz

The BER performance is shown in Figure 2.6. *Full* is the quantization scheme without feedback compression, i.e., for each subcarrier 6 bits are used to quantize the optimal beamforming vector. *Perfect* is the feedback scheme that assumes perfect channel information is available at the transmitter, meaning that the optimal beamforming vectors are used. Obviously having perfect channel information at the transmitter shows the best BER performance. At low SNR regime (SNR < 14 dB) the performance of the clustering and interpolation schemes is quite close to the scheme without feedback compression, while when SNR > 14 dB the performance of these two approaches shows the diversity
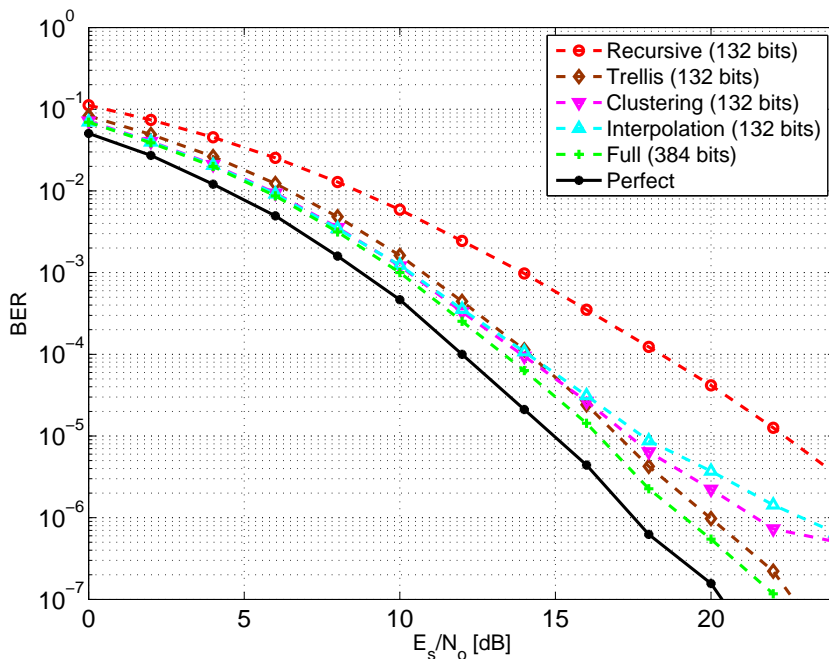
Figure 2.6: BER performance with different frequency-domain feedback algorithms under HIPERLAN/2 channel model B

loss effect and is degraded compared to the trellis-based scheme. At the BER of 10^{-6} the performance using clustering and interpolation approaches is 2 dB and 4 dB worse than the trellis-based scheme, respectively. And this performance difference is getting larger when the SNR is larger. For the whole SNR regime the difference between the trellis-based scheme and the approach without feedback compression is keeping 1 dB. However, the trellis-based scheme requires huge computational complexity which increases exponentially with the numbers of feedback bits and subcarriers [137]. On the other side, although the recursive algorithm shows the worst performance, this algorithm does not suffer from severe diversity loss when the SNR is high. Moreover, the recursive algorithm requires very low searching complexity. It only needs the neighboring codewords as mentioned in Section 2.3.2 to be stored at the receiver and transmitter.

RB-based recursive algorithm

Based on the previous observation and analysis in some applications such as the control systems or wireless sensor networks where the BER requirement is high, we propose to combine the RB-based feedback structure with the recursive and trellis-based schemes. The *RB-based recursive algorithm* is firstly given in the following:

- The feedback information is created independently for each RB.

- For the first OFDM symbol of a RB the first subcarrier uses B_{full} bits for feedback quantization and the optimal codeword which satisfies (2.8) is selected.

- For each of the remaining $N_{\text{sub}}-1$ subcarriers B_{sub} bits are used and the corresponding codebook $\widetilde{\mathcal{C}}(k)$ is chosen as a subset of $\mathcal{C}$ based on the previous optimal codeword as explained in Section 2.3.2. The optimal codeword is calculated according to

$$\mathbf{c}_{\text{opt}}(k) = \arg \max_{\mathbf{c}_i \in \widetilde{\mathcal{C}}(k)} \frac{E_{\text{s}}}{N_0} ||\mathbf{h}(k)\mathbf{c}_i||^2. \tag{2.16}$$

- After the beamforming vectors on all subcarriers in the first OFDM symbol are obtained by the transmitter, the remaining $N_{\text{sym}} - 1$ OFDM symbols within the same RB reuses the beamformers designed for the first OFDM symbol on the corresponding subcarriers.

In frequency direction this algorithm periodically feeds back the quantized optimal beamforming vector using B_{full} bits (with a period of N_{sub} subcarriers). In case that the transmitter loses track of the channel because of an abrupt channel variation or feedback error which may occur in the recursive and trellis-based algorithms, the *RB-based recursive algorithm* restores the channel state after a maximum of N_{sub} subcarriers so that error propagation can be avoided. In the following we show that error diffusion is restrained by the RB-based method. Moreover, the complexity of this algorithm keeps the same and is as low as for the recursive encoding.

If only one OFDM symbol is considered, a total of $\lceil \frac{N_{\text{c}}}{N_{\text{sub}}} \rceil (B_{\text{full}} - B_{\text{sub}}) + B_{\text{sub}} N_{\text{c}}$ feedback bits are required by the *RB-based recursive algorithm*. This corresponds to an increment of $\lceil \frac{N_{\text{c}}}{N_{\text{sub}}} - 1 \rceil (B_{\text{full}} - B_{\text{sub}})$ compared to the recursive and trellis-based algorithms. Notice that temporal correlation is considered in the *RB-based recursive algorithm*. The last $N_{\text{sym}} - 1$ OFDM symbols in a RB do not cause additional feedback overhead. Therefore, the feedback load is reduced by a factor of N_{sym}. In practice N_{sub} and N_{sym} can be and have to be chosen according the current channel conditions. In the sequel we also show that N_{sub} and N_{sym} can be chosen depending on the coherence bandwidth and the coherence time sophisticatedly. In addition, [69] verifies that in a slow fading environment infrequent high resolution feedback outperforms frequent low resolution feedback. Similar to this result, in the simulation analysis in Section 2.3.4 we confirm that spending a few more bits just on the first OFDM symbol of a RB in the *RB-based feedback algorithm* will gain much compared with the approaches without utilizing temporal correlation.

In order to show the quantization error of the channel, we compare the SNR and SNR loss on each subcarrier using different feedback schemes and the SNR loss is defined as the SNR difference between the quantization feedback scheme and the scheme with perfect

channel knowledge at the transmitter. The HIPERLAN/2 channel model B is used and the parameters are the same as given in Table 2.1. We fix the transmit symbol power and set the noise power so that the transmit SNR is 5 dB. For the *RB-based recursive algorithm* $N_{\text{sub}} = 5$ and $N_{\text{sym}} = 1$. The simulation is done based on 100000 channel realizations.
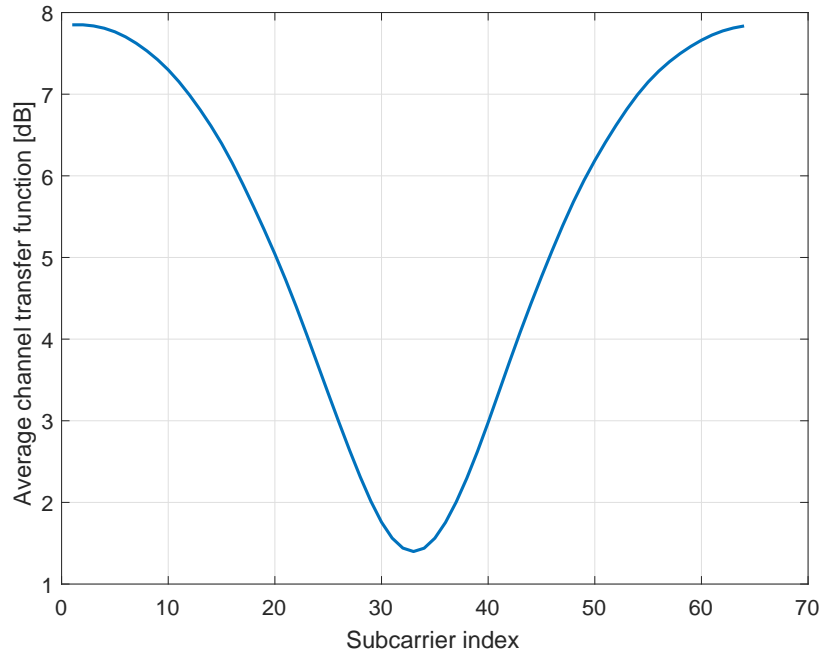
Figure 2.7: Average channel transfer function of the HIPERLAN/2 channel model B

Firstly, the average channel transfer function is shown in Figure 2.7 and the SNR results are given in Figure 2.8. Similar to Figure 2.6 *Perfect* is the optimal scheme using optimal beamforming vectors at the transmitter which shows the best performance (largest average received SNR) over the subcarriers. *Full* is the quantization scheme without feedback compression (with 6 feedback bits per subcarrier). This scheme has an SNR loss of 4 dB at the edge subcarriers and 1 dB at the middle subcarriers. This observation shows that when the channel condition is poor, the performance loss due to quantization error also becomes small. Moreover, the *Full* scheme, the *RB-based recursive algorithm* and the recursive approach all suffer from the quantization error. The recursive approach has the same SNR at the first subcarrier as the *Full* scheme because both approaches quantize the first subcarrier using 6 bits. However, the performance is getting worse compared to the *Full* scheme since the channel variations cannot be exactly tracked and at subcarrier 64 the SNR loss is about 9 dB. It can be clearly seen from the curves that for the first 5 subcarriers the *RB-based recursive algorithm* and the recursive approach
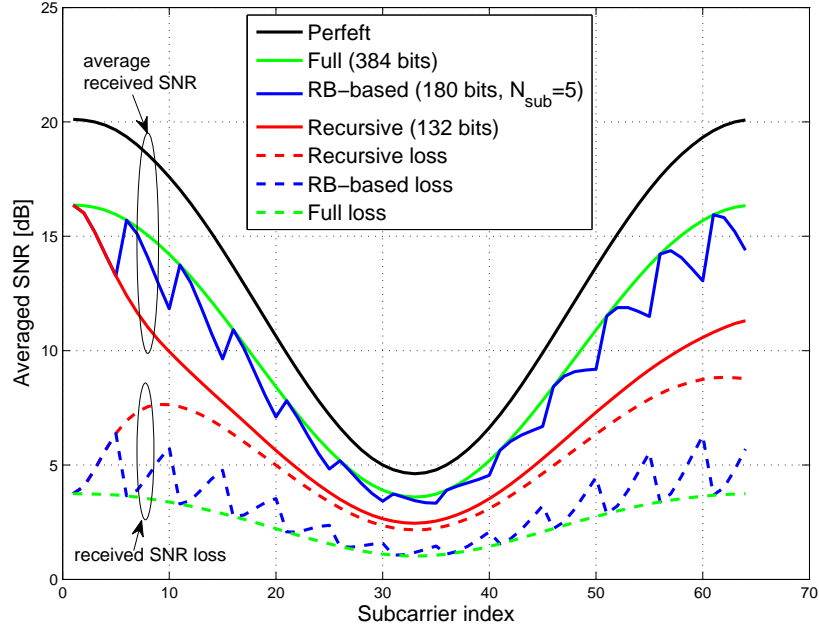
Figure 2.8: Received SNR and SNR loss using different feedback schemes under HIPER-
LAN/2 channel model B

perform the same because they implement the same algorithm. After that for each 5
subcarriers the *RB-based recursive algorithm* resets the channel tracking status the same
as the *Full* scheme using 6 bits so that the error propagation can be suppressed. The
SNR loss due to quantization is kept under 6 dB by the *RB-based recursive algorithm* and
this performance improvement is on the cost of extra feedback bits every 5 subcarriers.

RB-based trellis algorithm

For the *RB-based trellis algorithm*, different from the trellis-based approach in Section
2.3.2, a path is defined as the selection of one codeword for each subcarrier throughout
N_{sub} adjacent subcarriers within a RB instead of the whole bandwidth and the final
decision is made once for N_{sub} subcarriers. The RB-based trellis algorithm is shown in
the following:

- For the following steps $j = 1, \cdots, \left\lceil \frac{N_{\mathrm{c}}}{N_{\mathrm{sub}}} \right\rceil$ stands for the RB index along the fre-
  quency direction.

- The Viterbi algorithm is implemented subcarrier-wise and for the first OFDM sym-
  bol of each RB only. The paths start from all the codewords in $\mathcal{C}_{\mathrm{full}}$ and for each

codeword the BER metric on the first subcarrier of RB j

$$\text{Metric} = Q\left(\sqrt{\frac{E_s}{N_0}|\mathbf{h}((j-1)N_{\text{sub}}+1)\mathbf{c}_i|^2}\right), \quad \text{for } i = 1, \cdots, N, \quad (2.17)$$

is calculated.

- For the remaining subcarrier $(j-1)N_{\text{sub}}+k$ $(k = 2, \cdots, N_c)$ of RB j depending on the codeword used for subcarrier $(j-1)N_{\text{sub}}+k-1$, the paths select $2^{B_{\text{sub}}}$ neighboring codewords and calculate the metrics for subcarrier $(j-1)N_{\text{sub}}+k$. The metric is accumulated with the previous metrics of the same path.

- After the selection of the codewords for all N_{sub} subcarriers is finished, the cumulative metrics of all paths are compared and the one with the minimum cumulative metric is the optimal path. The codewords associated with the optimal path are the quantized beamforming vectors for the first OFDM symbol of each RB.

- The remaining $N_{\text{sym}}-1$ OFDM symbols within the same RB reuses the beamformers designed for the first OFDM symbol on the corresponding subcarriers.

RB-based clustering algorithm

For some applications in the mobile cellular networks such as telephoning, video streaming, etc., where the demand for latency or data rate is high while the BER requirement is not very high and mobile terminals may move at a high velocity, we propose to combine the RB structure with the clustering scheme. The interpolation scheme is not considered since the clustering scheme needs much less memory size and computational complexity. The *RB-based clustering algorithm* is described as followings:

- The RB parameter N_{sub} is set to the cluster size K_c in the frequency-domain clustering scheme in Section 2.3.2.

- In RB j $(j = 1, \cdots, \lceil \frac{N_c}{N_{\text{sub}}} \rceil)$ the beamforming vector on the central subcarrier of the first OFDM symbol is chosen as

$$\mathbf{w}((j-1)N_{\text{sub}}+\lceil \tfrac{N_{\text{sub}}}{2} \rceil) = \arg \max_{\mathbf{c}_i \in \mathcal{C}_{\text{full}}} |\mathbf{h}((j-1)N_{\text{sub}}+\lceil \tfrac{N_{\text{sub}}}{2} \rceil)\mathbf{c}_i|^2. \quad (2.18)$$

- $\mathbf{w}((j-1)N_{\text{sub}}+\lceil \tfrac{N_{\text{sub}}}{2} \rceil)$ is selected as the beamforming vector for the whole RB.

2.3.4   Simulation results and analysis

First we compare the *RB-based feedback algorithm* under HIPERLAN/2 channel model B. The same simulation settings are used as in Table 2.1. $B_{\text{full}} = 6$, $B_{\text{sub}} = 2$ and the Grassmannian codebook is given in Table B.2. For HIPERLAN/2 channel model B the RMS delay spread σ_τ is 98.998 ns. As mentioned in Section 2.2.2 a general approximation of the coherence bandwidth B_c can be calculated proportional to the reciprocal of σ_τ: $B_c \approx \frac{k}{\sigma_\tau} \approx 10.101k$ MHz, where k depends on the PDP of the channel [50]. For example, it is shown that $B_c \approx \frac{0.2}{\sigma_\tau}$ approximates the range of frequencies over which channel correlation exceeds 0.5. Since for HIPERLAN/2 channel models the channel bandwidth is 20 MHz [12], the subcarrier spacing is 0.3125 MHz and $\frac{0.2}{\sigma_\tau}$ corresponds to about 6.5 subcarriers. We analyze in the following the BER performance using N_{sub} corresponding to different numbers of subcarriers.
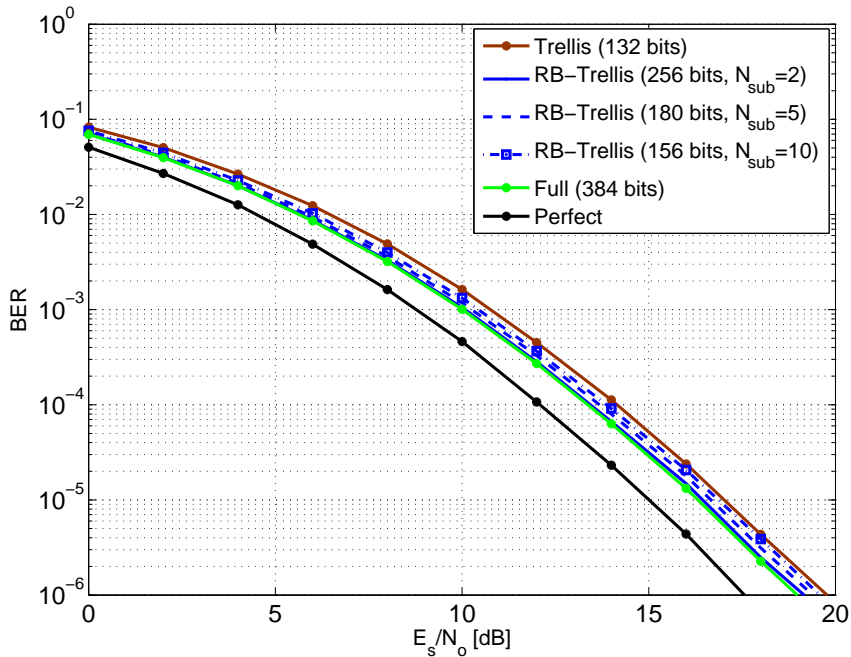
Figure 2.9: BER performance with *RB-based trellis algorithm* under HIPERLAN/2 channel model B

Figure 2.9 shows the simulation result using *RB-based trellis algorithm* with $N_{\text{sym}} = 1$ and $N_{\text{sub}} = 2$, 5, 10. *Perfect* indicates the beamforming strategy with perfect channel knowledge at the transmitter, hence exhibiting the best BER performance. Compared with the optimal case (*Perfect*) the scheme without feedback compression (*Full*) has degradation of 1 dB at low SNR regime and 2 dB at the SNR of 10^{-6}. This difference is caused by the quantization error. Moreover, the system has slightly better performance

improvement when N_{sub} is smaller, i.e., more feedback bits are used. Notice that when $N_{sub} = 2$ the *RB-based trellis algorithm* has a negligible performance loss in comparison with *Full* while saving 33% feedback bits.
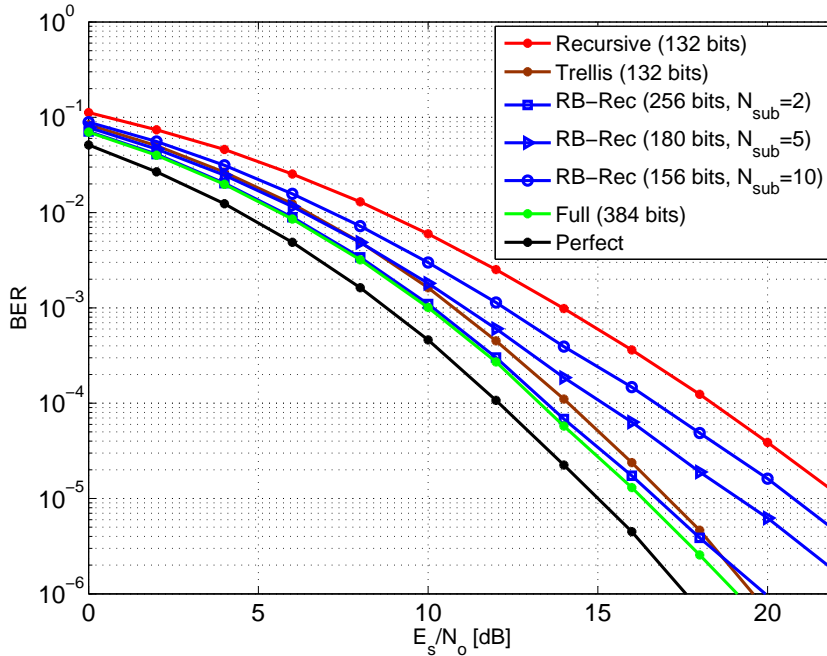
Figure 2.10: BER performance with *RB-based recursive algorithm* under HIPERLAN/2 channel model B

Figure 2.10 shows the BER versus average received SNR with *RB-based recursive algorithm*. We also set $N_{sym} = 1$ and $N_{sub} = 2$, 5, 10 for comparison. The simulation shows that the *RB-based recursive algorithm* outperforms the recursive approach with additional feedback bits. The smaller N_{sub} is, the better is the BER performance of the system and the more feedback bits the system needs. With $N_{sub} = 2$ the gap between the *RB-based recursive algorithm* and the scheme without feedback compression (*Full*) is negligible at low SNR regime and is about 1 dB at the BER of 10^{-6}, while the RB-based feedback saves 33% feedback overhead. Furthermore, the *RB-based recursive algorithm* with $N_{sub} = 2$ outperforms the trellis-based scheme by 1 dB at low SNR regime and performs similarly at high SNR, but still incurs slight diversity loss and requires almost 100% more feedback bits. As mentioned previously, the trellis-based scheme requires high memory size and computational complexity which increase exponentially with the numbers of feedback bits and subcarriers [137]. Therefore, with variable N_{sub} the *RB-based recursive algorithm* can be implemented in an adaptive way to find a compromise among feedback overhead, performance gain and complexity.

In order to further reduce the feedback overhead, temporal correlation should be exploited. In the following the simulation results under ITU typical urban model are shown, which models an urban scenario where the terminals may move at high velocity. The PDP of the ITU typical urban model with reduced setting (6 taps) are given in Table 2.2 [11]. For the simulations we use $N_\text{t} = 4$, $N_\text{r} = 1$, $N_\text{c} = 1024$ and $N_\text{g} = 216$. For the transmissions we assume a carrier frequency of $f_\text{c} = 5.2$ GHz and sampling rate of 20 MHz. Also no spatial correlation exists between antennas.

Table 2.2: ITU typical urban model

Path Number	Average Path Gain (dB)	Path Delay (ns)
1	-3	0
2	0	200
3	-2	500
4	-6	1600
5	-8	2300
6	-10	5000

In this simulation the frequency-domain clustering scheme and the *RB-based clustering algorithm* are compared. The frequency-domain clustering scheme uses a cluster size $K_\text{c} = 8$ and 4 feedback bits for each cluster. The quantized beamforming vectors will be fed back every OFDM symbol and hence the temporal correlation is not utilized. The Grassmannian codebook with 16 codewords is given in Table B.1. The terminal velocity is assumed to be 3 km/h. Therefore, the maximum Doppler frequency is 14.44 Hz and the coherence time T_c mentioned in Section 2.2.2 is 0.0293 s, which corresponds to 472 OFDM symbols. For the *RB-based clustering algorithm* we set $N_\text{sub} = 8$ and $N_\text{sym} = 4$, 20, 80 for comparison. Within each RB 8 bits are used for quantization.

Figure 2.11 shows the result when the terminal velocity is low. The BER curve for the *RB-based clustering algorithm* with $N_\text{sym} = 4$ and $N_\text{sym} = 20$ almost overlap with each other and both outperform the frequency-domain clustering scheme by 1 dB. The proposed algorithm with $N_\text{sym} = 80$ performs similar to the frequency-domain clustering scheme except slightly better when the SNR is lower than 7 dB. Furthermore, the algorithm with $N_\text{sym} = 80$ reduces the feedback overhead by a factor of 53 compared with the scheme without utilizing temporal correlation. We find out that in low speed scenario by exploiting temporal correlation and spending some more bits on the first OFDM symbol to increase the quantization resolution gain much more than the scheme feeding back for each OFDM symbol with fewer bits.
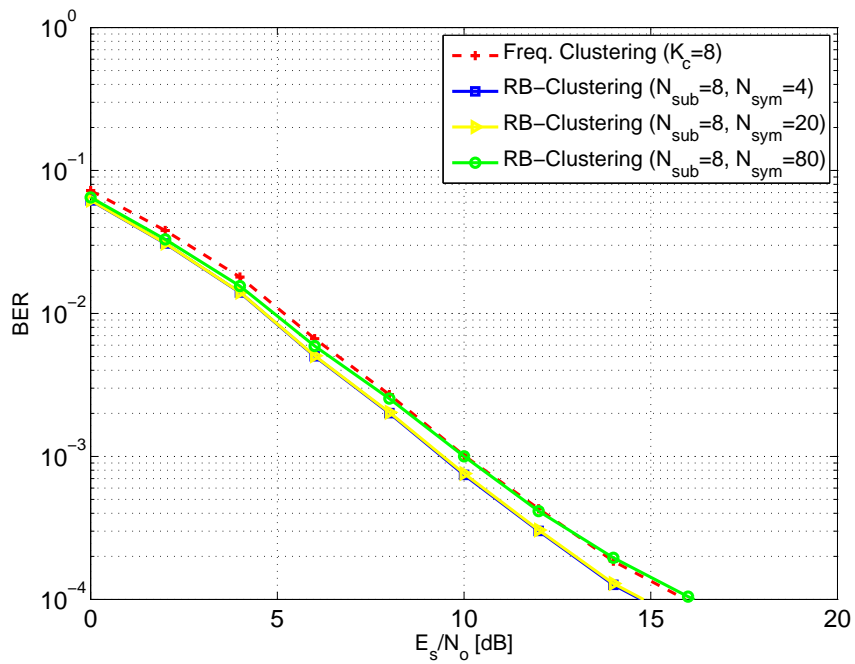
Figure 2.11: BER performance with the *RB-based clustering algorithm* under ITU typical urban model (terminal speed 3 km/h)
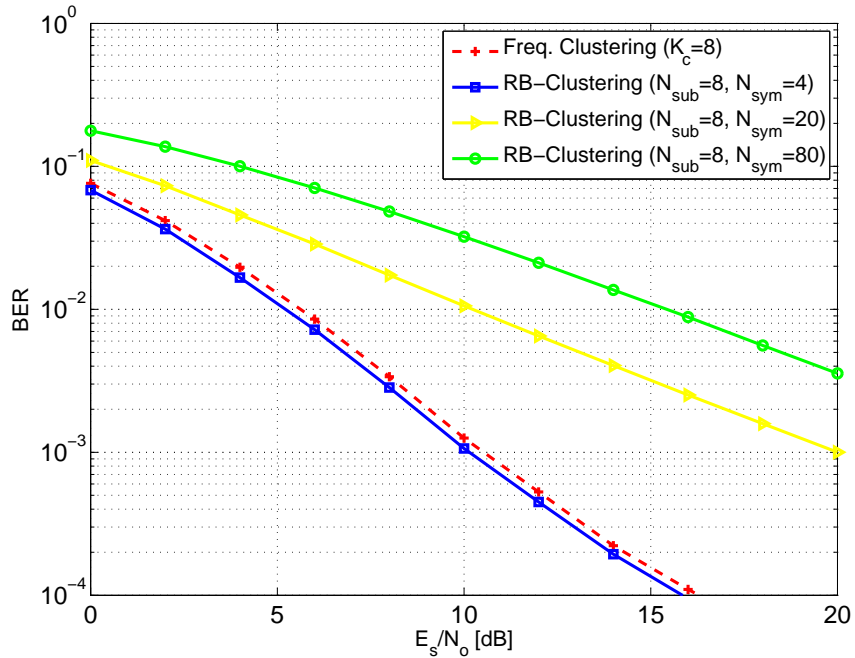
Figure 2.12: BER performance with the *RB-based clustering algorithm* under ITU typical urban model (terminal speed 50 km/h)

Figure 2.12 shows the simulation result when the terminal velocity is 50 km/h. The other simulation parameters are the same as in Figure 2.11. One observation is that when the velocity is high, the performance of the proposed RB-based algorithm is worse than that of the scenario with low velocity. This is because the coherence time is smaller in high speed scenario and the channel varies more quickly with time. We also observe that the performance with the proposed algorithm gets better when N_{sym} is smaller. Although the proposed algorithm with $N_{\mathrm{sym}} = 20$ and $N_{\mathrm{sym}} = 80$ performs much worse than the frequency-domain clustering scheme, the algorithm with $N_{\mathrm{sym}} = 4$ performs slightly better and can still guarantee a feedback reduction of a factor of 2.67. Moreover, when the terminal velocity is low, the proposed approach with $N_{\mathrm{sym}} = 80$ shows similar performance as the frequency-domain clustering scheme and $N_{\mathrm{sym}} = 80$ corresponds to 17% of the coherence time. When the terminal velocity is high, the coherence time is 0.0018 s which covers around 28 OFDM symbols and $N_{\mathrm{sym}} = 4$ corresponds to 14% of the coherence time where the proposed approach performs similar to the frequency-domain clustering scheme. We conclude that about 15% of the coherence time is a good choice for the parameter N_{sym} for the ITU typical urban model if we want to maintain similar performance to the frequency-domain clustering scheme and gain feedback reduction simultaneously.

2.4 Conclusion

Within this chapter the concept of OFDM was briefly introduced and the mobile radio channels were characterized. The state of the art of the feedback techniques for OFDM systems were presented. Taking both frequency correlation and temporal correlation into account a RB-based feedback structure was proposed which is combined with different feedback reduction schemes. The *RB-based feedback algorithm* can be implemented adaptively for different applications. In case that the BER requirement is high, the *RB-based trellis algorithm* and *RB-based recursive algorithm* were recommended. It was shown that both algorithms outperform the scheme without RB-based structure with additional feedback overhead when no temporal correlation is utilized and the performance of both algorithms approaches the scheme without feedback reduction while saving 33% feedback overhead. In case that the demand for latency or data rate is high and the feedback rate is limited, the *RB-based clustering algorithm* can be used. When the temporal correlation is considered, the feedback overhead could be dramatically reduced and the performance is still maintained. Moreover, it was pointed out that the coherence bandwidth and the coherence time are important for the design of parameters of the RB structure.

CHAPTER 3

Limited feedback for CoMP-CB system

In Chapter 2 the feedback problem for a single link in a multi-carrier system was discussed. In a cellular system the disturbance does not only come from the additive noise at the receiver but also from the interference of other BSs or users. Especially, when the data rate and the requirement for high quality of service (QoS) is increasing, the interference becomes the limiting factor for the whole system [80]. Therefore, how to cope with the interference in a cellular system is always an important problem [22, 48, 128]. One approach to reduce the inter-cell interference (ICI) is to increase the frequency reuse factor K, where K is the number of cells that use different frequency bands within the available bandwidth [104]. Figure 3.1 illustrates an example of the frequency allocation in a cellular system. By this means the ICI within this K-cell cluster can be avoided. However, due to decreased bandwidth for each cell the peak data rate can be significantly reduced [30]. Therefore, in the 4G/5G systems the concept of CoMP is proposed [6]. CoMP aims at increasing the overall throughput and cell-edge data rate by base station cooperation. With sophisticated transmission strategies the so-called cochannel interference (CCI), which is caused by sharing the same frequency resource among multiple cells or users [128], can be well managed. In this chapter the frequency reuse factor of 1 is considered.
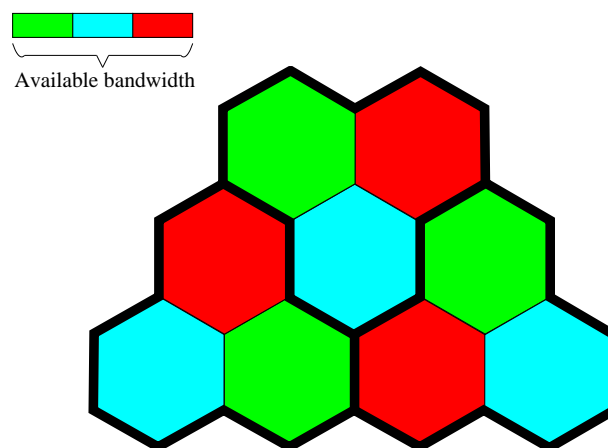
Figure 3.1: Illustration of bandwidth occupation in a cellular system with frequency reuse factor $K = 3$

3.1 Introduction to the CoMP system

3.1.1 Categories of the CoMP system

With explicit BS cooperation CoMP has two types [6, 80]:

- Coordinated scheduling/beamforming (CS/CB): data is only available in the serving cell, but user scheduling/beamforming is performed with coordination among cells within the same CoMP cooperation set.

- Joint processing (JP): data is available at each transmission point (TP) in CoMP cooperation set, where TP refers to a set of collocated antennas in a cell [72].

JP can be further categorized into:

- Joint transmission (JT): data transmission occurs from multiple TPs within the CoMP cooperation set at a time.

- Dynamic cell selection (DCS): data transmission is only from one TP at a time and the TP varies in the CoMP cooperation set according to changes in channel and interference conditions.

Since in this dissertation only DL transmission is considered, the CoMP cooperation set is the set of cells participating in the DL coordinated transmission to the user equipments (UEs).

Figure 3.2 shows the three CoMP schemes in a cooperation set with three cells. The dedicated transmission is indicated by the solid lines and the dashed lines shows the interference. The CS/CB scheme is illustrated in Figure 3.2a. Each UE is only served by its anchor (serving) BS. However, the scheduling decisions of neighboring TPs and the CSI of all UEs are coordinated within the cooperation set. With this coordinated information the transmit beamforming weights for each UE are generated to reduce the interference to other UEs scheduled within the cooperation set. Therefore, the user throughput, particularly the cell-edge user throughput, can be improved due to the increase in the received SINR [105].

Figure 3.2b shows the JT scheme and each UE is served by three BSs at the same time. Especially for the cell-edge users, converting an interference signal from the neighboring cells to a useful signal will be very helpful for improving the performance [72]. Generally, the transmission could be coherent or non-coherent. In coherent JT all user data and CSI are shared within the cooperation set and each BS knows the local CSI between itself and UEs as well as the CSI between other BSs and UEs. Therefore, the whole cooperation
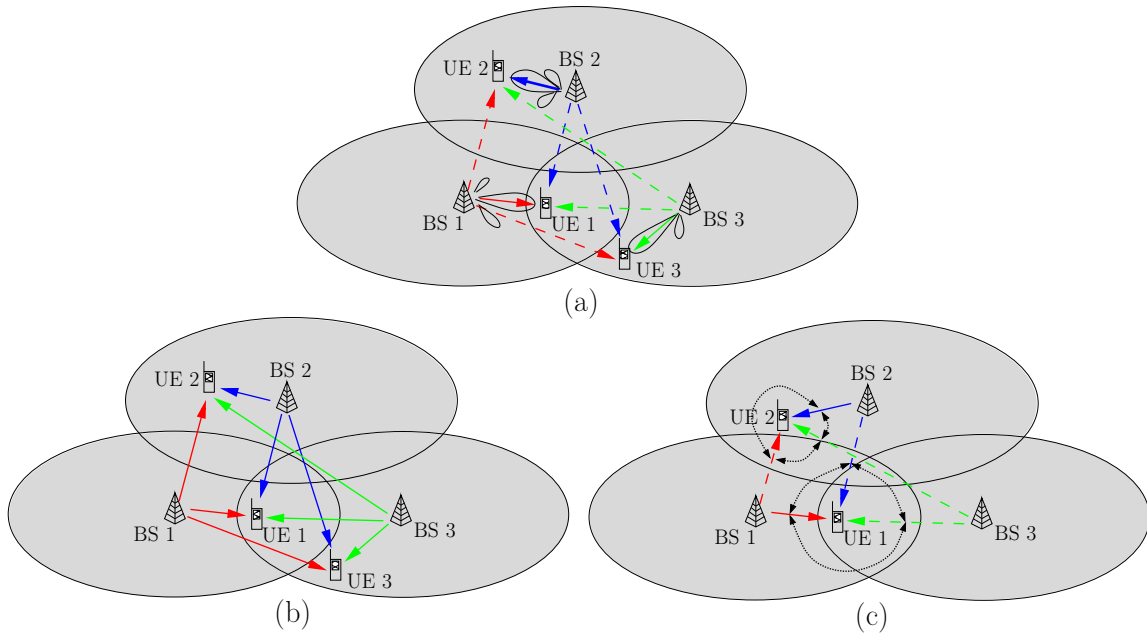
Figure 3.2: Illustration of different DL CoMP schemes: (a) CS/CB, (b) JT, (c) DCS

set can be seen as a virtual broadcast system, where the antennas of the transmitter are located at different places. The transmit signals are usually phase aligned to achieve constructive combining at the receiver side. This may include pre-processing at the transmitter or combing techniques at the receiver based on the CSI. The well-known zero forcing (ZF) algorithm, minimum mean square error (MMSE) algorithm, dirty paper encoding, etc., fall into this category. On the other hand, non-coherent JT does not perform such phase alignment [79]. Only local CSI and data are available at each BS. Open-loop transmission approaches are usually used to enhance the transmit power and to increase the diversity gain. The cyclic delay diversity (CDD) scheme or the space time/frequency coding scheme such as Alamouti encoding may be used [72].

The DCS scheme is shown in Figure 3.2c, where the dotted circles with arrows indicate the transmission links from the serving cell and the potential serving cells in the cooperation set. In DCS UEs are dynamically scheduled by the most suitable TP according to the channel condition in the cooperation set. For instance, the TP which incurs the minimum path loss can be chosen as the serving TP, whereas other TPs in the cooperation set are muted, so that the interference from neighboring cells can be significantly reduced [105].

3.1.2 Challenges in CoMP system

The CoMP technique has been intensively discussed and has shown much gain compared with the traditional non-coordinated system [72, 105]. However, many practical

constraints restrict the benefits that CoMP can provide.

Feedback and backhaul overhead

In order to enable CoMP the CSI needs to be available at the transmitter. In TDD DL systems BSs can obtain DL channel information by exploiting channel reciprocity. However, in FDD systems the DL CSI has to be fed back through uplink (UL) channels to BSs by UEs. Each UE needs to feed back the CSI from all BSs in its cooperation set to its serving BS. Since it's not realistic to transmit perfect CSI back to the BSs, in practice the codebook based feedback scheme is often used [55]. It has been mentioned that the throughput of a CoMP system heavily relies on the quality or accuracy of CSI available at the transmitter [49] and the amount of feedback scales with performance requirement [73]. Therefore, in a CoMP system the feedback overhead grows proportional to the QoS, number of UEs and TPs in the cooperation set, etc. Especially in a large cellular network, to ensure some transmission quality this feedback load is huge unless some smart feedback techniques are employed.

For BS cooperation the CSI fed back from UEs must be exchanged between BSs within the cooperation set. An additional infrastructure is required to connect the BSs, which can be optical fiber, copper or microwave [99], often referred to as **backhaul**. For CS/CB systems only CSI or some control signaling information needs to be exchanged via the backhaul to mitigate the interference. In case of JP it is also necessary to distribute user data throughout the cooperation set. The DCS method may have a trade-off between transmission algorithm complexity, backhaul overhead and system performance [43], whereas JT provides potential benefits such as macro-diversity gains, beamforming gains and interference cancellation at the cost of high-capacity backhaul links with tight synchronization and delay constraints, which implies a high deployment cost [39, 91]. Therefore, all CoMP schemes, particularly JT, come with extra requirement on the backhaul compared to the non-cooperating schemes. Along with the increasing demand in data traffic in the mobile networks the backhaul infrastructure tends to be the system bottleneck [36, 81].

Channel estimation and prediction

The CSI must be available to some extent at the receiver before it is fed back to the transmitter in FDD systems. In CoMP DL systems the channel not only from the anchor BS but also from other BSs causing strong interference or participating in the coordinated transmission, needs to be measured by the terminal. Especially for wideband frequency-selective channels the number of channel components to be estimated is n-fold increased. The reference signals from different BSs for channel estimation may interfere with each

other. Therefore, orthogonal resources must be assigned to these reference signals to avoid collision. This leads to a loss of spectral efficiency since a huge amount of resources is used for transmitting non-data signals [72]. Accurate channel estimation is crucial for CoMP systems. Specifically, joint precoding is highly sensitive to estimation errors in a JP system [80].

Practical system consideration

A prerequisite of CoMP is clustering, i.e., to determine the cooperation set. Generally, large clusters improve the system performance such as overall system throughput, cell-edge user experience, etc. In practice, too large clusters are not allowed due to a huge amount of overhead that needs to be exchanged either through backhaul or between BSs and UEs. Also, it does not make much sense to incorporate the cells that cause weak interference or give a minor contribution in the joint transmission into the cooperation set. The static and dynamic clustering are two schemes often discussed theoretically and practically [26, 61, 96, 97]. Static clustering keeps the clusters fixed over time and is usually designed based on geographical criteria. Dynamic clustering adapts the clusters to time-varying parameters such as user locations, interference conditions, etc. Taking some practical constraints into account, dynamic clustering is more flexible but complicated, and is still an ongoing research topic [80, 90, 92, 113].

Multi-cell coordination also brings out the problem that difficulties with respect to the design of resource optimization algorithms arise, since compared with a non-coordinated system more factors must be considered and optimized by the coordinated system. Therefore, robust and efficient algorithms should be developed for hardware implementation. There are other practical considerations associated with CoMP such as synchronization (time, frequency and phase synchronization), higher data processing requirement on user terminals due to increased data rates, etc. These challenges still need a continuous research.

3.1.3 Coordinated transmission in a CoMP-CB system with limited feedback

As mentioned in Section 3.1.2, coordination between BSs requires the exchange of CSI which is critical in FDD DL systems since users have to feedback CSI to BSs using limited resources [9]. This signaling overhead generated in the UL channel and backhaul must be kept as low as possible. Therefore, full cooperation among multiple cells that requires full CSI at the transmitters is not realistic. An intuitive method is to exchange quantized CSI with a finite number of feedback bits. This brings the problem of an optimal quantization codebook design. On the other hand, since coordinated transmission requires the users to

feedback CSI of both the desired link and interfering links under the constraint of limited feedback overhead, another problem is how to distribute the limited feedback resources to both types of links.

The limited feedback technique has been investigated to some extent for a single-cell broadcast channel or multi-cell systems [29, 65, 73, 130]. Some cooperative beamforming design has also been proposed in the literature. The regularized zero forcing (RZF) beamforming, which is also called MMSE beamforming, was introduced in [95]. In [130] the eigen-beamforming and interference cancellation (IC) beamforming were discussed and the question whether it is better to do IC or simply eigen-beamforming was analytically explored. It was shown that in a multi-cell system with one user in each cell the eigen-beamforming is preferred when the cell-edge SNR is lower than 0 dB and IC should be implemented when the cell-edge SNR is over 10 dB. At medium SNR multiple BSs should jointly determine the transmission strategy depending on user location. In [29] a generalized eigenvector approach was designed to maximize the sum-rate at high SNR for the soft hand-off model [111]. This approach was proved to be always able to benefit an interference nulling (IN) ability from the IC beamforming, at the same time maintaining the desired signal power at a low interference-to-signal ratio (ISR) regime.

Codebook design for quantizing CSI is crucial for the performance of single-cell systems [77]. In [78] the Grassmannian line packing problem was intensively discussed which tries to optimally place several lines passing through the origin in order to maximize the minimum angle separation between any two lines. Since Grassmannian line packing captures the essential problem in quantized beamforming codebook design for Rayleigh fading MIMO channels, [78] proposed the Grassmannian beamforming which takes the advantage of algorithms of the Grassmannian line packing for codebook construction. In [102] the random vector quantization (RVQ) was proposed, where quantized vectors in the codebook are chosen independently from an isotropic distribution on a unit hypersphere. As the number of antennas scales to infinity RVQ was shown to have good asymptotic properties compared with the case of perfect CSI at the transmitter [103]. Therefore, RVQ will be used in this chapter to facilitate the analysis. Alternatively, the codebook can also be constructed by using vector quantization (VQ) techniques [47, 101]. For multi-cell systems the aforementioned schemes can be directly used for quantization of each link separately [112].

Coordinated transmission requires DL CSI from the desired TP and interfering TPs to be available at the BSs for cooperation. In FDD systems users need to feed back CSI using limited resources. For quantization-based feedback, which is an assumption throughout this dissertation, a fixed number of feedback bits can be used for quantizing the CSI of

the desired link and interfering links. Conventional approaches consider average distribution of feedback bits to both links. However, how to adaptively partition the bits is an ongoing research recently and it was shown that sophisticated design of the allocation of feedback bits can increase the system throughput dramatically [29, 73]. In [29] based on the generalized eigenvector beamforming proposed for the soft hand-off model, the rate loss due to quantization using RVQ was derived in a closed form. A feedback allocation strategy was proposed to minimize the upper bound of the rate loss. Simulation results have shown that this bit allocation strategy is effective under the assumption that only a single interferer exists. The feedback bit allocation problem under the multi-cell interfering broadcast channel was discussed in [73], where users incur inter-user interference (IUI) as well as ICI. By implementing a coordinated ZF beamforming scheme a feedback bit allocation method was proposed which minimizes the performance degradation due to quantization. This method shows significant gain compared to the equal allocation of feedback bits to all links. Unlike the aforementioned bit partitioning algorithms, which try to minimize the rate loss due to quantization errors, in the following we propose bit partitioning schemes, attempting to directly maximize the channel capacity of the whole system [133]. Furthermore, cooperative beamforming strategies are developed, which adaptively chooses ZF or eigen-beamforming in order to maximize the sum-rate in different scenarios.

3.2 Cooperative beamforming in a two-cell system with limited feedback

3.2.1 System model

In this section we consider a CoMP-CB system with two cells, each of which has one BS and one user as shown in Figure 3.3. Each BS is equipped with N_t transmit antennas and each user has a single antenna. The cell-edge users suffer from the interference from the neighboring cell which is illustrated as dashed lines in Figure 3.3. The desired links are shown as solid lines. A backhaul channel exists between the two BSs to exchange CSI for cooperative beamforming. The received signal at UE i served by the i-th BS ($i = 1, 2$) is given by:

$$y_i = \sqrt{P_{i,i}}\mathbf{h}_{i,i}\mathbf{w}_i x_i + \sqrt{P_{i,\bar{i}}}\mathbf{h}_{i,\bar{i}}\mathbf{w}_{\bar{i}} x_{\bar{i}} + n_i \tag{3.1}$$

where $i \in \{1, 2\}$ and $\bar{i}$ is the complement element of i in $\{1, 2\}$. $P_{i,j}$ is the average received power at UE i from BS j. We assume a narrow band flat-fading Rayleigh channel and $\mathbf{h}_{i,j} \in \mathbb{C}^{1 \times N_t}$ represents the channel from BS j to UE i, whose elements are independently complex Gaussian distributed with zero mean and unit variance. $\mathbf{w}_i \in \mathbb{C}^{N_t \times 1}$ is the

beamforming vector at BS i which fulfills the normalization condition $||\mathbf{w}_i|| = 1$ and x_i is the transmit signal for UE i with the power constraint $\mathbb{E}\{|x_i|^2\} = 1$. The received signal is disturbed by the additive white Gaussian noise n_i with values distributed according to $\mathcal{CN}(0, N_0)$.
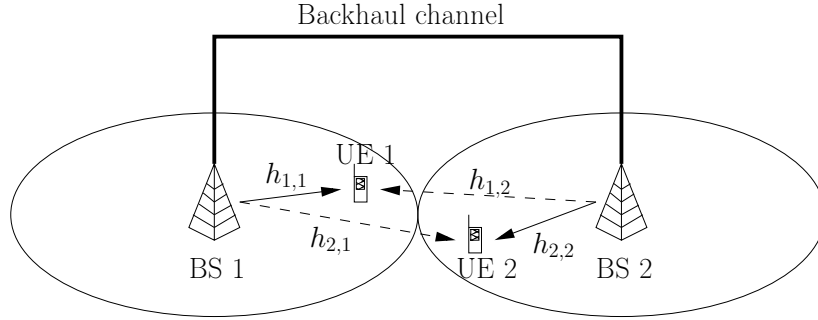
Figure 3.3:　A two-cell MISO system with one user at each cell

Therefore, the received SINR at UE i is calculated as:

$$\text{SINR}_i = \frac{P_{i,i}|\mathbf{h}_{i,i}\mathbf{w}_i|^2}{N_0 + P_{i,\bar{i}}|\mathbf{h}_{i,\bar{i}}\mathbf{w}_{\bar{i}}|^2}. \tag{3.2}$$

Consequently, the average normalized achievable rate of UE i is obtained by:

$$R_i = \mathbb{E}\{\log_2(1 + \text{SINR}_i)\}, \tag{3.3}$$

which is the expectation with respect to the random channel. The objective of our design is to maximize the sum-rate of the system

$$R = \sum_{i=1}^{2} R_i. \tag{3.4}$$

Transmit Beamforming Strategies

The sum-rate (3.4) greatly depends on the design of the beamforming vector $\mathbf{w}_i$. In this dissertation we consider two typical beamforming strategies.

- **ZF beamforming**: ZF beamforming nulls out the interference caused to the users in other cells. In the meanwhile, it tries to maximize the desired signal power. A BS with N_t transmit antennas can perfectly cancel the interference to $N_\text{t} - 1$ users with single receive antennas in other cells. Taking BS 1 in Figure 3.3 as an example, the beamforming vector $\mathbf{w}_1$ needs to fulfill the orthogonality condition: $\mathbf{h}_{2,1}\mathbf{w}_1 = 0$, so that no interference from BS 1 to UE 2 appears. We assume that $\mathbf{h} = \mathbf{h}_{2,1}$ is the

interference channel from BS 1 to other users. Under the condition that perfect CSI is available at the BS $\mathbf{w}_1$ can be chosen in the direction of the projection of $\mathbf{h}_{1,1}$ on the null space of $\mathbf{h}$ [66], i.e., $\mathbf{w}_1$ is given as the normalized version of $(\mathbf{I}_{N_t} - \mathbf{P})\mathbf{h}_{1,1}^{\mathrm{H}}$

$$\mathbf{w}_1 = \frac{(\mathbf{I}_{N_t} - \mathbf{P})\mathbf{h}_{1,1}^{\mathrm{H}}}{||(\mathbf{I}_{N_t} - \mathbf{P})\mathbf{h}_{1,1}^{\mathrm{H}}||}, \tag{3.5}$$

where $\mathbf{P} = \mathbf{h}^{\mathrm{H}}(\mathbf{h}\mathbf{h}^{\mathrm{H}})^{-1}\mathbf{h}$ and $\mathbf{I}_{N_t}$ is the identity matrix. When a BS creates interference to more than one users in other cells, $\mathbf{h}$ is selected as the concatenation of all the interfering channels, which is a matrix. ZF beamforming is often used when the system is interference limited, where interference dominates the system performance [130].

- **Eigen-beamforming or maximum ratio transmission (MRT)**: Without considering the interference to other users the beamforming vector is designed according to the direction of the desired channel to maximize the received power of the desired signal [115]. When perfect CSI is present at BS i, the beamforming vector of BS i is given by

$$\mathbf{w}_i = \mathbf{h}_{i,i}^{\mathrm{H}}/||\mathbf{h}_{i,i}^{\mathrm{H}}||. \tag{3.6}$$

The eigen-beamforming maximizes the received SNR and hence is suitable in the noise-limited systems.

Limited Feedback Channel

In this dissertation it is assumed that each user obtains perfect channel knowledge by channel estimation and sends back CSI using a finite rate feedback channel with no delay and zero error. The full CSI can be splitted into channel direction information (CDI) and channel quality information (CQI) [125]. CQI, which is the channel gain $||\mathbf{h}_{i,j}||$, does not affect the beamforming design in (3.5) and (3.6). For more sophisticated beamforming design CQI can be easily quantized by scalar quantization scheme. In our work only CDI, i.e., $\tilde{\mathbf{h}}_{i,j} = \mathbf{h}_{i,j}/||\mathbf{h}_{i,j}||$, is necessary for the design of beamforming vectors. ZF beamforming needs both CDI of the desired channel and the interfering channels while the eigen-beamforming only requires the CDI of the desired link. Here RVQ is adopted for analytical reasons and all the channels $\mathbf{h}_{i,j}$ use separate codebooks $\mathcal{C}_{i,j} = \{\mathbf{c}_1, \mathbf{c}_2, \cdots, \mathbf{c}_{2^{B_{i,j}}}\}$ which are known at both the transmitter and receiver. $B_{i,j}$ is the number of bits used for quantizing $\mathbf{h}_{i,j}$ The users search for the codeword which has the smallest angular separation from the actual CDI

$$n_{i,j} = \arg\max_{1 \le n \le 2^{B_{i,j}}} |\mathbf{c}_n^{\mathrm{H}}\tilde{\mathbf{h}}_{i,j}^{\mathrm{T}}|^2, \tag{3.7}$$

and send the index $n_{i,j}$ to the serving BS. The BS uses the corresponding codeword as the estimated CDI: $\hat{\mathbf{h}}_{i,j} = \mathbf{c}_{n_{i,j}}$. The usage of the estimated CDI leads to a performance degradation in the sum-rate due to quantization errors. In the following the effect of this error will be discussed analytically and a bit partitioning scheme for ZF beamforming is proposed, which adaptively allocates the feedback bits for quantizing the desired link and interfering link.

3.2.2   Adaptive feedback bit partitioning scheme

The ZF beamforming nulls out the interference to the undesired users if the BS holds full channel knowledge. In case of a limited feedback channel, the interference term in the denominator of (3.2) cannot be eliminated, i.e., limited feedback causes residual interference. Additionally, the desired power degrades due to the quantization error. We assume uncorrelated Rayleigh channels and hence each component of $\mathbf{h}_{i,j}$ is independent and identically distributed (i.i.d.) according to $\mathcal{CN}(0,1)$. Since eigen-beamforming is not a cooperative beamforming, no bit partitioning problem exists. Therefore, in this subsection we consider that the two BSs always perform ZF beamforming assuming that both users are experiencing non-negligible interference.

Under the assumption of perfect channel information at the BS and the beamforming vector $\mathbf{w}_{i,\text{perf}}$ is created by (3.5), the desired power term in (3.2) has been proved to be distributed as $|\mathbf{h}_{i,i}\mathbf{w}_{i,\text{perf}}|^2 \sim \chi^2_{2(N_t-1)}$[1] [66], where $\chi^2_{2(N_t-1)}$ is the chi-squared distribution with $2(N_t-1)$ degrees of freedom[2]. The reason is that $\mathbf{w}_{i,\text{perf}}$ is designed to be normalized projection of $\mathbf{h}_{i,i}$ on the null space of $\mathbf{h}_{\bar{i},i}$. This null space is N_t-1 dimensional due to the property of i.i.d. Gaussian vectors. The distribution of the desired power term can be obtained by simply applying Lemma 1 in [66]. In case of quantized channel information at the BSs, the beamforming vector $\mathbf{w}_i$ is designed according to (3.5) based on the quantized CDI $\hat{\mathbf{h}}_{i,j}$. Here the random vector quantization (RVQ) is used, where the codebook is constructed by the complex standard Gaussian random vectors. Using RVQ, the desired signal term in (3.2) is shown in [130] to be $|\mathbf{h}_{i,i}\mathbf{w}_i|^2 = \xi_{i,i}\mathbf{Z}$, where $\mathbf{Z} \sim \chi^2_{2(N_t-1)}$ and $\xi_{i,i}$ is the degradation factor of the desired signal power due to quantization. If $B_{i,i}$ bits are used for quantizing $\mathbf{h}_{i,i}$, $\xi_{i,i}$ can be calculated as [23]

$$\xi_{i,i} = 1 - 2^{B_{i,i}} \cdot \beta\left(2^{B_{i,i}}, \frac{N_t}{N_t - 1}\right), \tag{3.8}$$

where $\beta(\cdot)$ denotes the Beta function. Implementing theorem 3 in [130] for a two-cell

---

[1] "$\sim$" denotes the distribution of a random variable

[2] if $\mathbf{Z_1}$, $\mathbf{Z_2}, \ldots, \mathbf{Z_k}$ are independent standard normal random variables, the sum of their squares $\mathbf{X} = \sum_{i=1}^{k} \mathbf{Z_i^2}$ is distributed according to the chi-square distribution with k degrees of freedom.

scenario, the average rate of UE i (3.3) can be written as

$$R_i(P_{i,i}, P_{i,\bar{i}}, B_{i,i}, B_{i,\bar{i}}) = \mathbb{E}\left\{\log_2\left(1 + \frac{\xi_{i,i}P_{i,i}\boldsymbol{Z}}{N_0 + \kappa_{i,\bar{i}}P_{i,\bar{i}}\boldsymbol{Y}}\right)\right\}, \tag{3.9}$$

where $|\mathbf{h}_{i,\bar{i}}\mathbf{w}_{\bar{i}}|^2 = \kappa_{i,\bar{i}}\boldsymbol{Y}$ and $\boldsymbol{Y} \sim \chi_2^2$. $\kappa_{i,\bar{i}} = 2^{-\frac{B_{i,\bar{i}}}{N_t-1}}$ is the residual interference factor caused by quantization [130] and the residual interference term $\kappa_{i,\bar{i}}P_{i,\bar{i}}\boldsymbol{Y}$ is zero when ZF beamforming is implemented and full CDI is available at BS $\bar{i}$.

In this chapter we assume that each user has a fixed number of feedback bits B available, which can be used for quantizing the desired and interfering channels. Instead of maximizing the sum-rate in (3.4), we attempt to maximize the rate of each user (3.9) separately. This leads to the optimization problem (for UE i):

$$\begin{aligned}
\max \quad & R_i(P_{i,i}, P_{i,\bar{i}}, B_{i,i}, B_{i,\bar{i}}) \\
\text{subject to} \quad & B_{i,i} + B_{i,\bar{i}} = B \\
& B_{i,i}, \ B_{i,\bar{i}} \text{ are non-negative integers.}
\end{aligned} \tag{3.10}$$

In the high SINR regime by using the property $\log_2(1 + \text{SINR}) \approx \log_2(\text{SINR})$, the rate of UE i can be approximated as

$$\begin{aligned}
R_i(P_{i,i}, P_{i,\bar{i}}, B_{i,i}, B_{i,\bar{i}}) &\approx \mathbb{E}\left\{\log_2\left(\frac{\xi_{i,i}P_{i,i}\boldsymbol{Z}}{N_0 + \kappa_{i,\bar{i}}P_{i,\bar{i}}\boldsymbol{Y}}\right)\right\} \\
&= \log_2(\xi_{i,i}) + \log_2(P_{i,i}) + \mathbb{E}\{\log_2(\boldsymbol{Z})\} - \mathbb{E}\{\log_2(N_0 + \kappa_{i,\bar{i}}P_{i,\bar{i}}\boldsymbol{Y})\}.
\end{aligned} \tag{3.11}$$

Using the concave property of the logarithmic function and Jensen's inequality, (3.11) can be further written as

$$\begin{aligned}
& R_i(P_{i,i}, P_{i,\bar{i}}, B_{i,i}, B_{i,\bar{i}}) \\
&\geq \log_2(\xi_{i,i}) + \log_2(P_{i,i}) + \mathbb{E}\{\log_2(\boldsymbol{Z})\} - \log_2(N_0 + \kappa_{i,\bar{i}}P_{i,\bar{i}}\mathbb{E}\{\boldsymbol{Y}\}) \\
&= \log_2(\xi_{i,i}) + \log_2(P_{i,i}) + \frac{1}{\ln 2}\psi(N_t - 1) - \log_2(N_0 + \kappa_{i,\bar{i}}P_{i,\bar{i}}),
\end{aligned} \tag{3.12}$$

where $\psi(\cdot)$ is Euler's psi function [86].

At low SINR since $\ln(1 + \text{SINR}) \approx \text{SINR}$ for $\text{SINR} \approx 0$, (3.9) can be approximated as

$$\begin{aligned}
R_i(P_{i,i}, P_{i,\bar{i}}, B_{i,i}, B_{i,\bar{i}}) &\approx \mathbb{E}\left\{\frac{1}{\ln 2} \cdot \frac{\xi_{i,i}P_{i,i}\boldsymbol{Z}}{N_0 + \kappa_{i,\bar{i}}P_{i,\bar{i}}\boldsymbol{Y}}\right\} \\
&\geq \frac{1}{\ln 2} \cdot \mathbb{E}\left\{\xi_{i,i}P_{i,i}\boldsymbol{Z}\right\} \cdot \frac{1}{N_0 + \kappa_{i,\bar{i}}P_{i,\bar{i}}\mathbb{E}\{\boldsymbol{Y}\}} = \frac{1}{\ln 2} \cdot \frac{\xi_{i,i}P_{i,i}(N_t - 1)}{N_0 + \kappa_{i,\bar{i}}P_{i,\bar{i}}}.
\end{aligned} \tag{3.13}$$

Because the logarithmic function is a strictly monotonic increasing function, maximizing (3.13) is equivalent to maximizing (3.12). Therefore, in the following (3.12) will be considered without loss of generality. Simulation results will show that the algorithms based on the approximation in (3.11) guarantee performance gain at different SINR regions.

Since the derivative of the Beta function in (3.8) is very complicated, for later calculations we use a lower bound of the degradation factor [65]

$$\xi_{i,i} \geq 1 - 2^{-\frac{B_{i,i}}{N_\mathrm{t}-1}}. \tag{3.14}$$

Hence the rate of UE i in (3.12) is lower bounded by

$$R_i(P_{i,i}, P_{i,\bar{i}}, B_{i,i}, B_{i,\bar{i}})$$

$$\geq \log_2(1 - 2^{-\frac{B_{i,i}}{N_\mathrm{t}-1}}) + \log_2(P_{i,i}) + \frac{1}{\ln 2}\psi(N_\mathrm{t}-1) - \log_2(N_0 + \kappa_{i,\bar{i}}P_{i,\bar{i}}) \triangleq R_i^{\mathrm{LB2}}. \tag{3.15}$$

As a result the optimization problem (3.10) can be converted to

$$\begin{aligned} \max \quad & R_i^{\mathrm{LB2}} \\ \text{subject to} \quad & B_{i,i} + B_{i,\bar{i}} = B \\ & B_{i,i},\ B_{i,\bar{i}} \text{ are non-negative integers.} \end{aligned} \tag{3.16}$$

To find the solution of (3.16) we construct the Lagrange function with the help of the Lagrange multiplier λ

$$L(B_{i,i}, B_{i,\bar{i}}, \lambda) = R_i^{\mathrm{LB2}} + \lambda(B_{i,i} + B_{i,\bar{i}} - B). \tag{3.17}$$

We set all partial derivatives of (3.17) to zero with respect to $B_{i,i}$, $B_{i,\bar{i}}$ and λ

$$\frac{\partial L}{\partial B_{i,i}} = \frac{\partial L}{\partial B_{i,\bar{i}}} = \frac{\partial L}{\partial \lambda} = 0. \tag{3.18}$$

By solving the set of 3 equations, we obtain the intermediate solution of (3.16)

$$\begin{aligned} B_{i,i}^{\mathrm{temp}} &= (N_\mathrm{t}-1)\log_2\left(\frac{\sqrt{\rho_{i,\bar{i}}C} + \sqrt{\rho_{i,\bar{i}}C+1}}{\sqrt{\rho_{i,\bar{i}}C}}\right), \\ B_{i,\bar{i}}^{\mathrm{temp}} &= (N_\mathrm{t}-1)\log_2\left(\frac{\rho_{i,\bar{i}}\left(\sqrt{\rho_{i,\bar{i}}C+1} - \sqrt{\rho_{i,\bar{i}}C}\right)}{\sqrt{\rho_{i,\bar{i}}C}}\right), \end{aligned} \tag{3.19}$$

where $\rho_{i,\bar{i}} = \frac{P_{i,\bar{i}}}{N_0}$ is the received interference-to-noise ratio (INR) at UE i and $C = 2^{-\frac{B}{N_\mathrm{t}-1}}$. Taking the integer constraint in (3.16) into account, $B_{i,i}$ and $B_{i,\bar{i}}$ must be determined by B and rounded versions of (3.19). In case that the calculated $B_{i,i}^{\mathrm{temp}}$ is not an integer, we need to consider $\lceil B_{i,i}^{\mathrm{temp}} \rceil$ and $\lfloor B_{i,i}^{\mathrm{temp}} \rfloor$ and choose the one which maximizes (3.12) as the final solution $B_{i,i}$. The number of feedback bits for interfering channel $B_{i,\bar{i}}$ can be easily calculated by $B_{i,\bar{i}} = B - B_{i,i}$.

It can be observed that the results in (3.19) depend on the number of transmit antennas N_t, the total number of available feedback bits B and the received INR $\rho_{i,\bar{i}}$. As $\rho_{i,\bar{i}}$ decreases, $B_{i,i}$ increases up to B and $B_{i,\bar{i}}$ is decreased down to 0, meaning that when the interference becomes weaker, the number of bits spent on quantizing the interfering channel decreases. Furthermore, $B_{i,i}$ and $B_{i,\bar{i}}$ increase monotonically with B.

3.2.3 Cooperative beamforming strategies

Approach 1: cooperative approach considering limited feedback

In Section 3.2.2 it is assumed that in the two-cell scenario both BSs always adopt ZF beamforming. In fact ZF beamforming may not be the optimal choice when the users incur weak other-cell interference (OCI). In this case noise power dominates and a more proper transmission strategy is eigen-beamforming to increase the received signal power for the desired user regardless of interference to other users. In this subsection we consider that each BS can use either ZF beamforming or eigen-beamforming. Hence, in this two-cell system there are four possible beamforming strategies for the two BSs, namely, $\mathbf{BF}(BS_1, BS_2) \in \{(Z,Z), (E,E), (Z,E), (E,Z)\}$, where Z and E stand for ZF beamforming and eigen-beamforming, respectively. The problem is which strategy should be chosen for different interference scenarios to maximize the sum-rate of the system.

Similar to (3.11) we first give the rate of UE i if different strategies are used:

$$R_i(P_{i,i}, P_{i,\bar{i}}, B_{i,i}, B_{i,\bar{i}}) \approx$$
$$\begin{cases} \mathbb{E}\left\{\log_2\left(\frac{\xi_{i,i}P_{i,i}\boldsymbol{Z}}{N_0 + \kappa_{i,\bar{i}}P_{i,\bar{i}}\boldsymbol{Y}}\right)\right\}, \ \boldsymbol{Z} \sim \chi^2_{2(N_{\mathrm{t}}-1)}, \boldsymbol{Y} \sim \chi^2_2, \text{ if } \mathbf{BF}(BS_i, BS_{\bar{i}}) = (Z,Z); \\ \mathbb{E}\left\{\log_2\left(\frac{\xi_{i,i}P_{i,i}\boldsymbol{Z}}{N_0 + P_{i,\bar{i}}\boldsymbol{Y}}\right)\right\}, \ \boldsymbol{Z} \sim \chi^2_{2N_{\mathrm{t}}}, \boldsymbol{Y} \sim \chi^2_2, \text{ if } \mathbf{BF}(BS_i, BS_{\bar{i}}) = (E,E); \\ \mathbb{E}\left\{\log_2\left(\frac{\xi_{i,i}P_{i,i}\boldsymbol{Z}}{N_0 + P_{i,\bar{i}}\boldsymbol{Y}}\right)\right\}, \ \boldsymbol{Z} \sim \chi^2_{2(N_{\mathrm{t}}-1)}, \boldsymbol{Y} \sim \chi^2_2, \text{ if } \mathbf{BF}(BS_i, BS_{\bar{i}}) = (Z,E); \\ \mathbb{E}\left\{\log_2\left(\frac{\xi_{i,i}P_{i,i}\boldsymbol{Z}}{N_0 + \kappa_{i,\bar{i}}P_{i,\bar{i}}\boldsymbol{Y}}\right)\right\}, \ \boldsymbol{Z} \sim \chi^2_{2N_{\mathrm{t}}}, \boldsymbol{Y} \sim \chi^2_2, \text{ if } \mathbf{BF}(BS_i, BS_{\bar{i}}) = (E,Z). \end{cases}$$
$$(3.20)$$

$\boldsymbol{Y} \sim \chi^2_2$ is because in (3.2) the design of the eigen-beamforming vector $\mathbf{w}_{\bar{i}}$ at BS $\bar{i}$ is independent of $\mathbf{h}_{i,\bar{i}}$. $\boldsymbol{Z} \sim \chi^2_{2N_{\mathrm{t}}}$ for $\mathbf{BF}(BS_i) = (E)$ is simply due to the property of the eigen-beamforming vector in (3.6), resulting in $|\mathbf{h}_{i,i}\mathbf{w}_i|^2 = ||\mathbf{h}_{i,i}||^2$. The corresponding lower bound of each term in (3.20) that can be derived similar to (3.11) and (3.12) is

$$\begin{cases} \log_2\left(\frac{\xi_{i,i}}{1 + \kappa_{i,\bar{i}}\rho_{i,\bar{i}}}\right) + \frac{1}{\ln 2}\psi(N_{\mathrm{t}} - 1) + \log_2(\rho_{i,i}), \text{ if } \mathbf{BF}(BS_i, BS_{\bar{i}}) = (Z,Z); \\ \log_2\left(\frac{\xi_{i,i}}{1 + \rho_{i,\bar{i}}}\right) + \frac{1}{\ln 2}\psi(N_{\mathrm{t}}) + \log_2(\rho_{i,i}), \text{ if } \mathbf{BF}(BS_i, BS_{\bar{i}}) = (E,E); \\ \log_2\left(\frac{\xi_{i,i}}{1 + \rho_{i,\bar{i}}}\right) + \frac{1}{\ln 2}\psi(N_{\mathrm{t}} - 1) + \log_2(\rho_{i,i}), \text{ if } \mathbf{BF}(BS_i, BS_{\bar{i}}) = (Z,E); \\ \log_2\left(\frac{\xi_{i,i}}{1 + \kappa_{i,\bar{i}}\rho_{i,\bar{i}}}\right) + \frac{1}{\ln 2}\psi(N_{\mathrm{t}}) + \log_2(\rho_{i,i}), \text{ if } \mathbf{BF}(BS_i, BS_{\bar{i}}) = (E,Z), \end{cases}$$
$$(3.21)$$

where $\rho_{i,\bar{i}} = \frac{P_{i,\bar{i}}}{N_0}$ and $\rho_{i,i} = \frac{P_{i,i}}{N_0}$ is the received INR and SNR at UE i, respectively. Consequently, the sum-rate of the system $R_1 + R_2$ is lower bounded by the summation of

two formulas in (3.21) depending on the strategy used by the two BSs. As the number of search candidates is small, here the idea is to use the exhaustive search to find the strategy which maximizes the lower bound of the sum-rate in (3.21). It can be observed that each formula in (3.21) contains a common term related with the received SNR $\rho_{i,i}$. This means the lower bound of the sum-rate of the two-cell system must contain $\log_2(\rho_{i,i}) + \log_2(\rho_{\bar{i},\bar{i}})$, no matter which beamforming strategies the two BSs apply. As a result, $\rho_{i,i}$ does not affect the comparison result of different strategy combinations. Therefore, we only consider the first two terms in each formula in (3.21), which further depend on $B_{i,i}$, $B_{i,\bar{i}}$, N_{t} and $\rho_{i,\bar{i}}$. In addition, we recall that each user has B bits available for sending back CSI. So we have the *feedback rule*

$$
\begin{aligned}
B_{i,i} + B_{i,\bar{i}} = B, &\quad \text{if } BS_{\bar{i}} = Z \\
B_{i,i} = B, &\quad \text{if } BS_{\bar{i}} = E.
\end{aligned}
\tag{3.22}
$$

All of the above motivates the cooperative beamforming strategy design (*approach 1*):

- Both users measure the received INR and transmit this information to their serving BS;

- The two BSs calculate the number of bits for quantizing the serving channel and interfering channel for both users according to (3.19), assuming that both BSs implement ZF beamforming;

- The two BSs communicate via the backhaul channel and determine **jointly** the beamforming scheme which shows the maximal sum-rate lower bound according to (3.21);

- The users are informed by their serving BS which scheme has been selected and feed back CSI of serving channel or interfering channel based on the strategy and the *feedback rule* (3.22);

- The BSs carry out the corresponding beamforming strategy for this two-cell system.

In this cooperative beamforming strategy the users leave the work of choosing the most suitable beamforming scheme to the BSs, since the latter is more powerful and has a stable high-speed backhaul connection, and hence is more suitable for taking this decision. The users only need to send back the received INR, which is a scalar and can be quantized easily (scalar quantization). However, the cooperative strategy suffers from extra delay caused by the feedback of INR. One way to compensate this delay is to use some prediction schemes based on the transmit power of the BSs, the user location or additive noise level. Since this INR is an averaged quantity, in case that the users do not move at high speed,

the INR does not need to be fed back very often. In the following simulations this delay is neglected.

Approach 2: separating approach considering full CSI

Previous cooperative beamforming strategy directly takes the quantization of CSI into consideration and thus provides more accurate results when limited feedback is used. The strategy implements exhaustive search and jointly determines the beamforming schemes at each BS. When the number of BSs to be coordinated is large, approach 1 seems to be costly. Therefore, here a separating approach is proposed where each BS determines its own transmission scheme independently. This approach reduces the amount of information exchanged via the backhaul for calculating the lower bound in (3.21). In this separating approach it is assumed that full CSI is available at the BSs.

Similar to (3.11) under the assumption of high SINR the sum-rate of the two-cell system in Figure 3.3 can be approximated as

$$
\begin{aligned}
R &= \mathbb{E}\left\{\sum_{i=1}^{2}\log_2(1+\text{SINR}_i)\right\} \approx \mathbb{E}\left\{\sum_{i=1}^{2}\log_2(\text{SINR}_i)\right\} \\
&= \mathbb{E}\left\{\log_2\left(\frac{P_{1,1}|\mathbf{h}_{1,1}\mathbf{w}_1|^2}{N_0+P_{1,2}|\mathbf{h}_{1,2}\mathbf{w}_2|^2} \cdot \frac{P_{2,2}|\mathbf{h}_{2,2}\mathbf{w}_2|^2}{N_0+P_{2,1}|\mathbf{h}_{2,1}\mathbf{w}_1|^2}\right)\right\} \\
&= \mathbb{E}\left\{\log_2\left(\underbrace{\frac{P_{1,1}|\mathbf{h}_{1,1}\mathbf{w}_1|^2}{N_0+P_{2,1}|\mathbf{h}_{2,1}\mathbf{w}_1|^2}}_{\text{SLNR at UE 1}}\right)\right\} + \mathbb{E}\left\{\log_2\left(\underbrace{\frac{P_{2,2}|\mathbf{h}_{2,2}\mathbf{w}_2|^2}{N_0+P_{1,2}|\mathbf{h}_{1,2}\mathbf{w}_2|^2}}_{\text{SLNR at UE 2}}\right)\right\}, \quad (3.23)
\end{aligned}
$$

where the signal-to-leakage-plus-noise ratio (SLNR) at UE i is the ratio of received signal power at UE i to the received power of the signal intended for UE i at other UEs plus noise power. (3.23) approximates the sum-rate of the system by the summation of two terms, each of which only depends on the beamforming scheme of one BS. Therefore, the beamforming scheme of each BS can be determined separately.

Without loss of generality we take the first term in (3.23) as an example. Under the assumption of full CSI at each BS and an uncorrelated Rayleigh channel, $|\mathbf{h}_{1,1}\mathbf{w}_1|^2$ is a chi-squared distributed random variable $\boldsymbol{Z}$ [130], where

$$
\boldsymbol{Z} \sim \begin{cases} \chi^2_{2N_t} & \text{if } BS_1 = E \\ \chi^2_{2(N_t-1)} & \text{if } BS_1 = Z \end{cases}. \quad (3.24)
$$

The leakage $|\mathbf{h}_{2,1}\mathbf{w}_1|^2 = \boldsymbol{Y}$ is chi-squared distributed with 2 degrees of freedom when $BS_1 = E$ and is 0 when $BS_1 = Z$. Using Jensen's inequality the lower bound of the first

term in (3.23) is calculated as

$$\mathbb{E}\left\{\log_2\left(\frac{P_{1,1}\boldsymbol{Z}}{N_0 + P_{2,1}\boldsymbol{Y}}\right)\right\} = \mathbb{E}\{\log_2(P_{1,1}\boldsymbol{Z})\} - \mathbb{E}\{\log_2(N_0 + P_{2,1}\boldsymbol{Y})\}$$

$$\geq \log_2(P_{1,1}) + \mathbb{E}\{\log_2(\boldsymbol{Z})\} - \log_2(N_0 + P_{2,1}\mathbb{E}\{\boldsymbol{Y}\}) \triangleq T_1^{\text{LB2}}. \tag{3.25}$$

T_1^{LB2} can be further calculated when different transmission schemes are implemented at BS 1

$$T_1^{\text{LB2}} = \begin{cases} \log_2(P_{1,1}) + \dfrac{1}{\ln 2}\psi(N_t) - \log_2(N_0 + P_{2,1} \cdot 1) & \text{if } BS_1 = E \\ \log_2(P_{1,1}) + \dfrac{1}{\ln 2}\psi(N_t - 1) - \log_2 N_0 & \text{if } BS_1 = Z \end{cases}. \tag{3.26}$$

The purpose is to choose the beamforming strategy, which gives the larger lower bound in (3.25). Therefore, by comparing the two terms in T_1^{LB2} in (3.26) we can obtain the *transmission scheme determination rule* for this two-cell system:

$$\begin{aligned} \text{if} \quad & \frac{P_{2,1}}{N_0} < 2^{\frac{\psi(N_t)-\psi(N_t-1)}{\ln 2}} - 1 = e^{\frac{1}{N_t-1}} - 1, \quad \text{BS 1 uses eigen-beamforming} \\ & \qquad\qquad \text{else,} \qquad\qquad\qquad\qquad \text{BS 1 uses zero-forcing beamforming.} \end{aligned} \tag{3.27}$$

Therefore, only when the caused interference at UE 2 by BS 1 exceeds a certain threshold, BS 1 tries to cancel this interference by sacrificing the SNR of its serving user. Otherwise, BS 1 focuses all the transmit power on serving UE 1.

The cooperative beamforming strategy (*approach 2*) based on the separated transmission scheme determination is described as following:

- Both users measure the received INR and transmit this information to their serving BS;

- The two BSs exchange the received INR via the backhaul channel, **separately** determine the beamforming scheme according to the *transmission scheme determination rule* (3.27) and exchange the decision;

- The users are informed by their serving BS which scheme has been selected and feed back CSI of serving channel or interfering channel based on the scheme and the *feedback rule* (3.22) (calculation of number of bits for quantizing the serving and interfering channels according to (3.19) is necessary at UEs, if BS in the other cell employ zero-forcing beamforming);

- The BSs carry out the corresponding beamforming strategy for this two-cell system.

Although *approach 2* does not take the limited feedback into account when the BSs determine the beamforming scheme, simulation results will show that there is minor difference between *approach 2* and *approach 1*. Furthermore, when the number of coordinated cells is large, *approach 2* can be extended in the following sections so that each BS determines whether it should perform interference cancellation for a certain UE only depending on the interference and noise power level experienced by this UE.

3.2.4 Simulation results and analysis

In this subsection we consider the two-cell system shown in Figure 3.3. We set the number of transmit antennas of the BSs $N_t = 2$ since there is at most one interference that needs to be canceled. We assume that each user has some fixed received SNR values and incurs different interference-to-signal ratio (ISR) levels depending on the user channels. The channel is a narrow band flat-fading Rayleigh channel.

Performance with adaptive feedback bit partition scheme

First, we assume that both BSs use ZF beamforming and we compare the number of bits spent on the quantization of the serving channel and interfering channel. The user is assumed to be at a moderate SNR level, 10 dB. The ISR varies in the range of (-40 dB, 0 dB), which corresponds to the range of (-30 dB, 10 dB) for the INR. The total number of feedback bits available at each user is $B = 8$. In Figure 3.4, B_s shows the number of feedback bits for the serving channel and B_i for the interfering channel. The variation of the feedback bits with respect to the received INR using the algorithm in (3.19) is shown. As we can observe, B_i increases when the INR becomes larger, meaning that when OCI gets severe, more bits should be spent on the interference. When INR is lower than -21 dB, noise totally dominates and all of the feedback bits should be used for the serving channel to maximize the desired power. However, Figure 3.4 shows the results assuming that both BSs employ ZF beamforming. This does not mean that when INR is larger than -21 dB, performing ZF beamforming is always better than eigen-beamforming. The beamforming strategy should be determined cooperatively as described in *approach 1* and *approach 2*.

Figure 3.5 shows the sum-rate of the system at different average received SNRs per channel link with the ISR uniformly distributed within $(0, 1)$ using ZF beamforming, where ISR $= 0$ indicates no interference and ISR $= 1$ means that the interference can be at most the same as the desired signal power. The bit partitioning algorithm in (3.19) is denoted as *proposed* and *equal* is for equal allocation of the feedback bits. Obviously the performance when the BSs have full channel knowledge *perfect*, outperforms both algorithms. In case that we have the same number of bits $B = 8$ or $B = 4$, the pro-
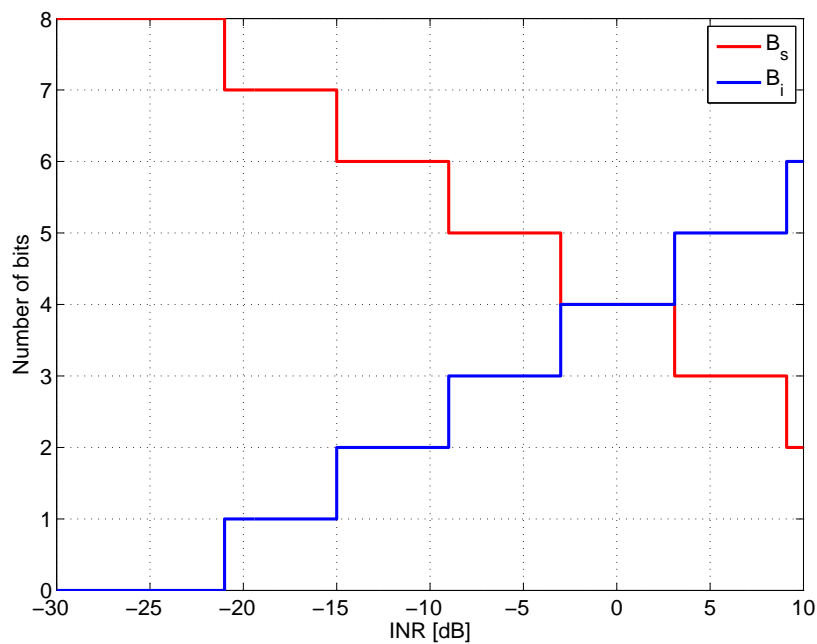
Figure 3.4:   Bit partitioning for SNR=10 dB and B=8
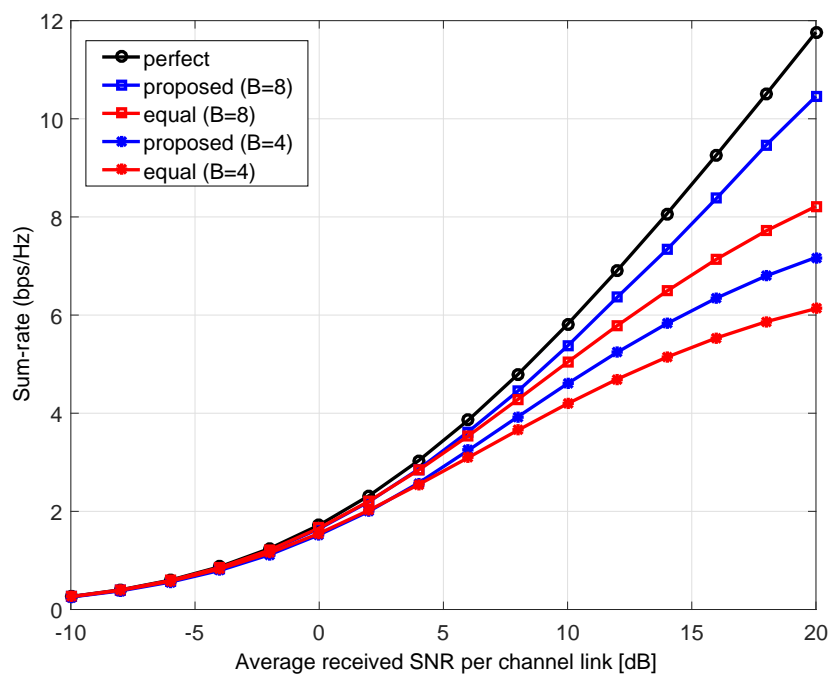
Figure 3.5: Sum-rate using ZF beamforming with different bit partitioning algorithms and different numbers of available feedback bits in a two-cell system

posed algorithm always outperforms equal bit distribution especially when the SNR is large. This is because in our simulation INR is large in the high SNR regime where the interference dominates the noise. In this case the ZF beamforming plays an important role and sophisticated design of the allocation of feedback bits gains much. Moreover, when there are more feedback bits available, with the proposed algorithm the potential of exploiting the adaptivity of feedback bit allocation is higher so that more sum-rate gain can be achieved.

Performance with cooperative beamforming strategy

Next, we implement the proposed cooperative beamforming strategy. We assume that each user has the fixed received SNR per channel link of 10 dB and experiences different ISR depending on the location of the user. Figure 3.6 and Figure 3.7 show the selection of beamforming schemes by the two BSs according to *approach 1* and *approach 2*, respectively. It can be seen that both approaches show the same results. This indicates that *approach 2* without considering the limited feedback can also determine the best transmission strategy when limited feedback is employed in the system. From (3.27) we can get that if one user has an INR higher than 2.35 dB (correspondingly ISR = −7.65 dB), the interfering BS (BS in the other cell) should perform ZF beamforming to cancel the strong interference to this user. Otherwise eigen-beamforming is used. This result coincides with the heuristic discussion in [130].
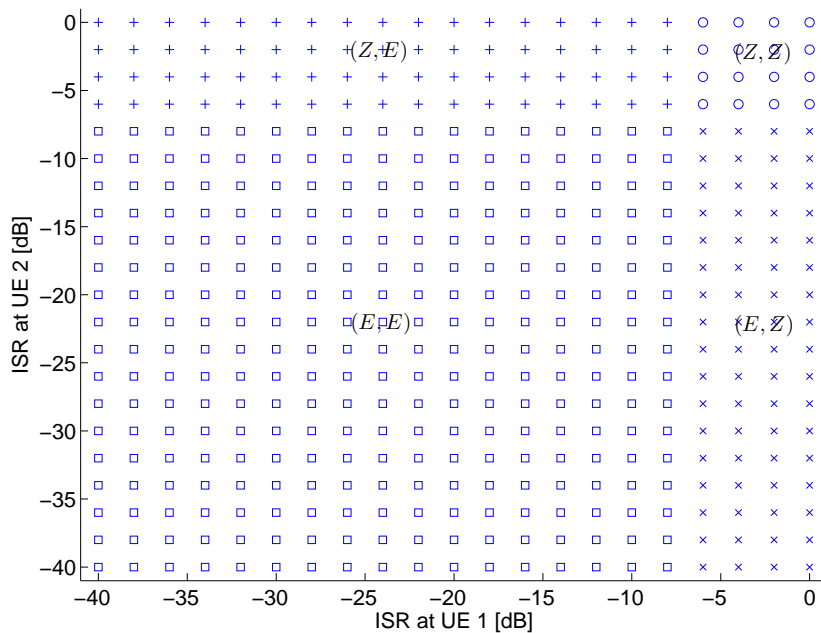
Figure 3.6: Cooperative beamforming strategy for SNR=10 dB with *approach 1*
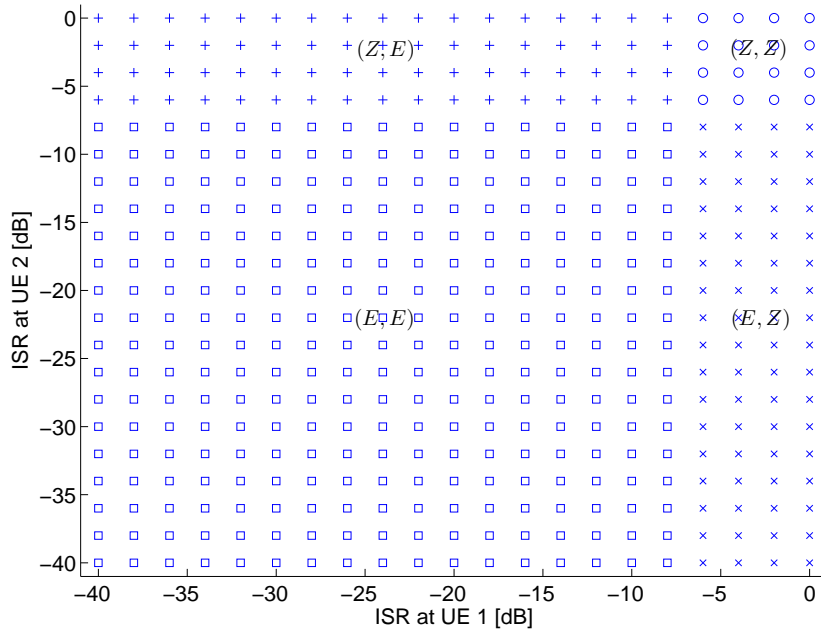
Figure 3.7: Cooperative beamforming strategy for SNR=10 dB with *approach 2*

In the following the achievable rates are compared at different SNR values. The ISR is assumed to be uniformly distributed within $(0, 1)$, representing different locations of the users in this two-cell system (0 represents the location very near the serving BS and 1 represents the location in the middle of the serving BS and interfering BS). Here, the proposed cooperative beamforming strategy is compared to some existing schemes:

- *eig* denotes the eigen-beamforming given by (3.6).

- *ZF* denotes the zero forcing beamforming given by (3.5).

- *mmse* denotes the regularized zero forcing scheme proposed in [95].

- *GE* denotes generalized eigenvector approach described in [29].

Figure 3.8 shows the performance comparison using different strategies assuming full CSI available at the BSs. *eig* outperforms ZF beamforming by 0.5 bps/Hz in the low SNR regime. When SNR is getting higher, i.e., the interference from neighboring cell is stronger, *eig* almost shows no sum-rate gain with the SNR whereas ZF beamforming exhibits its advantage in canceling the interference. The proposed beamforming strategy (*approach 2*) selects ZF beamforming or eigen-beamforming adaptively and thus outperforms both throughout the SNR region. The generalized eigenvector approach *GE* and the regularized zero forcing (RZF) *mmse* perform similarly and even have a performance

gain of less than 0.5 bps/Hz at medium SNR compared with the proposed scheme. At low or high SNR where the noise or the interference dominates, the lines of all three schemes converge. However, the generalized eigenvector approach is applicable in the Wyner model [111], where a linear array of cells is assumed and users are located close to the cell-edge, incurring interference only from a single neighboring cell. This approach may not be directly applied in a more complicated scenario, where users have more than one interferer. For the RZF scheme, to the best knowledge of the author, the bit allocation problem in a limited feedback scenario is not exploited yet. The advantage of the proposed approach is the easy extension to a multi-cell scenario as will be shown in the following sections. Note that in Figure 3.8 at the average received SNR per channel link of 0 dB the achievable rate per user using all beamforming methods except ZF beamforming exceeds 1 bps/Hz. This is due to the large diversity gain obtained by multiple antennas and the Rayleigh statistics of the channel [20]. The same reason holds for Figure 3.9.
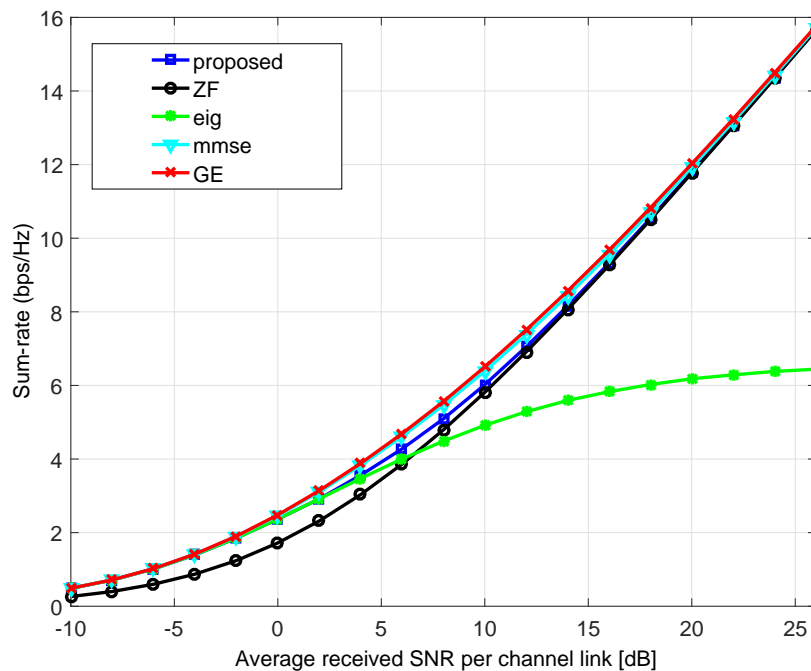
Figure 3.8: Performance comparison of different beamforming strategies with full CSI at BSs

Figure 3.9 illustrates the performance comparison using different beamforming schemes with limited feedback bits. The total number of available bits is $B = 6$. The same notation is used as in Figure 3.8. The eigen-beamforming *eig* on average achieves a gain of 0.75 bps/Hz in the low SNR regime in comparison to ZF beamforming with equally allocated feedback bits and in the high SNR regime *eig* shows poorer performance. Compared with Figure 3.8 *eig* does not lose evident performance because all 6 bits are used

to quantize the desired channel such that the quantization accuracy is sufficiently high. The RZF *mmse* with equally allocated feedback bits performs similar to *eig* at low SNR and approaches to ZF at high SNR. The proposed strategy with bit allocation scheme (3.19) outperforms *mmse* by 2 bps/Hz at SNR=20 dB and performs similar to eigen-beamforming at low SNR. ZF_{ref} is the coordinated ZF beamforming and adaptive bit allocation proposed in [73], which tries to eliminate the intra-cell interference and OCI without considering to enhance the desired power. Hence ZF_{ref} shows a performance degradation at low SNR and a slight gain at high SNR compared with the proposed approach. Again, the generalized eigenvector approach GE with limited feedback performs very similar to the proposed strategy in this single-interferer system, but it doesn't address the problem in a multiple interferer scenario. The proposed approach could be extended to a multi-cell system with multiple interferers.
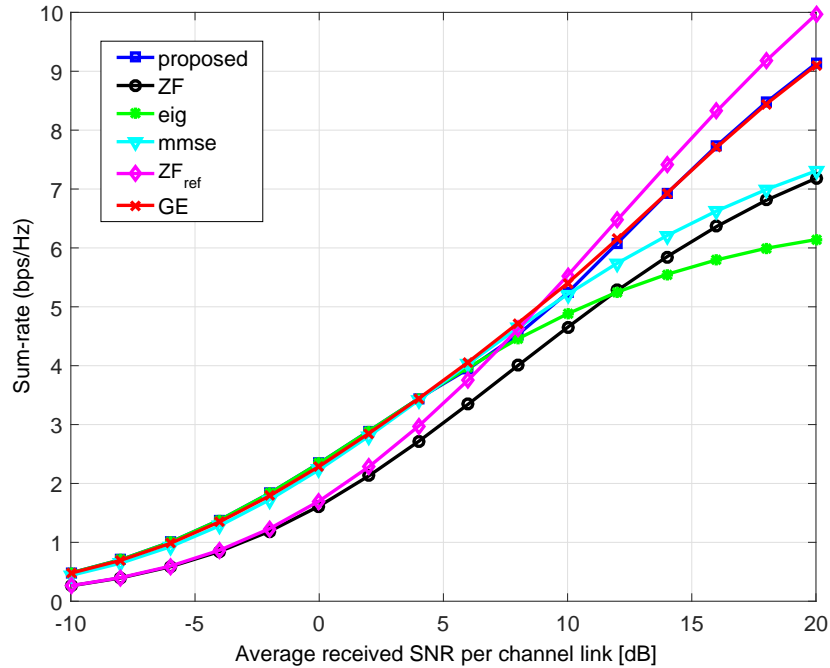
Figure 3.9:   Performance comparison of different beamforming strategies for $B = 6$

3.3   Cooperative beamforming in a three-cell system with limited feedback

In this section we investigate the limited feedback problem in a three-cell system. This three-cell system can be seen as a basic unit in a large multi-cell system and the approaches proposed in this section can be further used in a system with cell cluster size of

3.

3.3.1 System model

We consider a more practical scenario and a hexagonal cell layout is chosen in this system. BSs are located in the center of each cell as shown in Figure 3.10. The cell radius is $R = 166.7$ m. In this CoMP-CB system each user incurs the interference from neighboring two cells. The number of transmit antennas is $N_t = 3$ since each BS should be able to cancel the interference to at most two neighboring users. We also assume a stable backhaul connection between BSs.
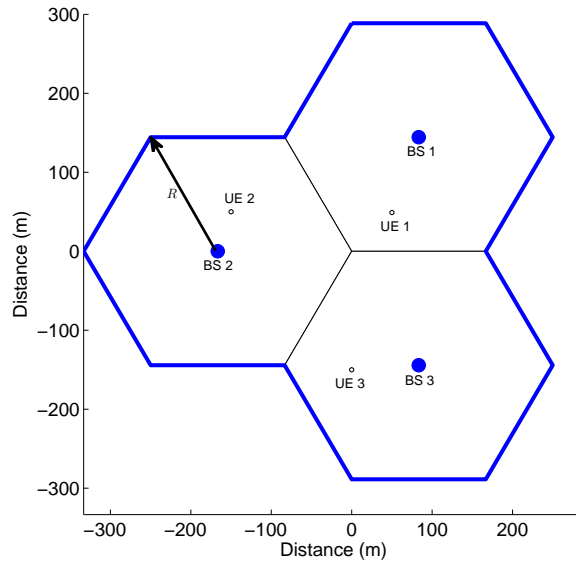
Figure 3.10: A three-cell MISO system with hexagonal cell layout

We take UE 1 as an example. The received signal at UE 1 served by BS 1 is given by

$$y_1 = \sqrt{P_{1,1}}\mathbf{h}_{1,1}\mathbf{w}_1 x_1 + \sqrt{P_{1,2}}\mathbf{h}_{1,2}\mathbf{w}_2 x_2 + \sqrt{P_{1,3}}\mathbf{h}_{1,3}\mathbf{w}_3 x_3 + n_1. \tag{3.28}$$

Hence the received SINR at UE 1 is calculated as

$$\text{SINR}_1 = \frac{P_{1,1}|\mathbf{h}_{1,1}\mathbf{w}_1|^2}{N_0 + P_{1,2}|\mathbf{h}_{1,2}\mathbf{w}_2|^2 + P_{1,3}|\mathbf{h}_{1,3}\mathbf{w}_3|^2}, \tag{3.29}$$

where N_0 is the power of the additive noise at UE 1 and $\mathbb{E}\{|x_i|^2\} = 1$.

The objective is to maximize the sum-rate of the system:

$$R = \sum_{i=1}^{3} R_i = \sum_{i=1}^{3} \mathbb{E}\{\log_2(1 + \text{SINR}_i)\}. \tag{3.30}$$

3.3.2   Adaptive feedback bit partitioning scheme

Similar to Section 3.2.2 in this part we assume that each BS performs ZF beamforming using (3.5) to null out the interference to the other two users in neighboring cells. When a finite-rate feedback channel is considered, each user should quantize the desired channel as well as the two interfering channels using a fixed number of feedback bits B. Under the assumption of uncorrelated Rayleigh channels and RVQ, the desired term in (3.29) is $|\mathbf{h}_{1,1}\mathbf{w}_1|^2 = \xi_{1,1}\mathbf{Z}$, where $\mathbf{Z}$ is a chi-squared random variable and $\xi_{1,1}$ is given by (3.8). From [130]

$$\mathbf{Z} \sim \chi^2_{2(N_t-m)}, \tag{3.31}$$

where m is the number of interferences that are nulled out by BS 1. In case that BS 1 uses eigen-beamforming, $m = 0$. Due to the quantization error, the interference terms cannot be completely canceled by the ZF beamforming. Similar to (3.9), the interference terms in (3.29) are $|\mathbf{h}_{1,2}\mathbf{w}_2|^2 = \kappa_{1,2}\mathbf{Y}_1$ and $|\mathbf{h}_{1,3}\mathbf{w}_3|^2 = \kappa_{1,3}\mathbf{Y}_2$, in which the residual interference factor $\kappa_{i,j} = 2^{-\frac{B_{i,j}}{N_t-1}}$ ($B_{i,j}$ is the number of bits used for quantizing $\mathbf{h}_{i,j}$ and $i \neq j$) and $\mathbf{Y}_1$, $\mathbf{Y}_2 \sim \chi^2_2$.

Here we also consider to maximize the rate of each user separately. Without loss of generality, the lower bound of the rate of UE 1 can be calculated analogous to the derivation in Section 3.2.2 as

$$R_1 = \mathbb{E}\left\{\log_2\left(1 + \frac{\xi_{1,1}P_{1,1}\mathbf{Z}}{N_0 + \kappa_{1,2}P_{1,2}\mathbf{Y}_1 + \kappa_{1,3}P_{1,3}\mathbf{Y}_2}\right)\right\}$$
$$\geq \log_2(1 - 2^{-\frac{B_{1,1}}{N_t-1}}) + \log_2(P_{1,1}) + \frac{1}{\ln 2}\psi(N_t - 2) - \log_2(N_0 + \kappa_{1,2}P_{1,2} + \kappa_{1,3}P_{1,3}) \triangleq R_1^{\text{LB3}}. \tag{3.32}$$

Therefore, the rate optimization problem of UE 1 is:

$$
\begin{aligned}
\max \quad & R_1^{\text{LB3}} \\
\text{subject to} \quad & B_{1,1} + B_{1,2} + B_{1,3} = B \\
& B_{1,i} \geq 0, \text{ for } i = 1, 2, 3.
\end{aligned}
\tag{3.33}
$$

As R_1^{LB3} is a concave function [1] with respect to $B_{i,j}$, the rate optimization problem has the standard form of a convex optimization problem [31], which can be solved by the Karush-Kuhn-Tucker (KKT) conditions. Since the KKT conditions for a nonlinear function

---

[1] A function f is called concave on the convex set $\mathcal{M}$, if $f(\lambda\mathbf{x} + (1-\lambda)\mathbf{x}') \geq \lambda f(\mathbf{x}) + (1-\lambda)f(\mathbf{x}')$ for all $\mathbf{x}, \mathbf{x}' \in \mathcal{M}$ and all $\lambda \in [0, 1]$.
Convex set: a set $\mathcal{M}$ is convex if $\lambda\mathbf{x} + (1-\lambda)\mathbf{x}' \in \mathcal{M}$, for any $\mathbf{x}, \mathbf{x}' \in \mathcal{M}$ and $\lambda \in [0, 1]$.

are difficult to solve analytically, we consider the equality constraint and the inequality constraints separately. Similar to (3.17), we first construct the Lagrange function

$$L(B_{1,1}, B_{1,2}, B_{1,3}, \lambda) = R_1^{\text{LB3}} + \lambda(B_{1,1} + B_{1,2} + B_{1,3} - B). \tag{3.34}$$

Then all partial derivatives of (3.34) are set to zero with respect to $B_{1,1}$, $B_{1,2}$, $B_{1,3}$ and λ:

$$\frac{\partial L}{\partial B_{1,1}} = \frac{\partial L}{\partial B_{1,2}} = \frac{\partial L}{\partial B_{1,3}} = \frac{\partial L}{\partial \lambda} = 0. \tag{3.35}$$

As given by Appendix C, after some steps of simplification, we get the following *key equation*

$$P^3 = P_{1,2}P_{1,3}B_{\text{e}}(3P + N_0), \tag{3.36}$$

where $B_{\text{e}} = 2^{-\frac{B}{N_t-1}}$ and

$$P = P_{1,2} \cdot 2^{-\frac{B_{1,2}}{N_t-1}} = P_{1,3} \cdot 2^{-\frac{B_{1,3}}{N_t-1}}. \tag{3.37}$$

As shown in Appendix D the number of positive roots of (3.36) is always one, which can be easily solved from the *key equation.*

It can be observed that when the received interference power at UE 1, e.g. $P_{1,2}$ from BS 2, increases, from the analysis in Appendix D the positive root of the *key equation* P_0 is also getting larger. By assuming that the interference power from BS 3 $P_{1,3}$ is fixed, from (3.37) we obtain that the number of bits $B_{1,3}$ for quantizing the interfering channel $\mathbf{h}_{1,3}$ is decreased. Furthermore, by slight transformation of (3.36) we get

$$\left(2^{-\frac{B_{1,2}}{N_t-1}}\right)^3 = \frac{P_{1,3}}{P_{1,2}^2} \cdot B_{\text{e}}(3P_{1,2}2^{-\frac{B_{1,2}}{N_t-1}} + N_0). \tag{3.38}$$

When $P_{1,2}$ increases and $P_{1,3}$ remains the same, $B_{1,2}$ increases, i.e., more bits are needed to quantize the strong interfering channel $\mathbf{h}_{1,2}$. From the intermediate result in (C.4) $2^{-\frac{B_{1,1}}{N_t-1}} = \frac{P_0}{3P_0+N_0}$, we can also see that when P_0 gets larger due to the increased interference $P_{1,2}$, the number of bits $B_{1,1}$ for quantizing the desired channel is decreased.

After obtaining the solution P_0 of (3.36), $B_{1,2}$ and $B_{1,3}$ can be calculated from (3.37). It is not guaranteed that $B_{1,2}$ and $B_{1,3}$ are non-negative. If one of them is negative, i.e., there is no necessity to quantize the interference of this link, we can consider this interference as part of the additive noise and solve the bit partitioning problem as in a two-cell system. Hence, for a three-cell system the following *bit partitioning algorithm I* is proposed (taking UE 1 as an example):

- Step 1: construct the *key equation* (3.36) by the interference and noise power levels;

- Step 2: solve for the positive root of (3.36) and calculate $B_{1,2}$ and $B_{1,3}$ from (3.37);

- Step 3: if $B_{1,2} \geq 0$ and $B_{1,3} \geq 0$, go to step 6;

- Step 4: if $B_{1,2} < 0$ and $B_{1,3} < 0$, set $B_{1,2} = 0$ and $B_{1,3} = 0$, then go to step 6;

- Step 5: if only $B_{1,i} < 0$ ($i = 2$ or 3), set $B_{1,i} = 0$, consider the interference from BS i as part of the noise and use (3.19) to calculate $B_{1,j}$ ($j \in \{2,3\}$, $j \neq i$), then go to step 6;

- Step 6: calculate $B_{1,1} = B - B_{1,2} - B_{1,3}$. In case that $B_{1,k}$ ($k = 1, 2, 3$) is not an integer, we should consider $\lceil B_{1,k} \rceil$ and $\lfloor B_{1,k} \rfloor$ which maximizes R_1^{LB3} in (3.32) as the final solution.

3.3.3 Separated approach for cooperative beamforming

As mentioned in Section 3.2.3 *approach 2* can be extended to a larger system. Similarly when high SINR is assumed, the sum-rate of this three-cell system in Figure 3.10 is

$$
\begin{aligned}
R &= \mathbb{E}\left\{\sum_{i=1}^{3} \log_2(1 + \text{SINR}_i)\right\} \approx \mathbb{E}\left\{\sum_{i=1}^{3} \log_2(\text{SINR}_i)\right\} \\
&= \mathbb{E}\left\{\log_2\left(\frac{P_{1,1}|\mathbf{h}_{1,1}\mathbf{w}_1|^2}{N_0 + P_{1,2}|\mathbf{h}_{1,2}\mathbf{w}_2|^2 + P_{1,3}|\mathbf{h}_{1,3}\mathbf{w}_3|^2}\right)\right\} \\
&\quad + \mathbb{E}\left\{\log_2\left(\frac{P_{2,2}|\mathbf{h}_{2,2}\mathbf{w}_2|^2}{N_0 + P_{2,1}|\mathbf{h}_{2,1}\mathbf{w}_1|^2 + P_{2,3}|\mathbf{h}_{2,3}\mathbf{w}_3|^2}\right)\right\} \\
&\quad + \mathbb{E}\left\{\log_2\left(\frac{P_{3,3}|\mathbf{h}_{3,3}\mathbf{w}_3|^2}{N_0 + P_{3,1}|\mathbf{h}_{3,1}\mathbf{w}_1|^2 + P_{3,2}|\mathbf{h}_{3,2}\mathbf{w}_2|^2}\right)\right\}.
\end{aligned}
\tag{3.39}
$$

In case of full CSI available at the BSs, without loss of generality, in (3.39) the desired term of UE 1 $|\mathbf{h}_{1,1}\mathbf{w}_1|^2 = \mathbf{Z}_1$ and the interference term from BS 2 to UE 1 $|\mathbf{h}_{1,2}\mathbf{w}_2|^2 = \mathbf{Y}_{1,2}$ are distributed as

$$
\mathbf{Z}_1 \sim \chi^2_{2(N_t - m)}, \qquad \mathbf{Y}_{1,2}
\begin{cases}
\sim \chi^2_2, & \text{if BS 2 does not perform ZF to UE 1} \\
= 0, & \text{if BS 2 performs ZF to UE 1}
\end{cases},
\tag{3.40}
$$

where m is the number of interferences that are nulled out by BS 1.

The target of this part is to determine whether it is worth to null out the interference to the users in neighboring cells. Notice that MRT does not cancel the interference to other users. Hence MRT not only increases received power at the serving UE, but also leads to increased interference to other UEs compared to ZF scheme. In the following we rewrite

(3.39) as

$$R \approx \boxed{\mathbb{E}\{\log_2(P_{1,1}\boldsymbol{Z}_1)\}} - \mathbb{E}\{\log_2(N_0 + P_{1,2}\boldsymbol{Y}_{1,2} + P_{1,3}\boldsymbol{Y}_{1,3})\}$$
$$+ \mathbb{E}\{\log_2(P_{2,2}\boldsymbol{Z}_2)\} \boxed{-\mathbb{E}\{\log_2(N_0 + P_{2,1}\boldsymbol{Y}_{2,1} + P_{2,3}\boldsymbol{Y}_{2,3})\}}$$
$$+ \mathbb{E}\{\log_2(P_{3,3}\boldsymbol{Z}_3)\} \boxed{-\mathbb{E}\{\log_2(N_0 + P_{3,1}\boldsymbol{Y}_{3,1} + P_{3,2}\boldsymbol{Y}_{3,2})\}}. \tag{3.41}$$

It can be seen from (3.41) that the beamforming vector of BS 1 $\mathbf{w}_1$ only affects the boxed term T_1, which is the combination of the received power at serving UE and the interference to UE 2 and UE 3. Instead of maximizing the sum-rate directly, we try to maximize T_1 assuming that beamforming vectors that is used in other BSs are fixed and simulation results later will show that this method can benefit from both MRT and ZF schemes.

Next, T_1 in (3.41) is further lower bounded as

$$T_1 \geq \mathbb{E}\{\log_2(P_{1,1})\} + \mathbb{E}\{\log_2(\boldsymbol{Z}_1)\} - \log_2(N_0 + P_{2,1}\mathbb{E}\{\boldsymbol{Y}_{2,1}\} + P_{2,3}\mathbb{E}\{\boldsymbol{Y}_{2,3}\})$$
$$- \log_2(N_0 + P_{3,1}\mathbb{E}\{\boldsymbol{Y}_{3,1}\} + P_{3,2}\mathbb{E}\{\boldsymbol{Y}_{3,2}\}) \triangleq T_1^{\mathrm{LB3}}. \tag{3.42}$$

In oder to determine the beamforming scheme $\mathbf{w}_1$ at BS 1, i.e., whether $\mathbf{w}_1$ does or does not perform IN to UE 2 or UE 3, we assume that UE 2 and UE 3 are also helped by other BSs besides BS 1. The reason behind this assumption is that when UE 2 or UE 3 is near the BS in the other cell (hence may incur strong interference from this BS), there is a high probability that this BS tries to null out the interference to UE 2 or UE 3. Under this assumption, in (3.42) $P_{2,3}\mathbb{E}\{\boldsymbol{Y}_{2,3}\} = 0$ and $P_{3,2}\mathbb{E}\{\boldsymbol{Y}_{3,2}\} = 0$. Therefore, depending on the scheme BS 1 uses, T_1^{LB3} can have different values:

$$T_1^{\mathrm{LB3}} =$$
$$\begin{cases} \mathbb{E}\{\log_2(P_{1,1})\} + \dfrac{1}{\ln 2}\psi(N_{\mathrm{t}} - 2) - 2\log_2(N_0), & \text{if } \mathbf{w}_1 \xrightarrow{\mathrm{ZF}} \text{UE 2 and } \mathbf{w}_1 \xrightarrow{\mathrm{ZF}} \text{UE 3;} \\[2mm] \mathbb{E}\{\log_2(P_{1,1})\} + \dfrac{1}{\ln 2}\psi(N_{\mathrm{t}} - 1) - \log_2(N_0) - \log_2(N_0 + P_{3,1}), & \text{if } \mathbf{w}_1 \xrightarrow{\mathrm{ZF}} \text{UE 2;} \\[2mm] \mathbb{E}\{\log_2(P_{1,1})\} + \dfrac{1}{\ln 2}\psi(N_{\mathrm{t}} - 1) - \log_2(N_0 + P_{2,1}) - \log_2(N_0), & \text{if } \mathbf{w}_1 \xrightarrow{\mathrm{ZF}} \text{UE 3;} \\[2mm] \mathbb{E}\{\log_2(P_{1,1})\} + \dfrac{1}{\ln 2}\psi(N_{\mathrm{t}}) - \log_2(N_0 + P_{2,1}) - \log_2(N_0 + P_{3,1}), & \text{if } \mathbf{w}_1 \text{ uses MRT,} \end{cases} \tag{3.43}$$

where $\mathbf{w}_1 \xrightarrow{\mathrm{ZF}}$ UE 2 indicates that BS 1 performs interference nulling to UE 2. $\psi(\cdot)$ is again Euler's psi function and the result of $\mathbb{E}\{\log_2(\boldsymbol{Z}_1)\}$ is given in [86]. By comparing the values in (3.43) the best beamforming scheme at BS 1 can be determined which maximizes T_1^{LB3}. The comparison only requires the noise and interference power level at UE 2 and UE 3 from BS 1 and does not need a joint determination of beamforming schemes at all

BSs. Hence, the beamforming vectors at each BS are determined **separately**. However, the information about the noise and interference power level at UE 2 or UE 3 must be conveyed from neighboring BSs to BS 1, which only causes a minor burden on the backhaul connection.

After determination of beamforming schemes used at each BSs, the users know which channel information should be fed back. Since *bit partitioning algorithm I* is under the assumption that all BSs perform ZF beamforming, it does not ensure maximal rate if MRT is also included. Therefore, the following *bit allocation scheme* for this three-cell system should be used to determine the number of bits for quantizing corresponding CSI (taking UE 1 as an example):

$$
\begin{cases}
\text{if } \mathbf{w}_2 \xrightarrow{\text{ZF}} \text{UE 1 and } \mathbf{w}_3 \xrightarrow{\text{ZF}} \text{UE 1, use } \textit{bit partitioning algorithm I} \\
\text{if } \mathbf{w}_2 \xrightarrow{\text{ZF}} \text{UE 1 only, use (3.19) by taking } P_{1,3} \text{ as part of the noise} \\
\text{if } \mathbf{w}_3 \xrightarrow{\text{ZF}} \text{UE 1 only, use (3.19) by taking } P_{1,2} \text{ as part of the noise} \\
\text{if neither } \mathbf{w}_2 \xrightarrow{\text{ZF}} \text{UE 1 nor } \mathbf{w}_3 \xrightarrow{\text{ZF}} \text{UE 1, use all bits } B_{1,1} = B \text{ to quantize } \mathbf{h}_{1,1}
\end{cases}
\tag{3.44}
$$

All of the above motivates the separated approach for cooperative beamforming (*approach 3*):

- All users measure the noise and received interference power level or the received INR from each neighboring BS, and transmit this information to their serving BS;

- Each BS obtains from neighboring BSs the noise and interference information of the users in the neighboring cells and determines whether it should perform ZF to any of these users or just MRT by finding the maximum value in (3.43);

- The users are informed by their serving BS which beamforming schemes have been selected by neighboring BSs, i.e., whether the neighboring BSs need to cancel the interference to these users. Correspondingly, the users feed back CSI according to the *bit allocation scheme* (3.44);

- The BSs carry out the corresponding beamforming strategy for this three-cell system.

Notice that the interference and noise power level does not change much unless the users move at high velocity. Hence, the measurement of the INR and the exchange of this information do not take place very often. Furthermore, the interference highly depends on the location of the users in the cell. If the location and the noise power of the users do not vary much, the same bit allocation and beamforming schemes can be used without much performance loss.

3.3.4   Simulation results and analysis

In this subsection we show some simulation results in the three-cell scenario in Figure 3.10. There is only one user randomly located in each cell communicating with its serving BS. The number of transmit antennas at the BSs is 3 and each user has a single receive antenna.

Performance with adaptive feedback bit partition scheme

First we assume that each user has a fixed received SNR value and incurs different ISR depending on factors that could affect the interference power, e.g., location of the users. We also assume that each BS performs ZF beamforming to the two users in neighboring cells. To compare the number of bits for quantizing the desired and interfering channels, the users are assumed to be at an SNR of 10 dB. The ISR varies in the range of (-40 dB, 0 dB), which corresponds to the range of (-30 dB, 10 dB) for the INR. The total number of feedback bits available at each user is $B = 8$ and UE 1 is taken as an example.

Figure 3.11 and Figure 3.12 show the number of bits used by UE 1 to quantize the desired channel $\mathbf{h}_{1,1}$ and the interfering channel $\mathbf{h}_{1,2}$ according to *bit partitioning algorithm I* proposed in Section 3.3.2. In Figure 3.11 it is shown that when the interference becomes larger, fewer bits are used to quantize the desired channel. When the INR from both BS 2 and BS 3 is smaller than -10 dB, all 8 bits are used to quantize the desired link. Another observation is that even the interference power is the same as the signal power (INR=SNR=10 dB), some bits are always assigned to quantize the desired channel in order to ensure the transmission quality to the serving user. Figure 3.12 shows if the interference from BS 2 gets larger, more bits are used for the interfering channel $\mathbf{h}_{1,2}$. Provided that the INR from BS 2 is fixed while increasing the INR from BS 3, fewer bits are used for $\mathbf{h}_{1,2}$ since more bits are assigned to $\mathbf{h}_{1,3}$. All these observations coincide with the analysis in Section 3.3.2.

Next, the sum-rate in this three-cell system is compared when each BS always performs interference nulling to neighboring users. We use the channel model introduced in Section 2.2.1. The small-scale fading is assumed to be Rayleigh distributed and the received power at a distance of d according to the path loss model (2.1) is

$$P_{\mathrm{r}} = P_0 \left[\frac{d_0}{d} \right]^{\gamma}, \qquad (3.45)$$

where d_0 is the reference distance and P_0 is the received power at d_0. In this simulation we set d_0 equal to the cell radius R and the cell-edge SNR at R varies from -3 dB to 30 dB. The path loss exponent γ is 3.7. For each iteration each user is uniformly dropped
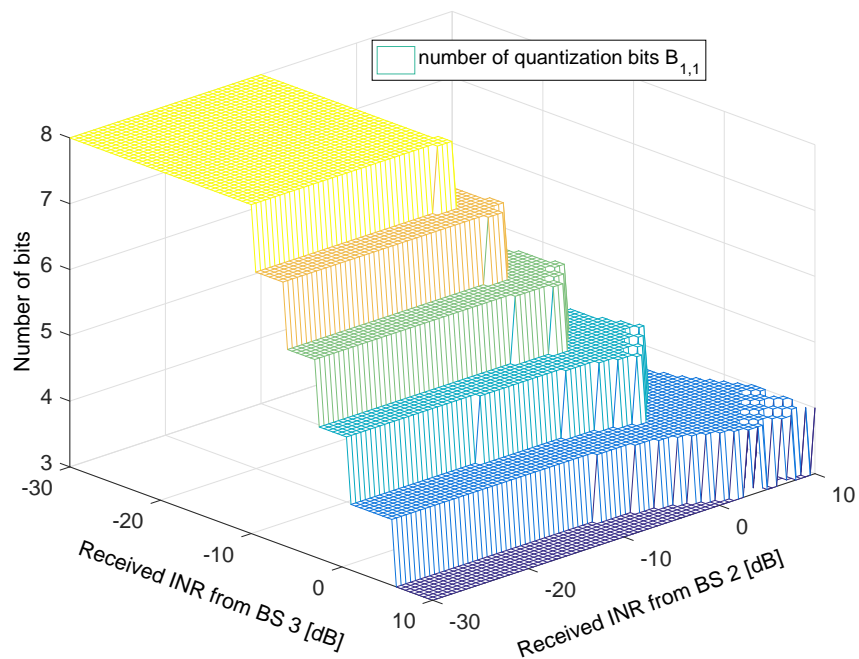
Figure 3.11: Number of bits to quantize the desired channel $\mathbf{h}_{1,1}$ for SNR=10 dB and B=8
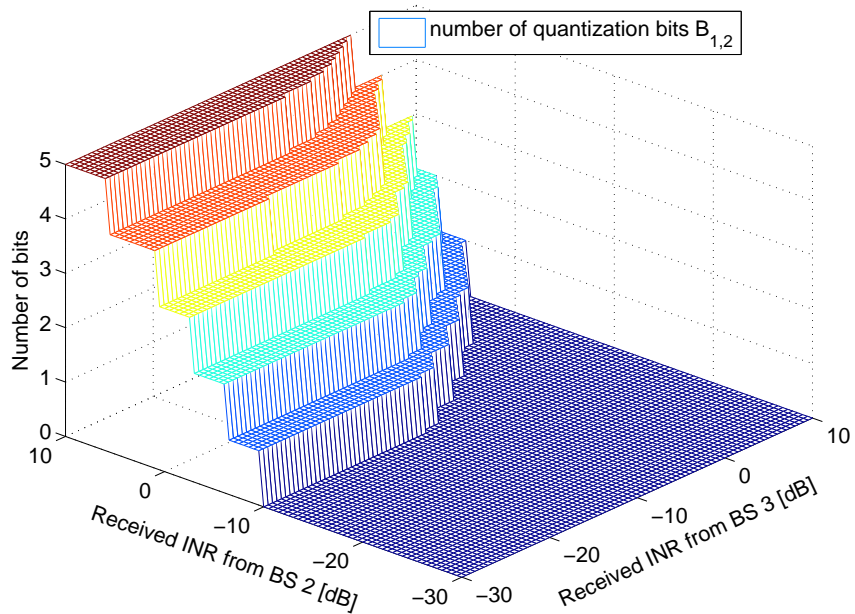
Figure 3.12: Number of bits to quantize the interfering channel $\mathbf{h}_{1,2}$ for SNR=10 dB and B=8

within the cells. Figure 3.13 shows the performance comparison using *bit partitioning algorithm I* (*proposed*) and equal bit allocation scheme (*equal*) for $B = 12$ and $B = 24$.
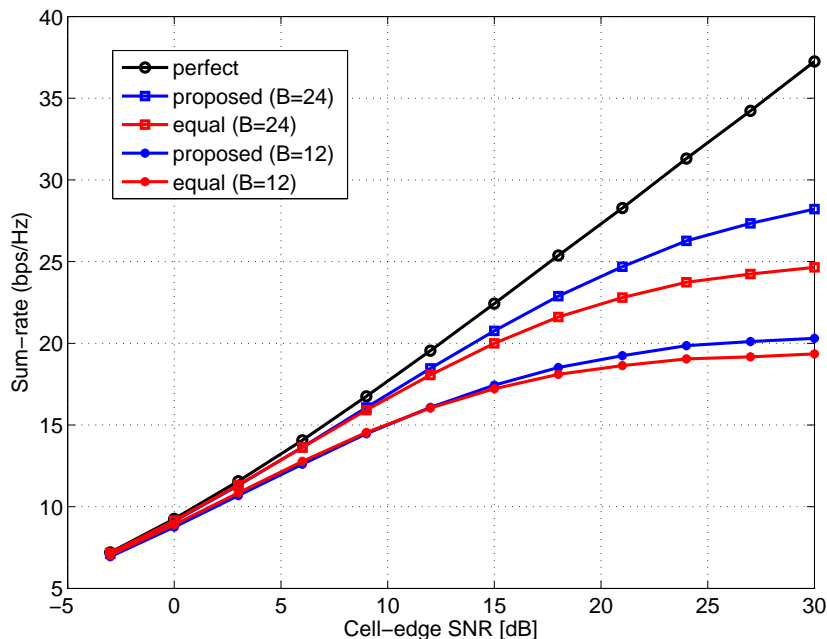
Figure 3.13: Sum-rate using ZF beamforming with different bit partitioning algorithms and different numbers of available feedback bits in a three-cell system

Similar to Figure 3.5 in a two-cell system, the performance when full CSI is available at BSs (*perfect*) always outperforms other schemes. As the cell-edge SNR increases, the difference is getting larger. When more bits are available at users, *proposed* obtains more performance gain compared to *equal* since the potential to exploit feedback bit allocation is higher. Moreover, the performance of ZF beamforming is limited due to quantization errors even if the cell-edge SNR is large, which is more obvious in the case $B = 12$.

Performance with a cooperative beamforming strategy

In this part the separated approach for cooperative beamforming *approach 3* is implemented. To illustrate how this approach works, we first consider one snapshot shown in Figure 3.14. UE 2 is at the cell edge and UE 3 is near its serving BS. When the cell-edge SNR is at moderate level (10 dB), (3.43) recommends BS 1 to perform interference nulling only to UE 2, because the interference from BS 1 to UE 3 is too weak. At low cell-edge SNR regime (-5 dB), the interference to both UE 2 and UE 3 needs not to be canceled by BS 1 according to (3.43). All transmit power at BS 1 is used to serve UE 1. If the cell-edge SNR is high (20 dB), BS 1 has to cancel the interference to both UEs in order to provide the best sum-rate performance of the whole system.

Next, we compare the performance of different strategies with full CSI and quantized CSI at the transmitter. In Figure 3.15 we can first see that there is no difference between
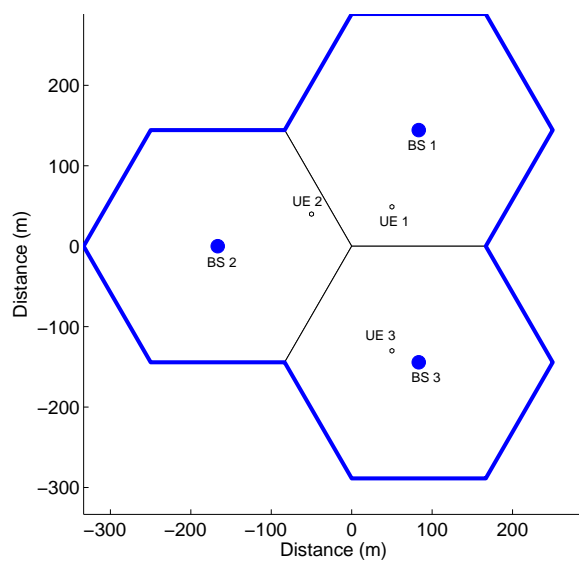
Figure 3.14:   One snapshot of a three-cell system with hexagonal cell layout
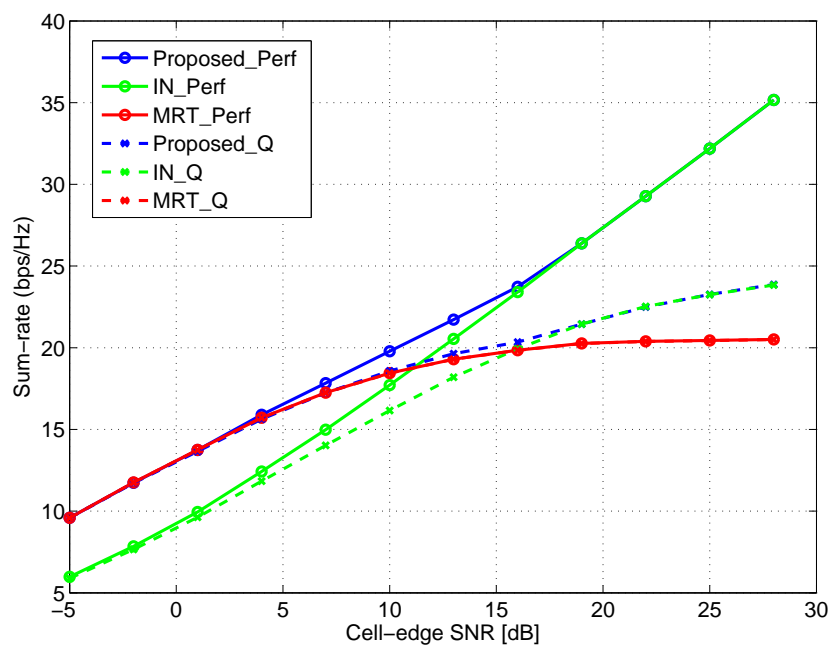
Figure 3.15: Performance comparison of different beamforming strategies with full CSI and quantized CSI ($B = 18$)

MRT with full CSI (MRT_Perf) and with quantized CSI (MRT_Q), showing that using $B = 18$ bits for quantizing the desired channel can provide sufficient accuracy for MRT. Similar to the two-cell scenario, at low cell-edge SNR regime MRT outperforms

IN scheme, where IN means the BS always nulls out interference to the two UEs in neighboring cells. At high cell-edge SNR regime, due to the strong inter-cell interference, IN scheme obtains much performance gain compared to MRT, especially for the full CSI case. With or without full CSI the proposed separated approach can benefit from both MRT and IN schemes at low SNR and high SNR regimes, respectively. Therefore, $Proposed\_Perf$ and $Proposed\_Q$ outperform MRT and IN schemes in both cases.

3.4   Cooperative beamforming in a multi-cell system with limited feedback

A practical mobile system consists of multiple cells, where resource assignment is usually problematic. Hence, feedback bit allocation and beamforming design become more complicated in this case. However, the approaches used in Section 3.2 and Section 3.3 can be extended in a multi-cell system. The purpose of this section is to provide some easy-to-implement schemes for feedback bit allocation and beamforming design.

3.4.1   System model
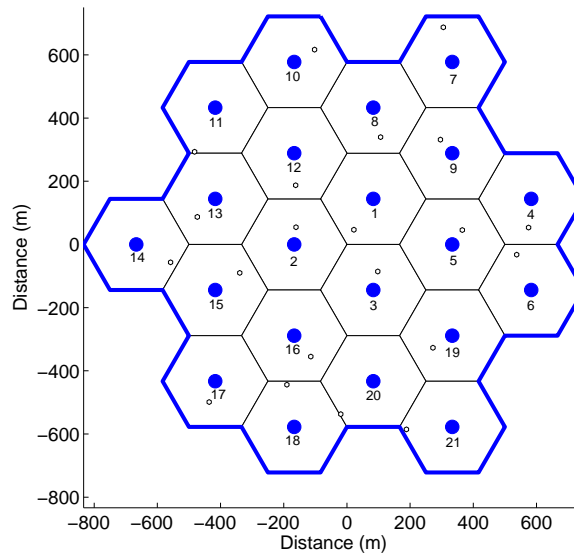
Figure 3.16:   A multi-cell MISO system with hexagonal cell layout

Figure 3.16 shows a cellular network consisting of $N_{ce} = 21$ cells. Each BS is equipped with N_t transmit antennas. We assume that in each time slot only one user is active in each cell. This is because the users that are served by the same BS are assumed to share orthogonal time or frequency resources and hence they do not interfere with each other.

In this system the received signal at each user is the accumulation of signals from all BSs, i.e., the received signal at UE i is

$$y_i = \sqrt{P_{i,i}}\mathbf{h}_{i,i}\mathbf{w}_i x_i + \sum_{j \in \mathcal{S}\backslash i} \sqrt{P_{i,j}}\mathbf{h}_{i,j}\mathbf{w}_j x_j + n_i, \tag{3.46}$$

where set $\mathcal{S} = \{1, 2, \cdots, N_{\text{ce}}\}$. Hence the received SINR at UE i is calculated as

$$\text{SINR}_i = \frac{P_{i,i}|\mathbf{h}_{i,i}\mathbf{w}_i|^2}{N_0 + \sum_{j \in \mathcal{S}\backslash i} P_{i,j}|\mathbf{h}_{i,j}\mathbf{w}_j|^2}, \tag{3.47}$$

where N_0 is the power of the additive noise at UE i.

Similarly, the objective of this part is to maximize the sum-rate of the multi-cell system:

$$R = \sum_{i=1}^{N} R_i = \sum_{i=1}^{N} \mathbb{E}\{\log_2(1 + \text{SINR}_i)\}. \tag{3.48}$$

3.4.2   Adaptive feedback bit partitioning scheme

In a large cellular system it is not necessary that all other BSs try to null out the interference to UE i. Therefore, we divide the BSs except BS i into two categories: BSs that perform IN to UE i whose indices are denoted in set $\mathcal{S}(i)$ and BSs that do not perform IN to UE i. The aim of this subsection is to adaptively partition the quantization bits at UE i for channel $\mathbf{h}_{i,j}$ ($j \in \{i \cup \mathcal{S}(i)\}$). Here we consider to maximize the rate of each user instead of the sum-rate and the algorithm proposed in this subsection can be adopted in a system either with cluster structure or with distributed ZF scheme as will be shown in the following sections.

Under the assumption of uncorrelated Rayleigh channels and RVQ, the rate of UE i is rewritten as

$$R_i = \mathbb{E}\left\{\log_2\left(1 + \frac{\xi_{i,i}P_{i,i}\boldsymbol{Z}}{N_0 + \sum_{j \in \mathcal{S}(i)} \kappa_{i,j}P_{i,j}\boldsymbol{Y}_j + \sum_{j \in \mathcal{S}\backslash\{i \cup \mathcal{S}(i)\}} P_{i,j}\boldsymbol{Y}_j}\right)\right\}. \tag{3.49}$$

In (3.49) $\boldsymbol{Z} \sim \chi^2_{2(N_t - m)}$, where m is the number of interferences that are nulled out by BS i, and $\boldsymbol{Y}_j \sim \chi^2_2$ for $j \in \{i \cup \mathcal{S}(i)\}$. $\xi_{i,i}$ is given in (3.8) and lower bounded by (3.14), and the residual interference factor $\kappa_{i,j} = 2^{-\frac{B_{i,j}}{N_t - 1}}$ ($i \neq j$). Based on the discussion in Section 3.2.2, the lower bound of the rate of UE i can be calculated as

$$R_i \geq \log_2(1 - 2^{-\frac{B_{i,i}}{N_t - 1}}) + \log_2(P_{i,i}) + \frac{1}{\ln 2}\psi(N_t - m)$$
$$- \log_2(N_0 + \sum_{j \in \mathcal{S}(i)} \kappa_{i,j}P_{i,j} + \sum_{j \in \mathcal{S}\backslash\{i \cup \mathcal{S}(i)\}} P_{i,j}) \triangleq R_i^{\text{LBM}}. \tag{3.50}$$

Consequently, the rate optimization problem of UE i in a multi-cell system is:

$$\begin{aligned} \max \quad & R_i^{\text{LBM}} \\ \text{subject to} \quad & \sum_{j \in \{i \cup \mathcal{S}(i)\}} B_{i,j} = B \\ & B_{i,j} \geq 0, \text{ for } j \in \{i \cup \mathcal{S}(i)\}. \end{aligned} \qquad (3.51)$$

Using a similar method as in Section 3.3.2 by avoiding solving the complicated KKT conditions, we construct the Lagrange function

$$L(\bigcup_{j \in \{i \cup \mathcal{S}(i)\}} B_{i,j}, \lambda) = R_i^{\text{LBM}} + \lambda(\sum_{j \in \{i \cup \mathcal{S}(i)\}} B_{i,j} - B), \qquad (3.52)$$

and then set all partial derivatives of (3.52) to zero with respect to $B_{i,j}$ ($j \in \{i \cup \mathcal{S}(i)\}$) and λ:

$$\frac{\partial L}{\partial B_{i,j}} = \frac{\partial L}{\partial \lambda} = 0, \ \forall \ j \in \{i \cup \mathcal{S}(i)\}. \qquad (3.53)$$

Although (3.53) is a system of equations consisting of multiple variables, it is not difficult to solve it due to the symmetric property of $B_{i,j}$ ($j \in \mathcal{S}(i)$). After some calculations, we can also get the following *key equation*, which has a similar form of (3.36):

$$P^{n+1} = (\prod_{j \in \mathcal{S}(i)} P_{i,j})B_{\text{e}}((n+1)P + N_0 + \sum_{j \in \mathcal{S} \setminus \{i \cup \mathcal{S}(i)\}} P_{i,j}), \qquad (3.54)$$

where $B_{\text{e}} = 2^{-\frac{B}{N_{\text{t}}-1}}$ and $n = |\mathcal{S}(i)|$. P is an intermediate parameter that exhibits the symmetric property of $B_{i,j}$ ($j \in \mathcal{S}(i)$):

$$P = P_{i,j} \cdot 2^{-\frac{B_{i,j}}{N_{\text{t}}-1}}, \text{ for } j \in \mathcal{S}(i). \qquad (3.55)$$

Notice that (3.54) is a polynomial equation with respect to P. The positive root is unique analogous to the analysis in Appendix D and the roots of a polynomial equation can be efficiently solved, since the order n is not too large in practice. The reason is that a user may only incur severe interference from neighboring cells, such that the amount of BSs that perform IN to this user won't be too high.

The analysis of (3.38) can be generalized to the case of N cells. It is not difficult to see that the number of bits $B_{i,j}$ ($j \in \mathcal{S}(i)$) used for quantizing the interfering channel $\mathbf{h}_{i,j}$ increases when the received interference power $P_{i,j}$ increases, and the same trend holds for the case of decrement. The result is intuitive since as one interferer gets stronger, it is worth to spend more bits to increase quantization accuracy for a rate gain.

After the positive root of (3.54) is obtained, $B_{i,j}$ can be calculated from (3.55). However, the inequality constraints in the optimization problem (3.51) are not considered yet. If

one of the results is negative, indicating that the interference from this link is so weak that there is no need to spend a bit on it, we can take this interference as additive noise and re-optimize the problem. Therefore, we propose a recursive method as shown in the following *bit partitioning algorithm II*:

- Step 1: Initialize $\mathcal{S}'(i) = \mathcal{S}(i)$;

- Step 2: construct the *key equation* (3.54) by the interference and noise power levels use $\mathcal{S}'(i)$ instead of $\mathcal{S}(i)$. Notice that the received signal from BSs that do not perform IN to UE i can be simply seen as a part of additive noise;

- Step 3: solve for the positive root of (3.54) and calculate $B_{i,j}$ for $j \in \mathcal{S}'(i)$ from (3.55);

- Step 4: if $B_{i,k} < 0$ ($k \in \mathcal{S}'(i)$), set $\mathcal{S}'(i) = \mathcal{S}'(i) \backslash k$ and go to step 2;

- Step 5: calculate $B_{i,i} = B - \sum_{j \in \mathcal{S}'(i)} B_{i,j}$. In case that $B_{i,j}$ ($j \in \{i \cup \mathcal{S}'(i)\}$) is not an integer, we should consider $\lceil B_{i,j} \rceil$ and $\lfloor B_{i,j} \rfloor$ which maximizes R_i^{LBM} in (3.50) as the final solution and $B_{i,j} = 0$ for $j \in \mathcal{S}(i) \backslash \mathcal{S}'(i)$.

$\mathcal{S}(i)$ is the set of BSs that may perform IN to UE i and is used as an initial value for this algorithm. One possible method for the determination of $\mathcal{S}(i)$ is described in *approach 4* in Section 3.4.3.

3.4.3 BS-specific approach for adaptive ZF beamforming

For a large system with multiple cells the beamforming design at each BS is not a trivial task. The aim of this part is to choose the beamforming strategy between MRT and ZF schemes and also to determine for each BS to which UEs the interference needs to be nulled out in terms of maximizing the sum-rate of the system. In order to reduce feedback and backhaul overhead in a cellular system, a clustering technique is proposed to shrink the cooperating size [80]. In the following we first compare the performance of ZF beamforming using static clustering and the MRT scheme, where static clustering means that each cluster is designed based on some geographical information such as BS location or potential user location and is fixed over time. For the ZF beamforming each BS nulls out the interference to users in other cells in the same cluster.

We consider a cellular system as shown in Figure 3.17 with $N = 57$ cells in total and for static clustering we assume a cluster size of 3 (3 cells in a cluster). The clusters are displayed in the gray area with different transparencies and there is no overlapping among clusters. Each BS has 3 transmit antennas and UEs have a single receive antenna. There

is only one user in each cell and the users are dropped uniformly within the cells for each iteration. We simulate for all 57 cells but only evaluate the inner 21 cells surrounded by the red dashed line.
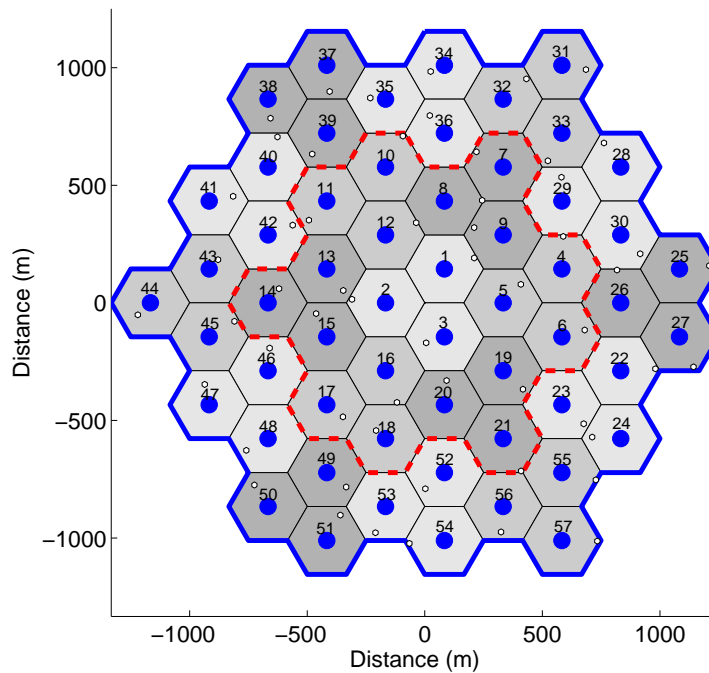
Figure 3.17: A multi-cell MISO system with 57 cells

Figure 3.18 shows the comparison of user data rate using MRT and ZF schemes. Since a CoMP technique is to increase data rate especially of cell-edge users, we also compare the data rate of cell-edge users. The cell-edge user throughput is defined by 3GPP as the 5% point of the cumulative distribution function (CDF) of the user throughput [8]. Here we adopt the same definition for cell-edge data rate. From Figure 3.18 we can see that the average user data rate using MRT ($MRT\_Average$) dramatically outperforms the average data rate using ZF scheme with static clustering ($IN\_Average$) in all SNR regimes. The same result also holds for the cell-edge user data rate. The reason is that in such a complicated scenario users undergo interference from multiple interferers. Note that the ZF scheme reduces the received power of the desired user in order to null out the interference. Without sophisticated design of interference selection, the interference nulling benefit of ZF scheme cannot compensate the received power loss of desired users. Even for cell-edge users for which ZF usually gains a lot, static clustering is not a good choice because the users may lie in the boundary of the cluster, such as the user in cell 2. It seems that a ZF scheme for static clustering is not suitable for such a multi-cell scenario.
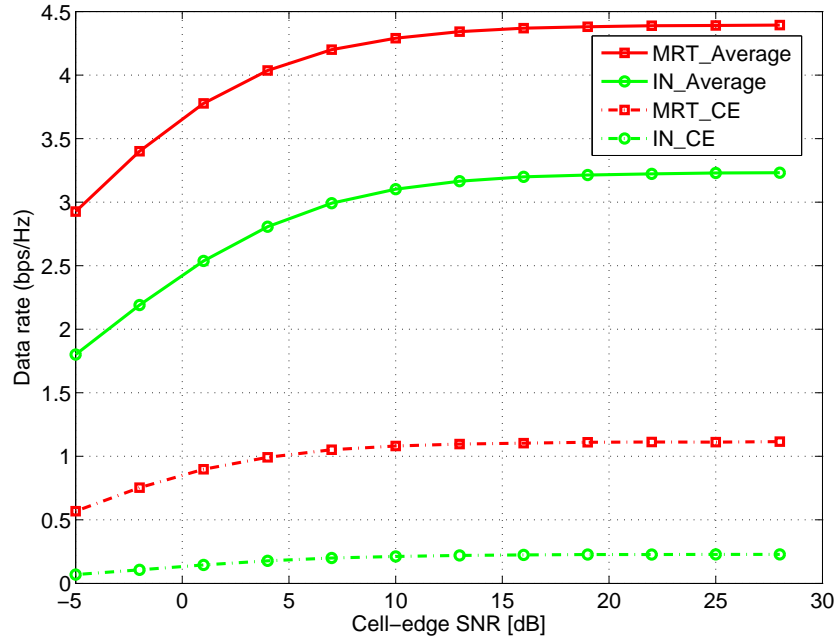
Figure 3.18:   Performance comparison of ZF beamforming using static clustering and MRT

Therefore, some advanced ZF approaches should be developed in order to outperform the MRT scheme.

Notice that in Figure 3.17 some users are at cell-edge, a straightforward method is to let BSs cancel the interference to the nearest users. Although a BS with N_{t} antennas can maximally null out $N_{\mathrm{t}} - 1$ interference, it may not be necessary to fully make use of interference nulling ability of the BS because nulling out interference also sacrifices received power at the desired user. Hence, in the following we try to find out whether and to which users the BS should perform ZF beamforming.

In the multi-cell system the achievable sum-rate under the assumption of high SINR is

$$
\begin{aligned}
R &= \mathbb{E}\left\{ \sum_{i \in \mathcal{S}} \log_2(1 + \mathrm{SINR}_i) \right\} \approx \mathbb{E}\left\{ \sum_{i \in \mathcal{S}} \log_2(\mathrm{SINR}_i) \right\} \\
&= \mathbb{E}\left\{ \sum_{i \in \mathcal{S}} \log_2\left(\frac{P_{i,i}|\mathbf{h}_{i,i}\mathbf{w}_i|^2}{N_0 + \sum_{j \in \mathcal{S}\setminus i} P_{i,j}|\mathbf{h}_{i,j}\mathbf{w}_j|^2} \right) \right\},
\end{aligned} \tag{3.56}
$$

where $\mathcal{S} = \{1, 2, \cdots, N\}$ contains indices of all cells. For the design of the beamforming vector $\mathbf{w}_n$ at BS n ($n \in \mathcal{S}$), we adopt a similar idea as is Section 3.3.3. Because directly maximizing the sum-rate needs a joint optimization whose complexity increases exponentially with the system size, we try to maximize the term affected by $\mathbf{w}_n$ assuming that beamforming vectors that are used in other BSs are fixed. In order to determine whether

BS n needs to perform ZF to UE l (UE l must be in the vicinity of BS n so that it makes sense for BS n to perform ZF to UE l and $n \neq l$), we rewrite (3.56) as

$$
\begin{aligned}
R \approx \mathbb{E} \bigg\{ & \log_2 \left(\frac{\boxed{P_{n,n}|\mathbf{h}_{n,n}\mathbf{w}_n|^2}}{N_0 + \sum_{j \in \mathcal{S}\backslash n} P_{n,j}|\mathbf{h}_{n,j}\mathbf{w}_j|^2} \right) \\
& + \log_2 \left(\frac{P_{l,l}|\mathbf{h}_{l,l}\mathbf{w}_l|^2}{N_0 + \boxed{P_{l,n}|\mathbf{h}_{l,n}\mathbf{w}_n|^2} + \sum_{j \in \mathcal{S}\backslash\{l,n\}} P_{l,j}|\mathbf{h}_{l,j}\mathbf{w}_j|^2} \right) \\
& + \sum_{i \in \mathcal{S}\backslash\{l,n\}} \log_2 \left(\frac{P_{i,i}|\mathbf{h}_{i,i}\mathbf{w}_i|^2}{N_0 + \sum_{j \in \mathcal{S}\backslash i} P_{i,j}|\mathbf{h}_{i,j}\mathbf{w}_j|^2} \right) \bigg\}
\end{aligned}
\tag{3.57}
$$

$$
\begin{aligned}
= \; & \underbrace{\mathbb{E} \left\{ \log_2 \left(\frac{P_{n,n}|\mathbf{h}_{n,n}\mathbf{w}_n|^2}{N_0 + P_{l,n}|\mathbf{h}_{l,n}\mathbf{w}_n|^2 + \sum_{j \in \mathcal{S}\backslash\{l,n\}} P_{l,j}|\mathbf{h}_{l,j}\mathbf{w}_j|^2} \right) \right\}}_{T_1} \\
& + \mathbb{E} \left\{ \log_2 \left(\frac{P_{l,l}|\mathbf{h}_{l,l}\mathbf{w}_l|^2}{N_0 + \sum_{j \in \mathcal{S}\backslash n} P_{n,j}|\mathbf{h}_{n,j}\mathbf{w}_j|^2} \right) \right\} \\
& + \mathbb{E} \left\{ \sum_{i \in \mathcal{S}\backslash\{l,n\}} \log_2 \left(\frac{P_{i,i}|\mathbf{h}_{i,i}\mathbf{w}_i|^2}{N_0 + \sum_{j \in \mathcal{S}\backslash i} P_{i,j}|\mathbf{h}_{i,j}\mathbf{w}_j|^2} \right) \right\}.
\end{aligned}
\tag{3.58}
$$

Although $\mathbf{w}_n$ also exists in the third term in (3.57), whether or not BS n performs ZF to UE l does not affect the statistical distribution of the interference term in the SINR at UE i ($i \in \mathcal{S}\backslash\{l,n\}$). It only affects the boxed terms in (3.57) and hence under the assumption that $\mathbf{w}_i$ ($i \in \mathcal{S}\backslash n$) is fixed we try to maximize T_1 in (3.58). With the help of (3.40), we can calculate the lower bound of T_1 as

$$
\begin{aligned}
T_1 &= \mathbb{E}\{\log_2(P_{n,n})\} + \mathbb{E}\{\log_2(\boldsymbol{Z})\} - \mathbb{E}\{\log_2(N_0 + P_{l,n}\boldsymbol{Y} + \sum_{j \in \mathcal{S}\backslash\{l,n\}} P_{l,j}|\mathbf{h}_{l,j}\mathbf{w}_j|^2)\} \\
&\geq \log_2(P_{n,n}) + \mathbb{E}\{\log_2(\boldsymbol{Z})\} - \log_2(N_0 + K + P_{l,n}\mathbb{E}\{\boldsymbol{Y}\}) \triangleq T_1^{\mathrm{LBM}}.
\end{aligned}
\tag{3.59}
$$

where $K = \mathbb{E}\{\sum_{j \in \mathcal{S}\backslash\{l,n\}} P_{l,j}|\mathbf{h}_{l,j}\mathbf{w}_j|^2\} = \sum_{j \in \mathcal{S}\backslash\{l,n\}} P_{l,j}$ is the total interference to UE l from other BSs except BS n assuming that these BSs do not cancel the interference to UE l. $\boldsymbol{Z} = |\mathbf{h}_{n,n}\mathbf{w}_n|^2$ and $\boldsymbol{Y} = |\mathbf{h}_{l,n}\mathbf{w}_n|^2$ are according to the distribution in (3.40). Depending on whether BS n performs ZF to UE l, the lower bound T_1^{LBM} can have different values:

$$
T_1^{\mathrm{LBM}} = \begin{cases} \log_2(P_{n,n}) + \dfrac{1}{\ln 2}\psi(N_\mathrm{t} - (m+1)) - \log_2(N_0 + K) & \text{if } \mathbf{w}_n \xrightarrow{\mathrm{ZF}} \text{UE } l \\[2mm] \log_2(P_{n,n}) + \dfrac{1}{\ln 2}\psi(N_\mathrm{t} - m) - \log_2(N_0 + K + P_{l,n}) & \text{else} \end{cases}, \tag{3.60}
$$

where m is the number of users except UE l that BS n performs ZF to. By comparing the two values in (3.60) we obtain the *transmission scheme determination rule* similar to *approach 2* for the two-cell system in Section 3.2.3:

$$
\begin{aligned}
&\text{if} \quad \frac{P_{l,n}}{N_0+K} > e^{\frac{1}{N_\mathrm{t}-m-1}} - 1, \quad \text{BS } n \text{ performs ZF to UE } l \\
&\text{else,} \qquad\qquad\qquad \text{BS } n \text{ does not perform ZF to UE } l.
\end{aligned}
\tag{3.61}
$$

The *transmission scheme determination rule* (3.61) shows that whether BS n should perform ZF to UE l depends on if the ratio of interference from BS n to UE l and noise plus interference from other BSs is larger than a threshold or not. And the threshold relies on the number of transmit antennas at BS n and the number of interferences that BS n nulls out. With this rule we can determine whether a BS should null out the interference to neighboring users. Since in this rule the number of users that a BS performs ZF to is required, we use (3.61) to check the potential UEs one by one near a BS and the determination order is from the nearest UE to the farthest within the surrounding $N_\mathrm{t}-1$ UEs. As a result the beamforming vector at each BS is determined at a time, **separately**. The following *approach 4* provides a method for *BS-specific beamforming* in a multiple cell system:

- Each BS communicates with neighboring BSs to exchange the location information of UEs in order to determine the $N_\mathrm{t}-1$ nearest UEs in neighboring cells (referred to as *victim UE*);

- Each UE measures the noise and received interference power level and transmit this information to its serving BS and this information is further conveyed to the BS whose *victim UEs* include this UE;

- Each BS determines whether it should perform ZF to the *victim UEs* using (3.61) and the determination order is from the nearest *victim UE* to the farthest. Notice that m in (3.61) should consider the *victim UEs* which the BS performs ZF to in the previous determination process;

- Each UE is informed by its serving BS which beamforming schemes have been taken by neighboring BSs, i.e., whether neighboring BSs need to null out the interference to this UE. In case of limited feedback, correspondingly the UE feeds back CSI according to the *bit partitioning algorithm II*;

- The BSs carry out the corresponding beamforming strategy.

This approach should be updated for a period of time which depends on the variation of noise and interference power of each UE. If the noise and interference condition does not

change abruptly, the update period of *approach 4* should be considerably large without much rate loss.

3.4.4 Simulation results and analysis

In this subsection we show some simulation results in the 57-cell system depicted in Figure 3.17. The channel model is the same as in Section 3.3.4. The small-scale fading is assumed to be Rayleigh distributed and the received power at a distance of d is given by (3.45). The number of transmit antennas at the BSs is 3, which means that each BS can maximally cancel the interference to 2 users. For each iteration only one user is uniformly dropped within each cell. The inner 21 cells surrounded by the red dashed line are evaluated for a fair comparison.
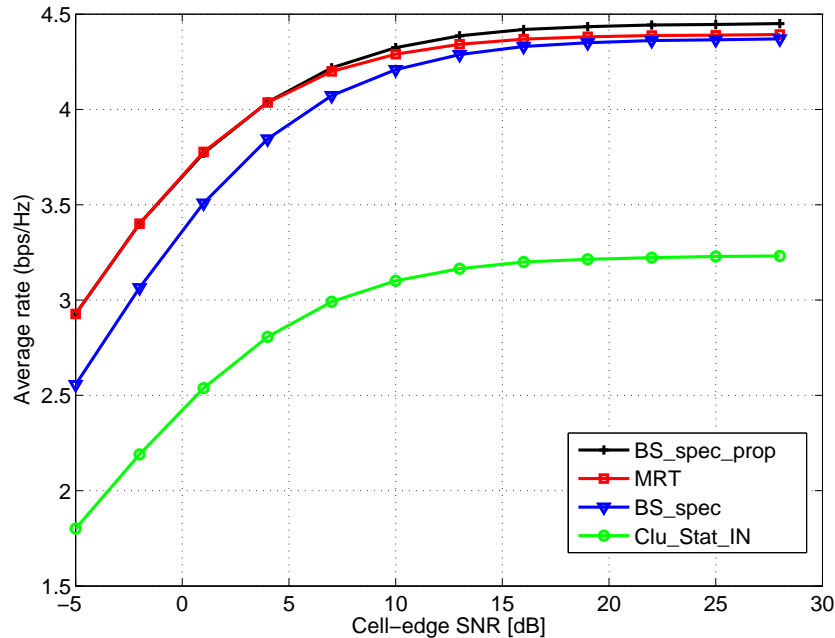
Figure 3.19: Average user data rate comparison of different beamforming approaches in a 57-cell system with full CSI

Figure 3.19 shows the performance comparison of the average user data rate using different beamforming strategies and full CSI is assumed to be available at the BSs. *BS_spec_prop* is the BS-specific beamforming scheme given by *approach 4*. *MRT* is the non-cooperative MRT scheme. In order to illustrate the advantage of *approach 4* in adaptively selecting IN *victim UEs*, we implement *BS_spec* which lets each BS always null out the interference to the $N_t - 1$ *victim UEs*. *Clu_Stat_IN* is the static clustering scheme which obviously underperforms other schemes. With the least feedback overhead

Figure 3.20: Cell-edge user data rate comparison of different beamforming approaches in a 57-cell system with full CSI

and least complexity the MRT beamforming performs really satisfactorily in this multi-cell system. It outperforms BS_spec even in the high SNR regime, indicating that the BS-specific approach without sophisticated IN user selection design is not worth being implemented. The proposed approach checks for each *victim UE* whether it is necessary to null out the interference. Therefore, when the SNR is low, it performs similarly to the MRT scheme. When the SNR is high, users incur high interference from neighboring cells and *approach 4* outperforms the MRT scheme slightly by canceling the interference to some users. Following simulation results will show that the gain of the proposed approach becomes higher when the number of transmit antennas is larger. Moreover, the performance difference at high SNR between BS_spec_prop and BS_spec also implies that it is also not necessary to always perform IN to all *victim UEs* around each BS.

Figure 3.20 shows for the same scenario the cell-edge user data rate, which is the 5% point of CDF of the user data rate. Because the BS-specific approaches are designed particularly for cell-edge users, both BS-specific approaches outperform the MRT scheme at high SNR. At the cell-edge SNR of 25 dB BS_spec gains 10% more user data rate in comparison with MRT and BS_spec_prop can have 15% improvement. Notice that from an SNR of 0 dB we can apparently see the improvement of the proposed approach. This reveals that even in the low SNR regime where cell-edge users usually receive low

power from the serving BSs, it is beneficial to use part of the serving power for nulling out the interference to neighboring users who experience non-negligible interference.
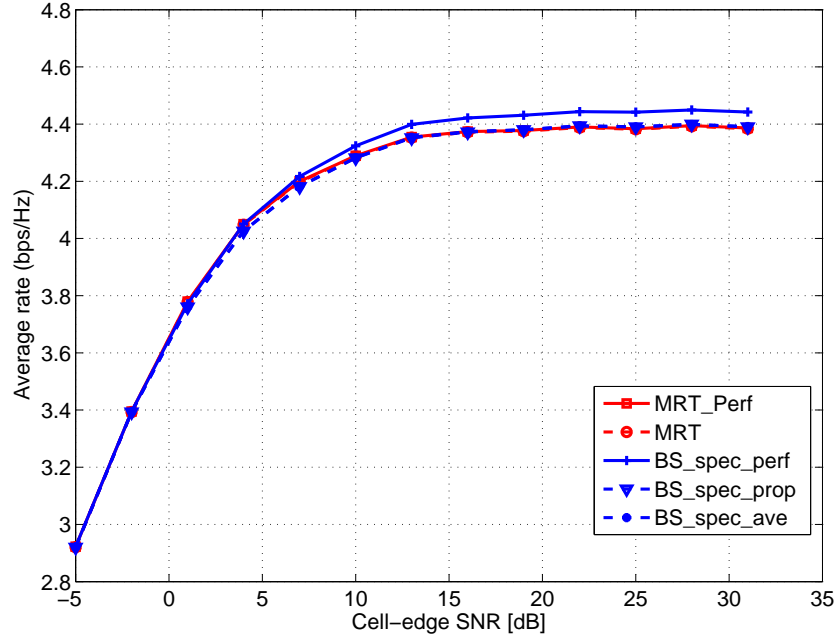
Figure 3.21: Average user data rate comparison of different beamforming approaches in a 57-cell system with quantized CSI

Next, we compare different beamforming approaches with imperfect CSI. The number of quantization bits available at each user is 18. In Figure 3.21 *BS_spec_prop* is *approach 4* with *bit partitioning algorithm II. BS_spec_ave* is *approach 4* with equal bit partitioning, i.e., after determination of IN *victim UEs* at each BS, in step 4 of *approach 4* each UE quantizes the desired channel and interfering channel using equal bits. The proposed *approach 4* with full CSI *BS_spec_perf* outperforms other four schemes and there is no distinct difference among the other four schemes. This means that 18 bits are sufficient for MRT to keep high quantization accuracy because only the desired channel needs to be quantized. However, the MRT scheme doesn't care about the cell-edge users even if they have severe interference. In Figure 3.22 we plot the CDF of the user data rate at the cell-edge SNR of 25 dB with these five approaches used in Figure 3.21. The curves using BS-specific approach has a higher slope compared with the curves using MRT in the area where most of the user data rate lies in (approximately 4.5 bps/Hz, corresponding to the probability of 0.6). This implies that most of the data rates using BS-specific approach are more close to the rate of 4.5 bps/Hz, whereas the data rates using the MRT scheme spread over a wider data rate range, although both schemes have similar average

data rate. Figure 3.22 shows that the BS-specific approach also guarantees some fairness between the users.
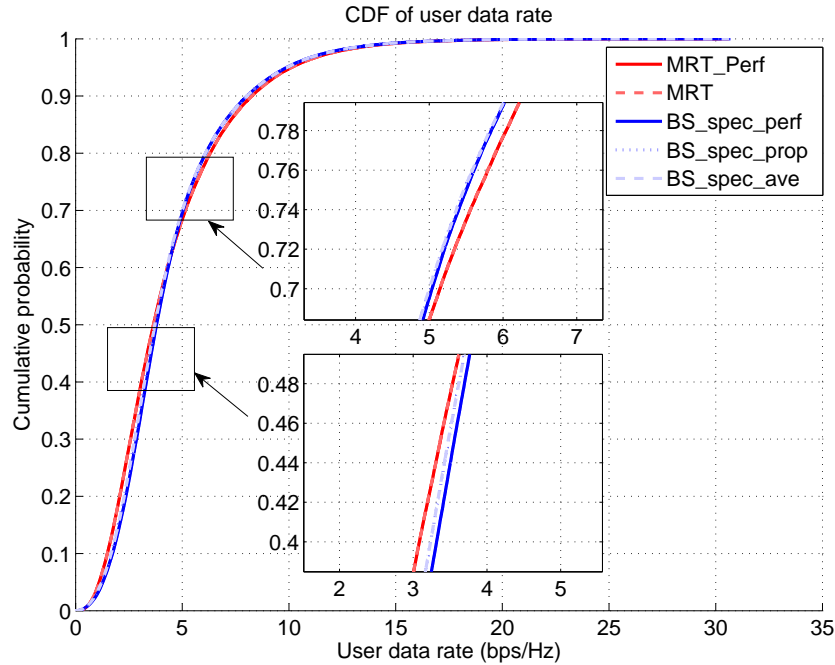
Figure 3.22: CDF of user data rate at the cell-edge SNR of 25 dB in a 57-cell system with quantized CSI

Figure 3.23 illustrates the cell-edge user data rate using the MRT and BS-specific approaches with quantized CSI. By canceling the interference to some cell-edge users the BS-specific approaches perform superior to the MRT scheme. With 18 quantization bits at each user the BS-specific approach has a degradation of 0.05 bps/Hz compared to the one with perfect CSI at the SNR of 30 dB. Another observation is that the proposed *bit partitioning algorithm II* has similar performance to the algorithm with equal bit allocation. The reason for this similarity is: when a user is near the cell-edge, the desired power is similar to the interference power from neighboring cells because we assume that each BS has the same transmit power and the large-scale fading model depends only on the distance. Therefore, *bit partitioning algorithm II* assigns almost the same quantization to each link.

Performance of *approach 4* with different numbers of transmit antennas

As mentioned in the analysis of Figure 3.19 *approach 4* provides only slight improvement compared with the MRT scheme for the average user data rate. Since the number of transmit antennas N_t is 3, there are not sufficient degrees of freedom for the BSs to make

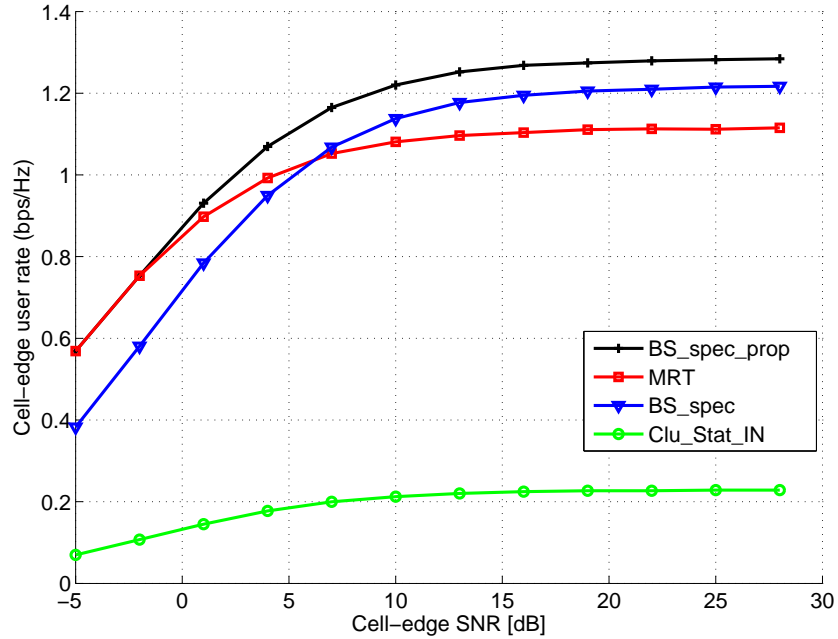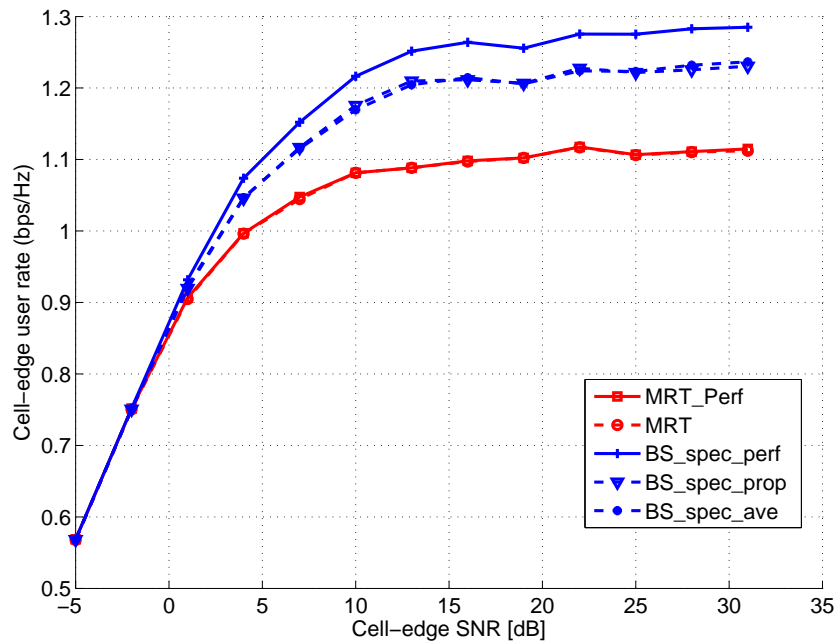**Figure 3.23:** Cell-edge user data rate comparison of different beamforming approaches in a 57-cell system with quantized CSI
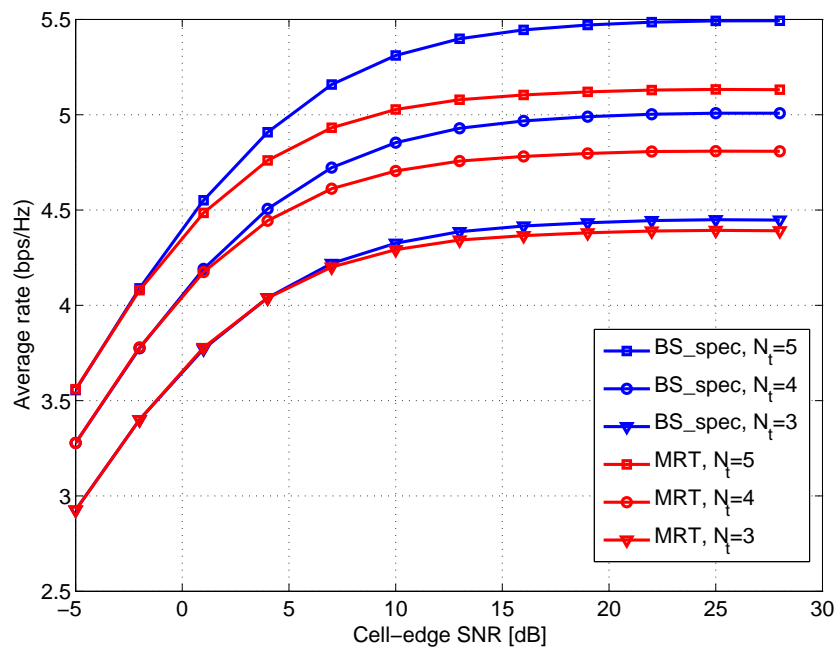
Figure 3.24: Average user data rate comparison with different numbers of transmit antennas in a 57-cell system
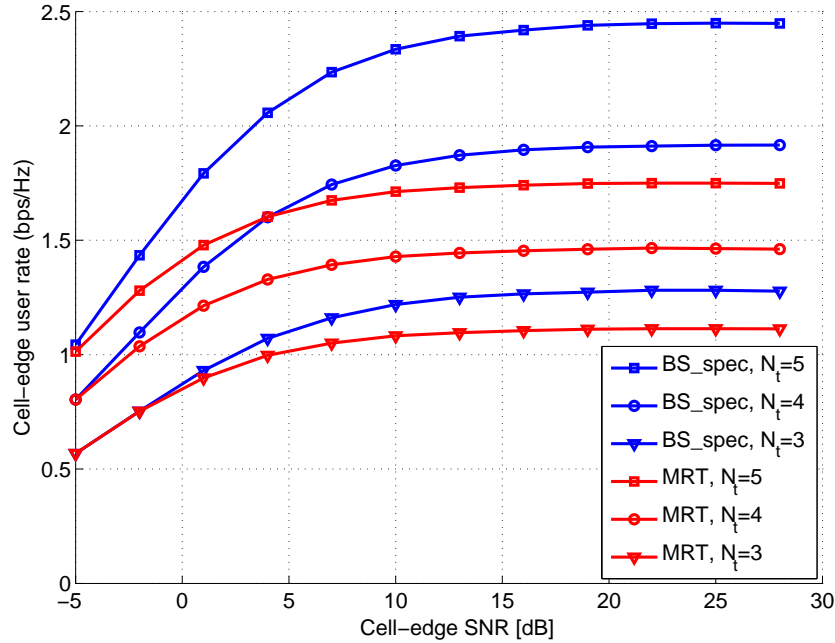
Figure 3.25: Cell-edge user data rate comparison with different numbers of transmit antennas in a 57-cell system

use of. On the other hand, the *transmission scheme determination rule* (3.61) depends on the interference and noise power level as well as N_t. Hence, in this part we simulate the same 57-cell environment and set the number of transmit antennas to 3, 4 and 5, respectively. We assume that full CSI is available at BSs. Figure 3.24 and Figure 3.25 illustrate the results using BS-specific and MRT schemes. A first observation is that the performance improvement is getting larger when N_t is larger for both the average rate and cell-edge user rate. This is because larger N_t provides more spatial degrees of freedom such that more advantage of *approach 4* can be exploited. With $N_t = 5$ the proposed scheme can outperform MRT by 0.4 bps/Hz at the SNR of 25 dB, which is approximately an improvement of 8%. For cell-edge users this improvement using the proposed approach is enlarged. For $N_t = 5$ the proposed scheme has a gain of 0.7 bps/Hz at the same cell-edge SNR, which is an enhancement of almost 40% compared to the MRT scheme. Moreover, for 5G systems much more transmit antennas are supported [8], so that it is expected to have much more gain with this proposed approach.

3.5   Conclusion

In this chapter the performance in the CoMP-CB system with limited feedback using ZF and MRT beamforming was analyzed. Firstly, we considered a two-cell system where the

two BSs can cooperate with each other. A bit partitioning algorithm was proposed which allocates the limited feedback bits available at each user for quantizing the serving and interfering channels. Simulation results show that adaptive partitioning can improve the system sum-rate especially in the OCI-dominated scenario. A cooperative beamforming strategy was also proposed which only requires the information about INR from the users. The presented strategy was proved to outperform the conventional schemes (ZF and MRT) and is suitable for different interference scenarios. Secondly, we proposed a bit partitioning algorithm for a three-cell system, which can be used in a larger system with cell cluster size of 3. A separated approach for cooperative beamforming was then introduced. In this approach each BS determines the beamforming vector separately and this does not need a joint optimization, which may have high complexity. The proposed bit partitioning algorithm was then extended to a general multiple cell system and this algorithm can be combined with the proposed BS-specific approach, in which a threshold is given to determine whether it is worth to cancel the interference to the neighboring users near a BS in terms of maximizing the achievable rate of the users. Simulation shows that the proposed BS-specific approach improves the data rate compared with the MRT scheme with and without limited feedback, especially for cell-edge users, revealing the advantage of the CoMP concept.

CHAPTER 4

Dynamic clustering with limited backhaul rate for CoMP-JT system

In Chapter 3 the limited feedback problem in the CoMP-CB system was discussed. It was shown that sophisticated design of the feedback bits can improve the system performance dramatically. Similar to a CoMP-CB system, the CoMP-JT system (described in Section 3.1.1) also exploits coordination among the BSs, where full data sharing exists among multiple network nodes on top of just CSI. Assuming theoretically infinite number of distributed antennas, one could transmit to any mobile terminal (MT) with the intended signal adding up at its position, while generating no interference for the other MTs [19, 48]. In this case, all the propagation links are exploited to carry useful data information, resulting in a more powerful cooperation among the BSs. Although CoMP-JT is a promising technique, which aims at directly improving the spectral efficiency, particularly for the cell-edge users, many issues still exist making the implementation challenging. Except the high bandwidth and low latency BS inter-connectivity [67], the feedback overhead is more severe in CoMP-JT systems and therefore these factors should be well handled.

4.1 Background and Motivation

In order to support full functionalities of the JT system, additional overhead/signaling compared to non-cooperating systems or the CoMP-CB system are expected. The overhead/signaling will result to a DL overhead increase due to multiple CSI-RSs (reference signals), UL overhead increase due to CSI measurement related to multiple points, UL overhead increase due to sounding reference signal (SRS) transmissions related to multiple points, and additional data sharing among the eNBs (evolved NodeBs) [7]. 3GPP has defined the X2 interface, as shown in Figure 4.1, which aims at connecting neighboring eNBs in a peer to peer fashion to facilitate handover and provide a means for coordination of resources [5, 87]. The X2 interface has many functions and the two essential functions are inter-cell interference coordination and data exchange for self-optimization. The inter-cell interference coordination function allows keeping the ICI under control. For UL this function allows indicating the UL interference overload such that neighboring eNBs can coordinate with each other to mitigate the mutual interference caused

by the UL radio resource allocation. For DL this function allows an eNB to inform its neighboring eNBs about DL power restrictions for interference aware scheduling. The data exchange function enables the X2 interface to carry user plane data and it is this function which dictates the bandwidth requirement [1].
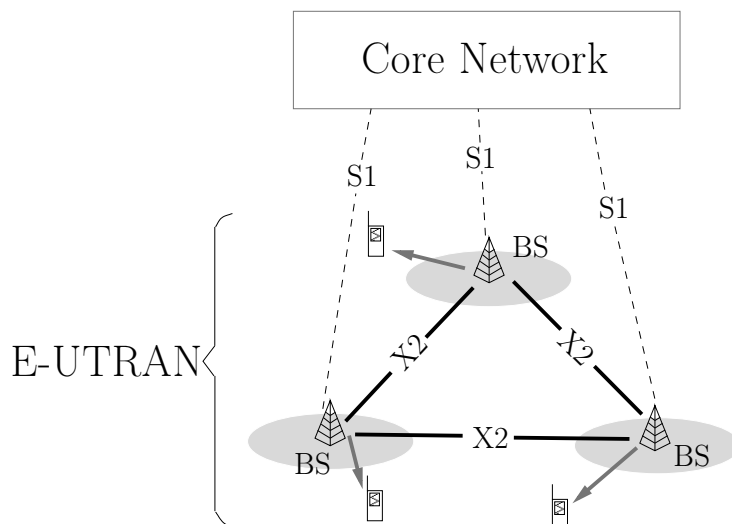
Figure 4.1: Architecture of evolved UMTS Terrestrial Radio Access Network (E-UTRAN) with X2 interface

A lot of research has been done on the topic of cell cooperation in multi-cell systems. However, most of them have made the assumption that the channel information or data is available and shared in the cooperation set to some extent with a zero-delay and infinite bandwidth X2 interface connection [51, 88], which is quite unrealistic. The practical limitation of the backhaul connectivity has prevented the efficient implementation of the cooperation schemes. The backhaul issue has been addressed in previous literature. In [124] some important factors restricting the promised potential of CoMP systems were analyzed including the imperfect backhaul links with limited capacity and latency. [87] modeled the X2 interface with a system level simulator and analyzed the influence of the X2 delay on the performance of the CoMP scheduler. A sparse multicell linear receive-filter design problem was formulated in [64], where a dynamic clustered cooperation was proposed aiming at reduced backhaul overhead. A comprehensive survey of the 5G backhaul paradigm was made in [62]. The hidden advantages and shortcomings, as well as the state-of-the-art research and solutions of the backhaul were explained. The unsolved backhaul challenges were also raised in the survey. Some more works considering the constrained backhaul have been mentioned in the references of [62, 64, 87], such as [134, 135, 138].

In order to overcome the backhaul challenge due to the ever-increasing demand for the data traffic, one straightforward way is to increase the capacity of the back link by using more stable and powerful backhaul cables, such as high-speed optical fibers. In spite of no technical challenges this approach causes high costs to the operators. Another method is to decrease the backhaul overhead while satisfying QoS of the users. An efficient and practical way to limit the number of BSs that exchange information is clustering. In a clustered cellular network, as long as the QoS of the users is fulfilled, the cluster size should be as small as possible in order to limit the cooperation set and information exchanged in the backhaul can be controlled. The CoMP-JT system has been intensively investigated and has shown its potential in increasing the overall cellular throughput. However, there is a lack of practical dynamic clustering method, particularly in the case of full CSI not available at the transmitter.

In general, clustering schemes can be specified by the cell/BS or UE. With respect to cell-specific cluster selection, it is distinguished between static and dynamic clustering algorithms. Static clustering is determined by the operation and maintenance system based on geographical criteria, such as position of BSs and the morphology of the surroundings. Dynamic clustering is determined relying on measurements, such as UE location or link quality. In a UE-specific selection the serving BS of a certain UE could request cooperation from other BSs, so that the UE always has the optimal cluster [80]. The dynamic clustering has attracted increased attention in the past few years. [92] has proposed a greedy algorithm to form the clusters with fixed cluster size, which first selects randomly a not assigned BS and then finds BSs maximizing the joint capacity until the specified cluster size is reached. In [113] a pattern selection algorithm was provided, where some patterns are first defined and the one with maximal throughput is selected. An exhaustive search approach was given in [90] based on the long term CSI, which is resilient to small-scale CSI inaccuracies. [26, 27] considered multiple antenna UEs and designed a two-step method to find the clusters: firstly a set of candidate clusters based on the large-scale channel fading are defined; then a weighted sum rate based on the small-scale fading is estimated for each cluster and a set of non-overlapping clusters are scheduled. [25] considered additionally a more realistic scenario, where only partial CSI (only channel links with an SNR over a threshold are fed back) is available at the BSs, and proposed a simple greedy clustering algorithm. 3GPP [97, 98] also discussed the possible clustering schemes, pointing out that adaptive clustering methods outperform the static clustering one. In [119] the clustering optimization problem was first reformulated as a set partition problem (SPP) or set covering problem (SCP) depending on whether the clusters are disjoint or not. Then a heuristic adaptive clustering algorithm was proposed which minimizes a cost function and this cost function is selected proportional to the size

of the clusters and inversely proportional to the radio condition within the clusters. The interference was not taken into account in the algorithm in [119] and it was mentioned that the performance of the adaptive clustering is very sensitive to the choice of the cost function. Therefore, the design of the adaptive clustering is still an important open topic. In this section a dynamic non-overlapping clustering scheme is proposed by solving the SPP.

4.2   Dynamic clustering scheme

4.2.1   System model

In this section we consider a CoMP-JT multi-cell system with totally K_B BSs and K_U users as shown in Figure 4.2. Each BS is equipped with N_t transmit antennas and each user has a single receive antenna. In a JT system with full cooperation all 21 BSs store the data for each user and can seamless communicate with each other via the backhaul. Therefore, the entire system behaves like a broadcast system with antennas deployed over the whole area, which can be seen as a performance upper bound in the following simulations. In practice a clustered method is usually considered in order to limit the amount of information exchange. Figure 4.2 shows a simple fixed cluster example with a cluster size K_{cl} of 3. In this chapter only non-overlapped cluster methods are discussed.
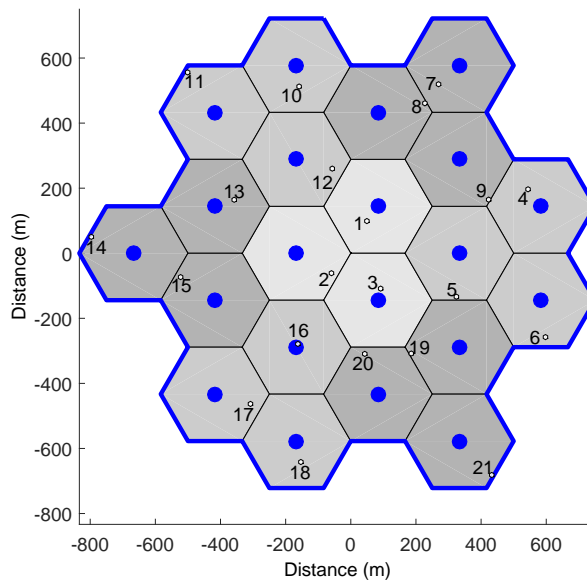
Figure 4.2:   A multi-cell MISO JT system with hexagonal cell layout

Full cooperation

Ideally, in a JT-system with fully cooperating BSs the received signal at each user is the accumulation of signals from all BSs. The received signal at UE k can be calculated as

$$y_k = \sqrt{P_k}\mathbf{h}_k\mathbf{w}_k x_k + \sum_{l=1, l\neq k}^{K_{\mathrm{U}}} \sqrt{P_l}\mathbf{h}_k\mathbf{w}_l x_l + n_k, \tag{4.1}$$

where $\mathbf{h}_k$ represents the $1 \times N_{\mathrm{t}}K_{\mathrm{B}}$ accumulated channel to UE k and P_k is the transmit power allocated to UE k. In this system the $N_{\mathrm{t}}K_{\mathrm{B}} \times 1$ beamforming vector $\mathbf{w}_k$ should be designed jointly by all the BSs, which is the main challenge and implementation difficulty in the CoMP-JT system.

Partial cooperation

In a clustered JT-system with partially cooperating BSs a user is served by only a limited number of BSs. Assume that the number of clusters in the whole system is C. The number of BSs and the number of users served in each cluster are denoted as $K_{\mathrm{B}}^{(c)}$ and $K_{\mathrm{U}}^{(c)}$. The received signal at UE k in cluster c is calculated as

$$\begin{aligned} y_k^{(c)} &= \sqrt{P_k^{(c)}}\mathbf{h}_k^{(c,c)}\mathbf{w}_k^{(c)} x_k^{(c)} + \sum_{l=1, l\neq k}^{K_{\mathrm{U}}^{(c)}} \sqrt{P_l^{(c)}}\mathbf{h}_k^{(c,c)}\mathbf{w}_l^{(c)} x_l^{(c)} \\ &\quad + \sum_{c'=1, c'\neq c}^{C} \mathbf{h}_k^{(c,c')} \sum_{l=1}^{K_{\mathrm{U}}^{(c')}} \sqrt{P_l^{(c')}}\mathbf{w}_l^{(c')} x_l^{(c')} + n_k^{(c)}, \end{aligned} \tag{4.2}$$

where the second term and the third term indicate the intra-cluster interference and the inter-cluster interference, respectively. $\mathbf{h}_k^{(c,c')} = [\mathbf{h}_{k,1}^{(c,c')}, \mathbf{h}_{k,2}^{(c,c')}, \cdots, \mathbf{h}_{k,K_{\mathrm{B}}(c')}^{(c,c')}]$ represents the accumulated channel vector from the BSs in cluster c' to UE k in cluster c and each element in $\mathbf{h}_k^{(c,c')}$ is given by the $1 \times N_{\mathrm{t}}$ channel coefficients from a single BS in cluster c'. $P_k^{(c)}$ is the transmit power allocated to UE k in cluster c and $\mathbf{w}_k^{(c)}$ is the beamforming vector designed by cluster c. The additive white Gaussian noise at UE k in cluster c is $n_k^{(c)}$ with values distributed according to $\mathcal{CN}(0, N_0)$. With the average symbol power $\mathbb{E}\{|x_k^{(c)}|^2\} = 1$ the received SINR at UE k in cluster c is calculated as:

$$\gamma_k^{(c)} = \frac{P_k^{(c)}|\mathbf{h}_k^{(c,c)}\mathbf{w}_k^{(c)}|^2}{N_0 + \sum\limits_{l=1, l\neq k}^{K_{\mathrm{U}}^{(c)}} P_l^{(c)}|\mathbf{h}_k^{(c,c)}\mathbf{w}_l^{(c)}|^2 + \sum\limits_{c'=1, c'\neq c}^{C} \sum\limits_{l=1}^{K_{\mathrm{U}}^{(c')}} P_l^{(c')}|\mathbf{h}_k^{(c,c')}\mathbf{w}_l^{(c')}|^2}. \tag{4.3}$$

Transmit Beamforming Strategies

The transmit beamforming strategies for a JT system in this chapter is similar to (3.5) and (3.6) for the CoMP-CB system.

- **ZF beamforming**: ZF beamforming is used to cancel the intra-cluster interference so that the second term in (4.2) will be zero if perfect channel state information is available at the BSs. We assume that $\mathbf{H} = ((\mathbf{h}_1^{(c,c)})^{\mathrm{H}}, \cdots, (\mathbf{h}_{k-1}^{(c,c)})^{\mathrm{H}}, (\mathbf{h}_{k+1}^{(c,c)})^{\mathrm{H}}, \cdots, (\mathbf{h}_{K_{\mathrm{U}}^{(c)}}^{(c,c)})^{\mathrm{H}})^{\mathrm{H}}$ is the equivalent $(K_{\mathrm{U}}^{(c)} - 1) \times N_{\mathrm{t}} K_{\mathrm{B}}^{(c)}$ channel matrix from all the BSs in cluster c to users in c except UE k. The beamforming vector for UE k designed by the BSs in c is given by [130]

$$\mathbf{w}_k^{(c)} = \frac{(\mathbf{I}_{N_{\mathrm{t}} K_{\mathrm{B}}^{(c)}} - \mathbf{P})(\mathbf{h}_k^{(c,c)})^{\mathrm{H}}}{||(\mathbf{I}_{N_{\mathrm{t}} K_{\mathrm{B}}^{(c)}} - \mathbf{P})(\mathbf{h}_k^{(c,c)})^{\mathrm{H}}||}, \tag{4.4}$$

where $\mathbf{P} = \mathbf{H}^{\mathrm{H}}(\mathbf{H}\mathbf{H}^{\mathrm{H}})^{-1}\mathbf{H}$ and $\mathbf{I}_{N_{\mathrm{t}} K_{\mathrm{B}}^{(c)}}$ is the identity matrix.

- **MRT beamforming**: without suppression of the intra-cell interference, the beamforming vector can be simply designed to maximize the received power of the desired signal:

$$\mathbf{w}_k^{(c)} = (\mathbf{h}_k^{(c,c)})^{\mathrm{H}}/||(\mathbf{h}_k^{(c,c)})^{\mathrm{H}}||. \tag{4.5}$$

To show the impact of clustering in CoMP-JT system we consider the 21-cell system in Figure 4.2. The ZF beamforming scheme (4.4) is performed within each cluster. The per-BS power constraint is considered:

$$\sum_{k=1}^{K_{\mathrm{U}}^{(c)}} ||\mathbf{w}_{k,b}^{(c)}|| \leq P_{\mathrm{B}}, \ b = 1, 2, \cdots, K_{\mathrm{B}}^{(c)}, \ c = 1, 2, \cdots, C, \tag{4.6}$$

where $\mathbf{w}_{k,b}^{(c)}$ are the $N_{\mathrm{t}} \times 1$ beamforming elements at BS b for UE k in cluster c. After design of each beamforming vector and in order to fulfill the per-BS power constraint (4.4) is scaled by the maximal transmit power of the BSs in each cluster. This beamformer design guarantees that the users within one cluster are assigned with equal transmit power and the ZF property is still maintained.

Figure 4.3 shows the average user data rate when different cluster sizes are used. In this system the number of transmit antennas at the BS is 2. The reference SNR used here is defined as the maximal received signal-to-noise power ratio at the cell edge. Fixed cluster schemes are adopted for each cluster size. It can be observed that full cooperation outperforms the other clustering schemes dramatically, especially in the high SNR regime. This is because full cooperation does not suffer from the inter-user/inter-cluster interference since the interference is totally suppressed. In the high SNR regime where the whole system is interference limited, the clustering schemes are always upper bounded due to inter-cluster interference. The performance of the full cooperation scheme increases linearly with the reference SNR since full cooperation can be seen as a clustering scheme
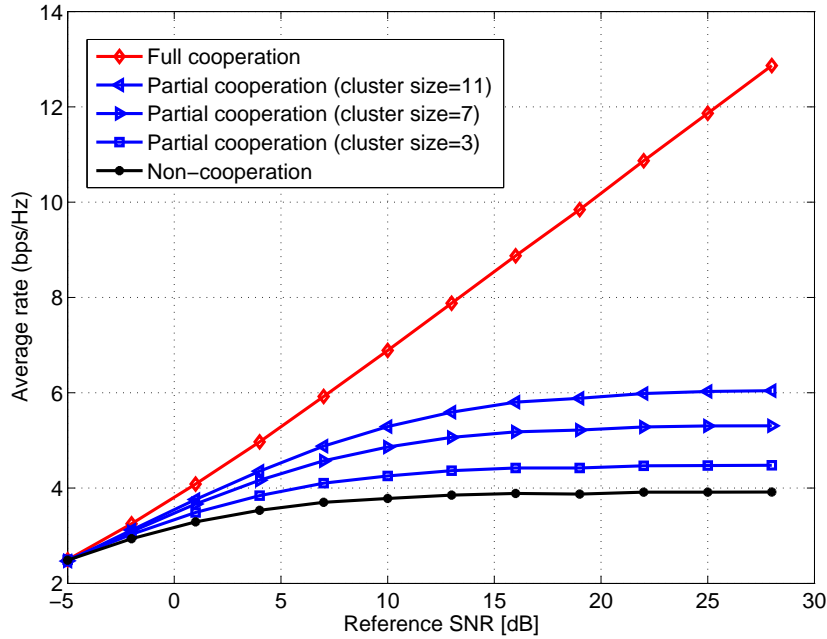
Figure 4.3: Average user data rate comparison with different cluster size in CoMP-JT system

with cluster size 21 and the intra-cluster and inter-cluster interference in (4.3) is equal to zero. The non-cooperation scheme has the worst performance because the inter-user interference is absolutely not handled. It can also be obviously seen that for the clustering schemes the larger the cluster size is, the larger is also the user rate of the system.

For clustering schemes with large clusters more information must be exchanged compared with small clusters. It was mentioned in [90, 93] that the overhead for the multi-cell cooperation is proportional to the number of BSs grouped together, i.e., the cluster size. Full cooperation requires massive information exchange among BSs and a huge feedback rate particularly for the channel information. All channel information to a user needs to be fed back to the BS and this information is either collected to a central unit or must be shared among the cooperating BSs. As can be seen there is still a large gap between the clustering scheme and full cooperation, when the interference in the system is not negligible.

4.2.2 Clustering problem formulation

In this section non-overlapping clusters are considered and we assume that all cells participate in the data transmission. Each cell in this system must be and can only be in one cluster, i.e., the optimal clusters cover the whole system. Assume that $\mathcal{S} = \{1, 2, \cdots, N_{ce}\}$ is the set of all cell indices, where N_{ce} is the number of cells in this system and is the same

as the number of BSs K_B. We first consider a fixed cluster size of K_cl. The total number of cluster candidates is $K_\mathrm{cc} = \binom{N_\mathrm{ce}}{K_\mathrm{cl}}$. Similar to [119], we introduce the characteristic matrix $\mathbf{A}$

$$\mathbf{A} = \left\{ \begin{array}{ccc} a_{11} & \cdots & a_{1K_\mathrm{cc}} \\ \vdots & \ddots & \vdots \\ a_{N_\mathrm{ce}1} & \cdots & a_{N_\mathrm{ce}K_\mathrm{cc}} \end{array} \right\} \tag{4.7}$$

with entries a_{ij}

$$a_{ij} = \begin{cases} 1, & \text{if cell } i \text{ is included in cluster } j \\ 0, & \text{otherwise} \end{cases}. \tag{4.8}$$

Note that once the cell topography of a cellular system is given, $\mathbf{A}$ is fixed. Since in a practical implementation the grouping of non-adjacent cells into a cluster is usually not efficient, the amount of the cluster candidates can be dramatically reduced. In addition a decision variable u_j is defined, which indicates if cluster j belongs to the final solution (the final solution consists of a subset of the whole cluster candidates) or not

$$u_j = \begin{cases} 1, & \text{if cluster } j \text{ is in the final solution} \\ 0, & \text{otherwise} \end{cases}. \tag{4.9}$$

Taking the aforementioned assumptions into account, the clustering problem can be formulated as

$$\begin{aligned} \min \quad & \sum_{j \in \mathcal{S}_\mathrm{cc}} c_j u_j \\ \text{subject to} \quad & \sum_{j \in \mathcal{S}_\mathrm{cc}} a_{ij} u_j = 1 \qquad \text{for } i = 1, 2, \cdots, N_\mathrm{ce} \\ & u_j \in \{0,\ 1\} \end{aligned} \tag{4.10}$$

where $\mathcal{S}_\mathrm{cc} = \{1, 2, \cdots, K_\mathrm{cc}\}$ is the index set of all cluster candidates. c_j is the cost variable/function of cluster j. The objective of (4.10) is to find the optimal decision variable u_j, which minimizes the overall costs of the whole system. The condition simply means that each cell should be involved in one and only one cluster in the final solution. Therefore, (4.10) belongs to the set partition problem, known as a special case of the set covering problem with equality constraints [24, 45, 82]. Now the problem lies on how to choose the cost function c_j and how to solve the SPP. As mentioned in [80] the performance of the adaptive clustering is very sensitive to the choice of the cost function and hence for different requirements the cost function should be chosen accordingly. On the other side, the partition problem is an NP-complete (nondeterministic polynomial time) problem and is difficult to solve. [24] has shown some methods, such as implicit enumeration and traditional cutting plane methods. In this section a *modified enumerative algorithm* is used and analyzed.

4.2.3 Implicit enumeration algorithm

As the SPP is an NP-complete problem and the problem size has substantial impact on the complexity of the algorithm, it is worth reducing the characteristic matrix $\mathbf{A}$ before the algorithm. Sometimes this reduction makes the optimization algorithm considerably easier. Some reduction rules are listed in Appendix E. In this section we assume that the cluster size is fixed to 3 and only the adjacent cells can form a cluster. Due to the special structure of the characteristic matrix $\mathbf{A}$ under this assumption, the reduction rule 1-4 in Appendix E will not further reduce the size of $\mathbf{A}$. One can only benefit from the reduction rule 5 by excluding some cell edge clusters. For instance, in Figure 4.2 the cluster containing cell 4, 8 and 9 cannot be in the optimal solution because otherwise cell 7 cannot be included in any cluster.

To start with, the rows $\mathbf{r}_i$ and the columns $\mathbf{a}_j$ of $\mathbf{A}$ are first permutated:

1. Rearrange the rows of $\mathbf{A}$ so that if $i \leq k$ then $\sum_{j \in \mathcal{S}_{cc}} a_{ij} \leq \sum_{j \in \mathcal{S}_{cc}} a_{kj}$;

2. The columns $\mathbf{a}_j$ of $\mathbf{A}$ are grouped in lists, with $\mathbf{a}_j$ being in list i if and only if $a_{1j} = \cdots = a_{i-1,j} = 0$ and $a_{ij} = 1$. An illustration of the rearranged $\mathbf{A}$ is shown in Figure 4.4;

3. Within each list the columns $\mathbf{a}_j$ are ordered by some heuristic criterion [24]: in order of nondecreasing cost c_j with ties broken arbitrarily.
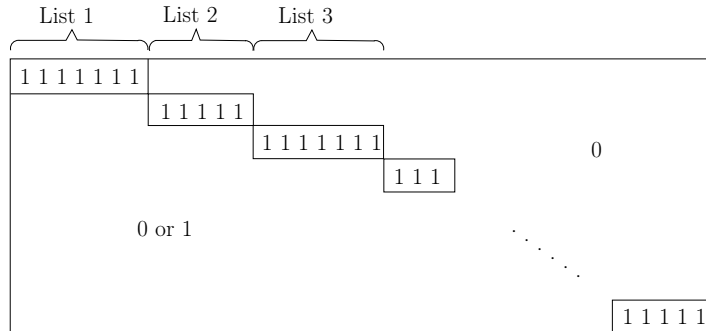
Figure 4.4: Rearranged $\mathbf{A}$ with lists

Assume that $\mathcal{M}$ and $\mathcal{N}$ are the row and column index set of the reduced $\mathbf{A}$. Denote by $\mathcal{W}$ the index set of a partial solution: $\mathcal{W} = \{j | j \in \mathcal{N} \text{ and } u_j = 1 \text{ in the partial solution}\}$, by $\mathcal{T}$ the row index set covered by the partial solution: $\mathcal{T} = \{i | i \in \mathcal{M} \text{ and } \sum_{j \in \mathcal{W}} a_{ij} = 1\}$. Let $z(\mathcal{W}) = \sum_{j \in \mathcal{W}} c_j$ be the total costs of the partial solution and $\bar{z}$ be the cost of the best solution found so far. In addition let $\mathcal{V} = \mathcal{M} \backslash \mathcal{T}$. Then the algorithm proceeds as follows.

- **Step 1** (initialization): Perform the reductions to obtain the reduced characteristic matrix and rearrange the rows and columns. Set $\mathcal{W} = \mathcal{T} = \varnothing$, $z(\mathcal{W}) = 0$, $\mathcal{V} = \mathcal{M}$ and $\overline{z} = +\infty$.

- **Step 2** (choose the next list): Let $\mathcal{V} = \mathcal{M} \backslash \mathcal{T}$ and $i^* = \min\{i | i \in \mathcal{V}\}$. Set an indicator at the top (lowest cost column) of list i^*. Then go to Step 3.

- **Step 3** (build the partial solution): Beginning at the indicated position in list i^*, examine all columns of the list in order of nondecreasing cost. If a column j is found such that $a_{ij} = 0$ for $\forall\, i \in \mathcal{T}$ and $z(\mathcal{W}) + c_j < \overline{z}$, go to Step 5. If list i^* is exhausted, go to Step 4.

- **Step 4** (backtrack): If $\mathcal{W} = \varnothing$, terminate with the current best solution found (if any). Otherwise, let t be the last column index included in $\mathcal{W}$. Set $\mathcal{W} = \mathcal{W} \backslash \{t\}$, $z(\mathcal{W}) = z(\mathcal{W}) - c_t$ and $\mathcal{T} = \mathcal{T} \backslash \{i | i \in \mathcal{M} \text{ and } a_{it} = 1\}$. Let i^* be the list where column t is stored. Set an indicator at the next column of t in list i^* and remove the previous indicator. Go to Step 3.

- **Step 5** (test new solution): Set $\mathcal{W} = \mathcal{W} \cup \{j\}$, $z(\mathcal{W}) = z(\mathcal{W}) + c_j$ and $\mathcal{T} = \mathcal{T} \cup \{i | i \in \mathcal{M} \text{ and } a_{ij} = 1\}$. If $\mathcal{T} = \mathcal{M}$, a better solution is found and set $\overline{z} = z(\mathcal{W})$. Then go to Step 4. Otherwise, go to Step 2.

Note that the aforementioned algorithm only works for non-negative costs. In case of negative costs, the *modified enumerative algorithm* can be given by reformulating step 3 of the original implicit enumeration algorithm:

- **Step 3** (build the partial solution): Beginning at the indicated position in list i^*, examine all columns of the list in order of nondecreasing cost. Depending on if a column j can be found such that $a_{ij} = 0$ for $\forall\, i \in \mathcal{T}$, do the followings:

  - column j found: If $\mathcal{T} \cup \{i | i \in \mathcal{M} \text{ and } a_{ij} = 1\} = \mathcal{M}$ and $z(\mathcal{W}) + c_j \geq \overline{z}$, go to Step 4. Otherwise, go to Step 5.

  - column j not found: Go to Step 4.

4.2.4   A large-scale fading based dynamic clustering approach

In this chapter the fading channel model introduced in Section 2.2.1 is used. The small-scale fading is assumed to be Rayleigh distributed and the average received power at a distance of d according to the path loss model (2.1) is

$$P_{\mathrm{r}} = P_0 \left[\frac{d_0}{d} \right]^\gamma, \tag{4.11}$$

where d_0 is the reference distance and P_0 is the received power at d_0. The path loss exponent γ is 3.7.

The objective of this section is to maximize the sum-rate of the whole system

$$\sum_{c=1}^{C} \sum_{k=1}^{K_{\mathrm{U}}^{(c)}} \log_2(1 + \gamma_k^{(c)}) \tag{4.12}$$

where $\gamma_k^{(c)}$ is the received SINR at UE k in cluster c given in (4.3). Since the *modified enumerative algorithm* allows negative cost functions, maximizing the positive sum-rate is equivalent to minimizing the corresponding negative rates. Here we introduce the negative rate based on the large-scale fading as the cost function for the cluster candidate c:

$$-\sum_{k=1}^{K_{\mathrm{U}}^{(c)}} \log_2\left(1 + \frac{\sum\limits_{b \in \mathcal{S}^{(c)}} P_{\mathrm{r}}^{(k,c,b)}}{N_0 + \sum\limits_{b \in \mathcal{S} \backslash \mathcal{S}^{(c)}} P_{\mathrm{r}}^{(k,c,b)}}\right), \qquad c \in \mathcal{S}_{\mathrm{cc}}. \tag{4.13}$$

In this case the average received power is determined by large-scale fading. And the large-scale fading is assumed to be only affected by the path loss, i.e., the distance between the BS and UE, given that the power received at a distance of d_0 and the path loss exponent are fixed. In practice the shadowing may also impact the average received power. $P_{\mathrm{r}}^{(k,c,b)}$ is the average received power at UE k in cluster c from BS b, which can be measured by the UE itself or calculated according to the geographical information of the UE. $\mathcal{S}^{(c)}$ is the set of BS indices in cluster c and $K_{\mathrm{U}}^{(c)}$ is the number of UEs served in cluster c. Maximizing the sum-rate of the system (4.12) is equivalent to minimizing the inverse sum-rate, which is always negative.

The proposed *large-scale fading based dynamic clustering approach* is described in the following:

- Each UE measures the large-scale fading information from each BS in the system to this UE, for instance by measuring the power received from each BS or the distance between the UE and other BSs;

- This information is fed back to the nearest BS to each UE;

- The large-scale fading information is gathered to a dominating BS or a central unit and the *modified enumerative algorithm* with negative costs shown in Section 4.2.3 is performed in order to find the optimal clustering;

- This clustering information is exchanged among all BSs and each UE is informed by the nearest BS to which cluster it belongs. In the meanwhile the clusters are formed;

- Each UE now measures the channel information from the BSs within the same cluster and feeds back the channel information to the nearest BS. The channel information is then exchanged among the BSs in the same cluster and the ZF beamforming can be performed within each cluster.

Notice that once the clusters have been formed, the large-scale fading based approach will not change the cluster formation very frequently. The reason is that the large-scale fading usually refers to path loss and shadowing, due to which signal variation occurs over a range of 10-1000 m [50]. Since signal degradation over multiple cells is considerably larger than over a single cell, for the calculation of (4.13) the interfering power from cells far away can be neglected. As a result, in the first step of the proposed approach each UE needs only to feed back the large-scale fading information from adjacent BSs, whose transmit power is not negligible. This could further reduce the amount of feedback information at the initial phase of the approach.

4.3 Simulation results and analysis

Here we consider a cellular system consisting of $K_B = 57$ cells with one user in each cell. It is assumed that in each cell the time division multiplexing or the frequency division multiplexing scheme is used so that at a time slot or frequency slot only one user is scheduled without being interfered by other users in the same cell. Each BS is equipped with 2 antennas and each user has a single antenna. The large-scale fading is modeled by (4.11) with the path loss exponent of 3.7 and no shadowing effect is considered. The small-scale fading is modeled by Rayleigh distribution. The *large-scale fading based dynamic clustering approach* is performed to find the optimal clustering and after the clusters are formed the ZF beamforming is used within each cluster to null out the intra-cluster interference.

Figure 4.5 shows a snapshot of the cluster formation based on the current large-scale information or user location information. The clustering approach is performed for the inner 30 cells and the surrounding 27 cells create the ambient interference. Note that the goal of this approach is to maximize the average data rate of the system by jointly selecting the optimal clusters. Ideally each UE should be served by the nearest 3 BSs based on the (4.11). Due to the per-BS power contraint (4.6) each BS is assumed to only serve UEs in adjacent 3 cells. Hence users are not always served by the nearest BSs. For instance, UE 8 is located in the overlapping area of BS 8, BS 10 and BS 36 but it is served by BS 1, BS 8 and BS 12 according to the global optimization of the whole system. This does not mean that the performance of certain UEs are sacrificed in order to achieve higher average data rate. On the contrary this approach guarantees the
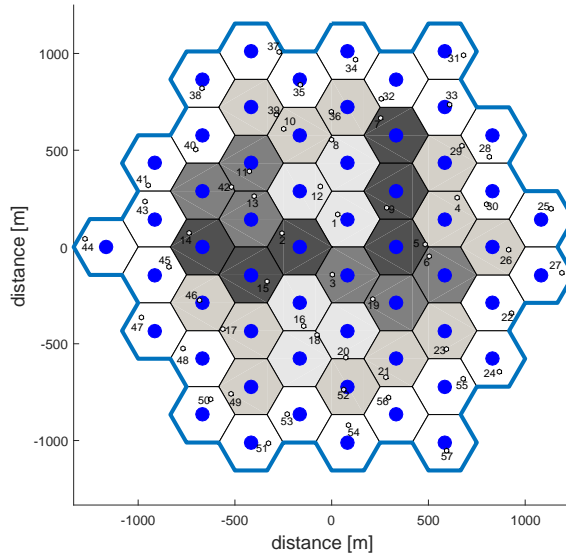
Figure 4.5: A snapshot of the clustering scheme within a 57-cell system

fairness of different users.

In the following the proposed dynamic clustering approach is performed for the inner 30 cells as shown in Figure 4.5 and the performance of the cell 1-21 is evaluated, such that all the evaluated users can benefit from the proposed method. The average data rate of the evaluated users is shown in Figure 4.6. Similar to Figure 4.3 full cooperation can provide the largest data rate at the cost of high-overload backhaul link with tight synchronization and delay constraints. The proposed approach outperforms the fixed clustering approach over all SNR regimes. For a reference SNR of 10 dB the proposed one can obtain consistently an average data rate gain of more than 3.3%, with a maximum of 3.7% (see Table 4.1). The data rate gain increases also with the reference SNR, which indicates in case of high inter-cluster interference users can benefit more from the proposed method.

Table 4.1: Data rate comparison with adaptive and fixed clustering schemes

SNR [dB]	1	4	7	10	13	16	19	22	25
Fixed (bps/Hz)	3.406	3.733	4.000	4.092	4.200	4.275	4.270	4.325	4.293
Adaptive (bps/Hz)	3.466	3.828	4.116	4.228	4.346	4.428	4.425	4.475	4.454
Gain (%)	1.76	2.56	2.96	3.32	3.48	3.58	3.64	3.46	3.75

In order to observe the distribution of the user data rates, the CDF of all the evaluated users at the reference SNR of 25 dB is shown in Figure 4.7. The adaptive clustering
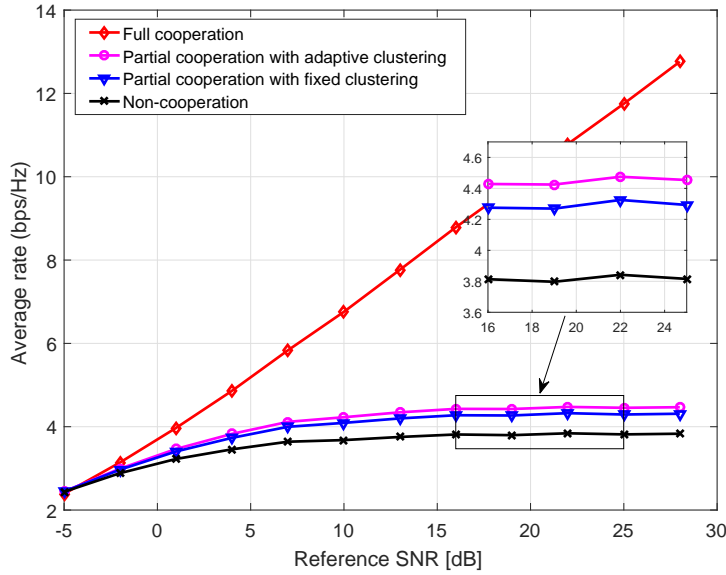
Figure 4.6:   Average user data rate comparison with different clustering schemes

approach lies on the right side of the fixed clustering for most of the users (80%). For
the rest of the users who probably reside near the BSs, the performance between the two
methods is similar. This implies that the proposed approach tries to improve the user
experience who suffers from a poor channel condition or high interference, such as the
cell-edge users. And the improvement is not at the expense of sacrificing the performance
of users under good channel condition, e.g., by decreasing serving BS power for the these
users.

Figure 4.8 shows the comparison of the average cell-edge user data rate (lowest 5% of
all data rates [8]) with different clustering schemes. Compared with the average data
rate of all users, the adaptive approach achieves a dramatic performance increase for the
cell-edge users. From the SNR of 7 dB the data rate gain can be maintained over 30%.

In the following, in order to evaluate the fairness using the clustering methods more
quantitatively, we use the fairness index introduced in [63]. Here the fairness index is
calculated as

$$\Gamma = \frac{[\sum r_i]^2}{K_{\mathrm{U}} \sum r_i^2} \tag{4.14}$$

where r_i indicates the data rate of user i and K_{U} is the number of users considered in
the evaluated system. Γ always lies between 0 and 1 and this boundedness aids intuitive
understanding of the fairness index. For instance, a fairness index of 0.8 means that
it is unfair to 20% of the users. The scenario where each user has the same rate, will
result in the maximal fairness index of 1. Figure 4.9 shows the fairness indices obtained
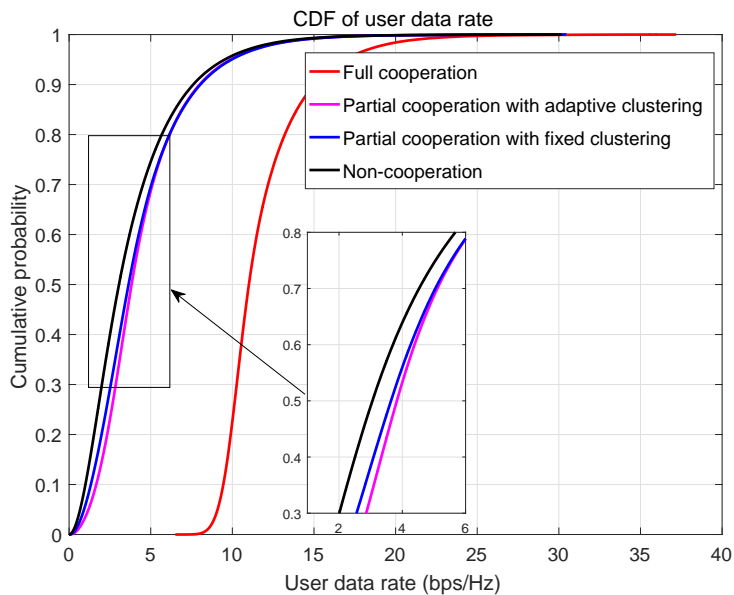
Figure 4.7: CDF of inner user data rate at the reference SNR of 25 dB
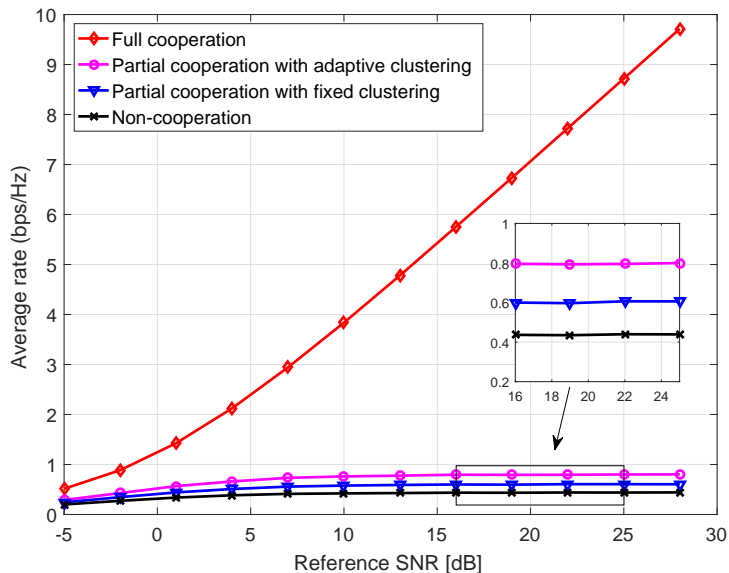
Figure 4.8: Comparison of the average cell-edge user data rate with different clustering schemes
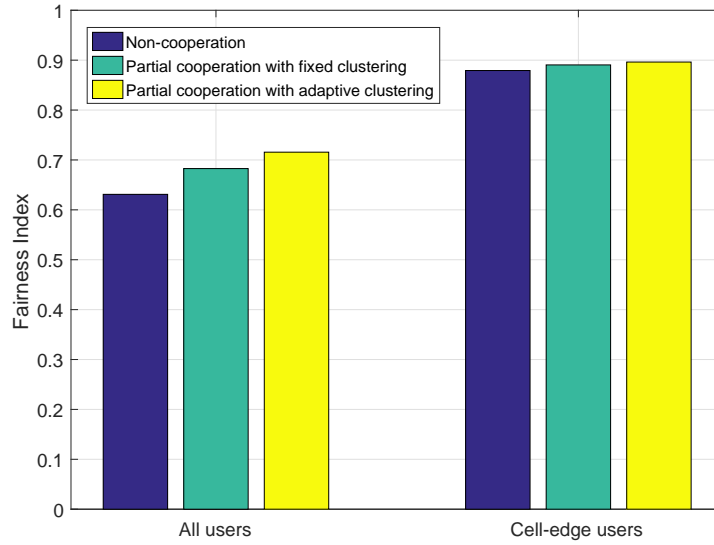
Figure 4.9:   Fairness comparison with different clustering schemes

by different schemes under an SNR of 25 dB. The indices of the cell-edge users are in average larger than the indices calculated for all users, because the cell-edge users are the lowest 5%-rate users and the relative difference is smaller. For both cases the adaptive clustering method achieves the highest fairness index. It gives fairness to 71.6% of the users overall, 3.3% more than the fixed clustering scheme, while still maintaining a higher average data rate. Although the fairness index of the non-cooperation scheme is not too small, the performance it provides is much worse than that of the clustering methods as depicted in Figure 4.6.

Besides the data rate gain and fairness improvement, we also observe the power consumed by different clustering approaches. The normalized power of each BS using the proposed approach is 0.87 and the one using fixed clustering is 0.90. Our proposed clustering method could additionally save 3.36% transmit power. The reason for the difference is the power scaling due to the per-BS power constraint (4.6). After the design of the ZF beamforming vector for all BSs within one clustering according to (4.4), the power of the BSs is scaled by the maximum power of the BSs calculated from the beamforming vectors, such that all the BSs will be kept under the maximum available power. The more difference the coefficients of the designed beamforming vectors have, the larger the scaling factor is. This implies that the adaptive clustering method implicitly adapts the power allocation across all BSs within one cluster during cluster design.

4.4   Conclusion

In this chapter we discussed the clustering problem in the CoMP-JT systems, whose practical implementation is limited by the stringent requirement for a high data rate and low-latency backhaul connectivity. Under the assumption of non-overlapping clusters, the clustering problem was first formulated as a classic set partition problem, which is NP-complete. Then a modified implicit enumeration algorithm was introduced using the negative cost function. With the enumerative algorithm we also proposed a large-scale fading based dynamic clustering approach. Simulations show that the proposed method outperforms the fixed clustering, especially for the cell-edge users. A data rate increase of over 30% can be obtained for cell-edge users for a reference SNR of 7 dB. In addition, we introduced a fairness index in order to evaluate the fairness of different schemes quantitatively. The proposed approach was shown to be able to provide 3.3% more fairness to the users. An interesting finding was the dynamic clustering scheme implicitly adapts the power allocation, consuming 3.36% less transmit power compared with the fixed clustering scheme.

CHAPTER 5

Conclusions

This dissertation has investigated the limited feedback problem in current communication systems. Different scenarios from a single OFDM link to coordinated systems were studied. Emphasis was placed on the efficient use of the available feedback resources for quantizing the CSI and design of practical cooperation approaches.

After a short introduction of the OFDM technique and the radio propagation channels, the feedback problem in an OFDM single link MISO system was addressed. Since the amount of CSI feedback in an OFDM system is proportional to the number of subcarriers, the channel feedback consumes a huge amount of resources of the backward link. There is correlation among the transfer function of adjacent subcarriers, this correlation could be utilized to reduce the amount of CSI feedback. In this part it was assumed that the receiver could perfectly estimate the channel and the feedback channel is error-free. The state of the art of the feedback techniques were firstly introduced. Then some feedback algorithms were explained in detail. An RB-based feedback structure was proposed which utilizes both frequency correlation and temporal correlation of the channel simultaneously. This structure was combined with the feedback reduction algorithms to decrease the BER performance loss caused by reduced feedback bits, and to further reduce the feedback amount by exploiting temporal correlation. Simulation results showed that the proposed approaches outperform the feedback reduction schemes, which do not take into account the RB structure, at the cost of a few additional bits. When temporal correlation is considered, the feedback overhead could be reduced by a factor proportional to the number of correlated OFDM symbols while still maintaining the performance. A decision rule has been given according to the coherence time of the channel, which gives a compromise with respect to performance and feedback reduction. It was also mentioned that different RB-based algorithms could be applied in different scenarios.

The feedback problem is more severe in a coordinated multicell system since the disturbance is not only caused from additive noise but also from interference from other cells. The BS cooperation requires the CSI to be available locally and globally. In the CoMP-CB system, where user scheduling/beamforming is performed within the same cooperation set without data sharing, the accuracy of the CSI is critical. In this dissertation an uncorrelated Rayleigh channel was assumed, whose stochastic properties can

be modeled easily. Two beamforming strategies were considered: ZF beamforming and MRT. The reason of choosing these two beamforming designs is the straightforwardness of extending to a more complicated system with more cells. Another reason is the known properties to some extent of these two beamformers under the uncorrelated Rayleigh channel. The target is to maximize the sum-rate of the whole system while applying quantization on the downlink CDI. In a two-cell system, a bit partitioning algorithm based on ZF beamforming was proposed, which allocates the limited available bits at each UE on the serving and interfering channels adaptively. It was shown that this adaptive bit allocation achieves a noticeable performance gain compared to the non-adaptive bit allocation. Since ZF beamforming is not always the best choice, especially in a noise-dominated system, several cooperative approaches were introduced in order to select the best suitable beamforming strategy. Simulation results showed that the proposed cooperative approaches could benefit from both ZF beamforming and MRT, and does not need high computational complexity to make the decision.

The adaptive bit partitioning algorithm was extended to a three-cell system as well as a multicell system. A generic separated cooperative approach was designed for the multicell system, where each BS determines separately the beamforming strategy for the *victim UEs*. This approach determines if a BS should carry out interference nulling (IN) to its surrounding UEs successively. The approach does not require a joint optimization, which may have high complexity. It was shown that the proposed approach outperforms dramatically the one, which always nulls out the interference to the *victim UEs*. An interesting finding was that the MRT without cooperation among BSs performs very close in average to the proposed approach, meaning that MRT is still very suitable in a practical multicell system. However, for the cell-edge users it's worth performing the proposed approach due to its noticeable gain. It was also observed that the more transmit antennas the BS has, the more data rate gain the UE could obtain using this approach. This observation reveals the advantage of the proposed method in a massive MIMO system.

In a CoMP-JT system, where full data sharing exists among BSs in addition to the CSI, the feedback overhead and backhaul load problems become more challenging. In order to limit the amount of feedback and backhaul the dynamic clustering problem was investigated in this dissertation. Assuming non-overlapping clusters, the clustering problem can be modeled by the NP-complete SPP. A modified implicit enumeration algorithm was introduced, which was then employed to form the proposed large-scale fading based dynamic clustering method. This approach does not require a frequent update because signal variation due to the large-scale fading occurs over a range of 10-1000 m. Simula-

tions showed that the proposed method could achieve a considerable gain compared to the fixed clustering and non-cooperation, especially for the cell-edge users. Along with the increased data rate, the fairness of the whole system was shown to be improved by evaluating a fairness index. It was also mentioned that the proposed dynamic clustering consumes around 3.4% less power in comparison with the fixed clustering.

Based on the results of this dissertation some aspects could be further investigated. For the analysis of the cooperative system the uncorrelated Rayleigh channel as well as the ZF and MRT beamforming schemes were assumed. It would be interesting to analyze other transmission and reception strategies, and to perform a possible feedback design. For the CoMP-JT system the small-scale fading could be considered, which might give a more suitable dynamic clustering. By exploiting temporal correlation, the small-scale fading method will not require a very frequent feedback from UEs. Also different cluster sizes may be allowed. Although the CSI exchange is negligible compared to data sharing in the JT system, it is still worth to study the feedback bit allocation for different channels as in CoMP-CB systems, since it could reduce the uplink channel overhead [126]. This dissertation considered as well a per-BS power constraint for the JT system, where some advanced power allocation schemes could be applied.

It was assumed that the feedback channel and backhaul link show zero delay and are error-free. Further research could be done to analyze the impact of delayed and imperfect channel feedback in practical systems. For the analytical reason, the RVQ was adopted here and codebook design was out of the scope of this dissertation. There are still many open aspects to be further investigated regarding limited feedback, along with the deployment of 5G. As the amount of CSI feedback increases proportional to the number of antennas, in massive MIMO the feedback problem becomes very challenging due to the increased dimension of the channel matrix [14, 18, 131]. Therefore, the CSI must be reduced/compressed before it is quantized and transmitted using the feedback channel [52, 107].

Power delay profile of HIPERLAN/2 channel model B

Table A.1:   HIPERLAN/2 channel model B

Path Number	Average Path Gain (dB)	Path Delay (ns)
1	-2.6	0
2	-3	10
3	-3.5	20
4	-3.9	30
5	0	50
6	-1.3	80
7	-2.6	110
8	-3.9	140
9	-3.4	180
10	-5.6	230
11	-7.7	280
12	-9.9	330
13	-12.1	380
14	-14.3	430
15	-15.4	490
16	-18.4	560
17	-20.7	640
18	-24.6	730

APPENDIX B

Grassmannian codebook used for OFDM systems

Table B.1: Grassmannian codebook for $N_\text{t} = 4$, $N_\text{r} = 1$ and 4 bits (16 codewords)[1]

-0.2832-0.3026j	0.7715	0.0490+0.2645j	0.6851
-0.4318+0.2306j	-0.1213+0.1684j	0.3039+0.1429j	0.1861+0.2946j
-0.4143-0.0092j	0.5813+0.0449j	0.1790+0.5045j	-0.3828-0.2366j
0.6457	-0.1475-0.0049j	0.7268	-0.1392+0.4328j
0.5480-0.0557j	0.7318	-0.2314-0.2726j	-0.2075-0.2030j
0.3246-0.1762j	-0.4010-0.3151j	-0.0087-0.0200j	-0.0327+0.0432j
0.0337-0.4986j	-0.3431-0.0759j	0.4820-0.3299j	0.8885
0.5572	-0.2387-0.1545j	0.7283	-0.3461+0.0595j
0.0573+0.3799j	-0.0681+0.1830j	0.6596	0.6576
-0.1914-0.5340j	-0.0628-0.6066j	-0.3825+0.1394j	0.3519+0.2595j
0.6762	-0.1660+0.0868j	-0.0604+0.1930j	-0.2176+0.0574j
0.2247+0.1510j	0.7449	0.5696+0.1838j	-0.1051-0.5610j
0.3039+0.5663j	0.1730+0.0383j	-0.1293-0.0810j	0.1200-0.3160j
0.6450	0.6533	0.7675	0.7791
-0.3047+0.2050j	-0.1297-0.6396j	-0.3124-0.0060j	0.5003+0.1412j
0.0075+0.1896j	-0.2886-0.1806j	0.4108-0.3483j	0.0638+0.0668j

---

[1]https://engineering.purdue.edu/~djlove/grass.html

Table B.2: Grassmannian codebook for $N_t = 4$, $N_r = 1$ and 6 bits (64 codewords)

0.5000	-0.4619+0.1913j	0.3536-0.3536j	-0.1913+0.4619j
0.5000	0.5000j	-0.5000	-0.5000j
0.5000	-0.5000	0.5000	-0.5000
0.5000	0.4976+0.0490j	0.4904+0.0975j	0.4785+0.1451j
-0.5000j	0.1913+0.4619j	-0.3536-0.3536j	0.4619+0.1913j
0.5000	0.5000j	-0.5000	-0.5000j
0.5000	-0.5000	0.5000	-0.5000
0.4619+0.1913j	0.4410+0.2357j	0.4157+0.2778j	0.3865+0.3172j
-0.5000	0.4619-0.1913j	-0.3536+0.3536j	0.1913-0.4619j
0.5000	0.5000j	-0.5000	-0.5000j
0.5000	-0.5000	0.5000	-0.5000
0.3536+0.3536j	0.3172+0.3865j	0.2778+0.4157j	0.2357+0.4410j
0.5000j	-0.1913-0.4619j	0.3536+0.3536j	-0.4619-0.1913j
0.5000	0.5000j	-0.5000	-0.5000j
0.5000	-0.5000	0.5000	-0.5000
0.1913+0.4619j	0.1451+0.4785j	0.0975+0.4904j	0.0490+0.4976j
0.5000	-0.4619+0.1913j	0.3536-0.3536j	-0.1913+0.4619j
0.5000	0.5000j	-0.5000	-0.5000j
0.5000	-0.5000	0.5000	-0.5000
0.5000j	-0.0490+0.4976j	-0.0975+0.4904j	-0.1451+0.4785j
0.5000j	0.1913+0.4619j	-0.3536-0.3536j	0.4619+0.1913j
0.5000	0.5000j	-0.5000	-0.5000j
0.5000	-0.5000	0.5000	-0.5000
-0.1913+0.4619j	-0.2357+0.4410j	-0.2778+0.4157j	-0.3172+0.3865j
-0.5000	0.4619-0.1913j	-0.3536+0.3536j	0.1913-0.4619j
0.5000	0.5000j	-0.5000	-0.5000j
0.5000	-0.5000	0.5000	-0.5000
-0.3536+0.3536j	-0.3865+0.3172j	-0.4157+0.2778j	-0.4410+0.2357j
0.5000j	-0.1913-0.4619j	0.3536+0.3536j	-0.4619-0.1913j
0.5000	0.5000j	-0.5000	-0.5000j
0.5000	-0.5000	0.5000	-0.5000
-0.4619+0.1913j	-0.4785+0.1451j	-0.4904+0.0975j	-0.4976+0.0490j
0.5000	-0.4619+0.1913j	0.3536-0.3536j	-0.1913+0.4619j
0.5000	0.5000j	-0.5000	-0.5000j
0.5000	-0.5000	0.5000	-0.5000
-0.5000	-0.4976-0.0490j	-0.4904-0.0975j	-0.4785-0.1451j

-0.5000j	0.1913+0.4619j	-0.3536-0.3536j	0.4619+0.1913j
0.5000	0.5000j	-0.5000	-0.5000j
0.5000	-0.5000	0.5000	-0.5000
-0.4619-0.1913j	-0.4410-0.2357j	-0.4157-0.2778j	-0.3865-0.3172j
-0.5000	0.4619-0.1913j	-0.3536+0.3536j	0.1913-0.4619j
0.5000	0.5000j	-0.5000	-0.5000j
0.5000	-0.5000	0.5000	-0.5000
-0.3536-0.3536j	-0.3172-0.3865j	-0.2778-0.4157j	-0.2357-0.4410j
0.5000j	-0.1913-0.4619j	0.3536+0.3536j	-0.4619-0.1913j
0.5000	0.5000j	-0.5000	-0.5000j
0.5000	-0.5000	0.5000	-0.5000
-0.1913-0.4619j	-0.1451-0.4785j	-0.0975-0.4904j	-0.0490-0.4976j
0.5000	-0.4619+0.1913j	0.3536-0.3536j	-0.1913+0.4619j
0.5000	0.5000j	-0.5000	-0.5000j
0.5000	-0.5000	0.5000	-0.5000
-0.5000j	0.0490-0.4976j	0.0975-0.4904j	0.1451-0.4785j
-0.5000j	0.1913+0.4619j	-0.3536-0.3536j	0.4619+0.1913j
0.5000	0.5000j	-0.5000	-0.5000j
0.5000	-0.5000	0.5000	-0.5000
0.1913-0.4619j	0.2357-0.4410j	0.2778-0.4157j	0.3172-0.3865j
-0.5000	0.4619-0.1913j	-0.3536+0.3536j	0.1913-0.4619j
0.5000	0.5000j	-0.5000	-0.5000j
0.5000	-0.5000	0.5000	-0.5000
0.3536-0.3536j	0.3865-0.3172j	0.4157-0.2778j	0.4410-0.2357j
0.5000j	-0.1913-0.4619j	0.3536+0.3536j	-0.4619-0.1913j
0.5000	0.5000j	-0.5000	-0.5000j
0.5000	-0.5000	0.5000	-0.5000
0.4619-0.1913j	0.4785-0.1451j	0.4904-0.0975j	0.4976-0.0490j

Derivation of the key equation in the three-cell CoMP-CB systems

By simplifying (3.35) and setting $B_1 = 2^{-\frac{B_{1,1}}{N_t-1}}$, $B_2 = 2^{-\frac{B_{1,2}}{N_t-1}}$, $B_3 = 2^{-\frac{B_{1,3}}{N_t-1}}$ and $B_e = 2^{-\frac{B_{1,1}+B_{1,2}+B_{1,3}}{N_t-1}}$, we get the following intermediate results:

$$\begin{cases} \dfrac{1}{N_t-1} \cdot \dfrac{B_1}{1-B_1} + \lambda = 0 & \text{(C.1a)} \\[3mm] \dfrac{P_{1,2}}{N_t-1} \cdot \dfrac{B_2}{N_0 + B_2 P_{1,2} + B_3 P_{1,3}} + \lambda = 0 & \text{(C.1b)} \\[3mm] \dfrac{P_{1,3}}{N_t-1} \cdot \dfrac{B_3}{N_0 + B_2 P_{1,2} + B_3 P_{1,3}} + \lambda = 0 & \text{(C.1c)} \\[3mm] B_{1,1} + B_{1,2} + B_{1,3} = B \;\Rightarrow\; B_1 \cdot B_2 \cdot B_3 = B_e & \text{(C.1d)} \end{cases}$$

By comparing (C.1b) and (C.1c) the following equation holds:

$$P_{1,2} \cdot B_2 = P_{1,3} \cdot B_3 \triangleq P. \tag{C.2}$$

By replacing $P_{1,2} \cdot B_2$ and $P_{1,3} \cdot B_3$ with P in (C.1b), we get

$$\frac{P}{(N_t-1)(N_0+2P)} + \lambda = 0 \;\Rightarrow\; \lambda(N_t-1) = -\frac{P}{N_0+2P}. \tag{C.3}$$

Inserting (C.3) into (C.1a) gives

$$B_1 = \frac{\lambda(N_t-1)}{\lambda(N_t-1)-1} = \frac{P}{3P+N_0}. \tag{C.4}$$

Slightly reformulate (C.1d), we get

$$B_1 \cdot P_{1,2}B_2 \cdot P_{1,3}B_3 = P_{1,2}P_{1,3}B_e \;\Rightarrow\; B_1 \cdot P \cdot P = P_{1,2}P_{1,3}B_e. \tag{C.5}$$

The *key equation* with respect to P in the three-cell CoMP-CB systems can be derived by combining (C.4) and (C.5):

$$P^3 = P_{1,2}P_{1,3}B_e(3P+N_0). \tag{C.6}$$

Analysis of the root of the key equation in the three-cell CoMP-CB systems

Since $P_{1,2}$, $P_{1,3}$, B_{e} and N_0 in the *key equation* (3.36) can be seen as constants, (3.36) has the same form as the following equation

$$P^3 = aP + b, \tag{D.1}$$

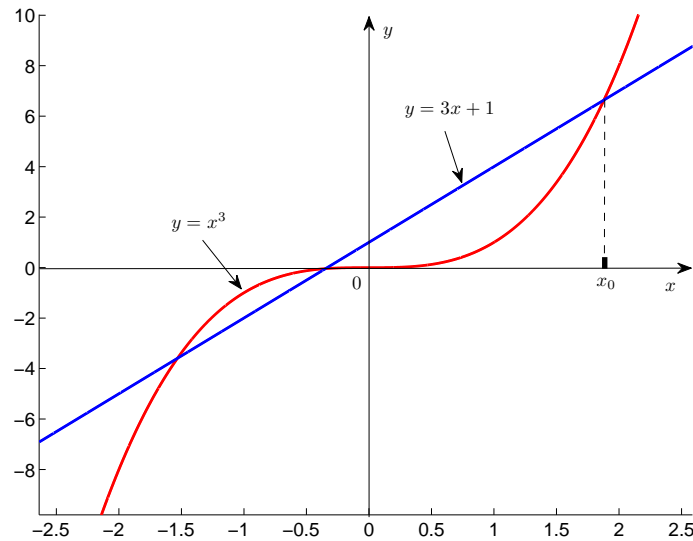where a and b are constants. An example for $a = 3$ and $b = 1$ is shown in Figure D.1:

Figure D.1: Illustration of the root of the *key equation*

Figure D.1 illustrates that if a and b are both positive, (D.1) always has a positive root x_0. Furthermore, if the slope a and the y-intercept b both increase, the root x_0 is getting larger, and vice versa.

<div align="center">

APPENDIX E

Reduction rules for the characteristic matrix in the set partition problem

</div>

Let $\mathcal{M}$ and $\mathcal{N}$ be the row and column index set of the characteristic matrix $\mathbf{A} = \{a_{ij}\}^{M \times N}$. Let $\mathbf{r}_i$ be the i-th row of $\mathbf{A}$ and $\mathbf{a}_j$ the j-th column of $\mathbf{A}$. c_j is the cost variable/function assigned to column j and u_j is the decision variable, which indicates if column j belongs to the final solution or not [24, 45].

- **Reduction 1**: If $\mathbf{r}_i$ is a null vector for a certain i, no solution exists.

- **Reduction 2** (unit row vector): If for some $i \in \mathcal{M}$ and $t \in \mathcal{N}$, $a_{it} = 1$, $a_{ij} = 0$, $\forall j \in \mathcal{N}\backslash\{t\}$, then

    - $u_t = 1$ in every solution and $\mathbf{a}_t$ can be deleted;
    - all rows $\mathbf{r}_k$ ($k \in \mathcal{M}$) such that $a_{kt} = 1$ can be deleted since they are covered by $\mathbf{a}_t$;
    - all columns $\mathbf{a}_j$ ($j \in \mathcal{N}\backslash\{t\}$) such that $\mathbf{a}_j^{\mathrm{T}}\mathbf{a}_t \geq 1$ can be deleted.

- **Reduction 3**: If $\mathbf{r}_k \geq \mathbf{r}_i$ in a vector sense ($i,\ k \in \mathcal{M}$), then

    - $\mathbf{r}_k$ can be deleted;
    - all columns $\mathbf{a}_t$ ($t \in \mathcal{N}$) such that $a_{kt} = 1$ and $a_{it} = 0$ can be deleted.

- **Reduction 4** (cost relevant reduction): If $\mathbf{a}_t = \sum_{\mathbf{a}_j \in \mathcal{N}'} \mathbf{a}_j$ and $c_t \geq \sum_{\mathbf{a}_j \in \mathcal{N}'} c_j$ for some $t \in \mathcal{N}$ and some subset $\mathcal{N}' \subseteq \mathcal{N}\backslash\{t\}$, then column $\mathbf{a}_t$ can be deleted.

- **Reduction 5**: For $i \in \mathcal{M}$, let $\mathcal{N}_i = \{j \in \mathcal{N} | a_{ij} = 1\}$. Then any column $\mathbf{a}_t$ ($t \in \mathcal{N}\backslash\mathcal{N}_i$) such that

$$\mathbf{a}_t^{\mathrm{T}}\mathbf{a}_j \geq 1, \quad \forall j \in \mathcal{N}_i \text{ and for some } i \in \mathcal{M} \tag{E.1}$$

    can be deleted.

Explanations to the reduction rules:

- **Reduction 1**: there exists one cell, which does not belong to any cluster.

- **Reduction 2** (unit row vector): cell i only belongs to cluster t

  - cluster t is in every solution and can be removed from the SPP;

  - all cells within cluster t can be removed from the SPP;

  - all other clusters, which have common cells with cluster t, can be removed from the SPP.

- **Reduction 3**: there exists cell k and cell i, such that all clusters containing cell i also contain cell k

  - cell k can be removed from the SPP;

  - all clusters, which contain cell k but not cell i, can be removed from the SPP.

- **Reduction 4** (cost relevant reduction): if there exists cluster t which is the union of some disjoint clusters, and the cost of cluster t is higher than the total cost of these disjoint clusters, cluster t can be removed from the SPP.

- **Reduction 5**: $\mathcal{N}_i$ is the set of all clusters containing cell i. If there exists cluster t, which does not contain cell i and has intersection with any cluster in $\mathcal{N}_i$, then cluster t can be removed from the SPP. The reason is that one of the clusters in $\mathcal{N}_i$ must be in the final solution and cluster t having common cells with this cluster cannot be in the solution any more. An example is, in Figure 4.2 the cluster containing cell 4, 8 and 9 cannot be in the final solution because it has common cells with all clusters containing cell 7.

Bibliography

[1] *Backhauling X2.* Cambridge Broadband Networks, 2011.

[2] NGMN 5G white paper. 2 2015.

[3] IEEE 5G and beyond technology roadmap white paper. 10 2017.

[4] 3GPP TR 25.814. Physical layer aspects for evolved universal terrestrial radio access (UTRA). 2006.

[5] 3GPP TR 36.420. Technical specification group radio access network; evolved universal terrestrial radio access network (E-UTRAN); X2 general aspects and principles (Release 14). 2017.

[6] 3GPP TR 36.814. Evolved universal terrestrial radio access (E-UTRA); further advancements for E-UTRA physical layer aspects (Release 9). 2011.

[7] 3GPP TR 36.819. Technical specification group radio access network; coordinated multi-point operation for LTE physical layer aspects (Release 11). 2013.

[8] 3GPP TR 36.913. Requirements for further advancements for Evolved Universal Terrestrial Radio Access (E-UTRA) (LTE-Advanced). 2018.

[9] 3GPP TS 38.211. NR; physical channels and modulation (Release 15). 2019.

[10] 3GPP TR 38.802. Technical Specification Group Radio Access Network; Study on New Radio Access Technology Physical Layer Aspects (Release 14). 2017.

[11] 3GPP TS 45.005. Radio transmission and reception (Release 10). 2011.

[12] ETSI TS 101 475. Broadband radio access networks (BRAN); HIPERLAN type 2; Physical (PHY) layer. 2000.

[13] ETSI TR 136 932. LTE; Scenarios and requirements for small cell enhancements for E-UTRA and E-UTRAN. 2016.

[14] I. Ahmed, H. Khammari, A. Shahid, A. Musa, K. S. Kim, E. De Poorter, and I. Moerman. A Survey on Hybrid Beamforming Techniques in 5G: Architecture and System Model Perspectives. *IEEE Communications Surveys Tutorials*, 20(4):3060–3097, 2018.

[15] T. Akbudak, M. Simsek, Bo Zhao, and A. Czylwik. Symmetric capacity of multi-user MIMO downlink under per-base station power constraints. In *2011 International ITG Workshop on Smart Antennas*, pages 1–4, Feb 2011.

[16] T. Akbudak, B. Zhao, M. Simsek, and A. Czylwik. A low-complexity resource allocation scheme for single-user MIMO transmission. In *2011 7th International Wireless Communications and Mobile Computing Conference*, pages 249–254, July 2011.

[17] Ian F. Akyildiz, Shuai Nie, Shih-Chun Lin, and Manoj Chandrasekaran. 5g roadmap. *Comput. Netw.*, 106(C):17–48, September 2016.

[18] Panos N. Alevizos, Xiao Fu, Nicholas D. Sidiropoulos, Ye Yang, and Aggelos Bletsas. Limited Feedback Channel Estimation in Massive MIMO with Non-uniform Directional Dictionaries. *CoRR*, abs/1712.10085, 2017.

[19] G. C. Alexandropoulos, P. Ferrand, J. m. Gorce, and C. B. Papadias. Advanced coordinated beamforming for the downlink of future LTE cellular networks. *IEEE Communications Magazine*, 54(7):54–60, July 2016.

[20] M.-S. Alouini and A. J. Goldsmith. Capacity of rayleigh fading channels under different adaptive transmission and diversity-combining techniques. *IEEE Transactions on Vehicular Technology*, 48(4):1165–1181, 1999.

[21] M. Amara and A. Feki. Downlink radio resource allocation with MU-MIMO and carrier aggregation in 5G networks. In *2017 IEEE 28th Annual International Symposium on Personal, Indoor, and Mobile Radio Communications (PIMRC)*, pages 1–6, Oct 2017.

[22] J. G. Andrews. Interference cancellation for cellular systems: a contemporary overview. *IEEE Wireless Communications*, 12(2):19–29, 2005.

[23] Chun Kin Au-Yeung and D. J. Love. On the performance of random vector quantization limited feedback beamforming in a MISO system. *IEEE Transactions on Wireless Communications*, 6(2):458–462, Feb. 2007.

[24] Egon Balas and Manfred W. Padberg. Set partitioning: A survey. *SIAM Review*, 18(4):710–760, 1976.

[25] P. Baracca, F. Boccardi, and V. Braun. A dynamic joint clustering scheduling algorithm for downlink CoMP systems with limited CSI. In *2012 International Symposium on Wireless Communication Systems (ISWCS)*, pages 830–834, Aug 2012.

[26] Paolo Baracca, Federico Boccardi, and Nevio Benvenuto. A dynamic clustering and resource allocation algorithm for downlink CoMP systems with multiple antenna UEs. *CoRR*, abs/1311.5114, 2013.

[27] Paolo Baracca, Federico Boccardi, and Nevio Benvenuto. A dynamic clustering algorithm for downlink CoMP systems with multiple antenna UEs. *EURASIP Journal on Wireless Communications and Networking*, 2014(1):125, Aug 2014.

[28] P. Bello. Characterization of randomly time-variant linear channels. *IEEE Transactions on Communications Systems*, 11(4):360–393, 1963.

[29] R. Bhagavatula and R. W. Heath. Adaptive limited feedback for sum-rate maximizing beamforming in cooperative multicell systems. *IEEE Transactions on Signal Processing*, 59(2):800–811, Feb. 2011.

[30] Ramya Bhagavatula. *Limited feedback for multicell cooperative systems*. PhD thesis, The university of Texas at Austin, 2010.

[31] S. P. Boyd and L. Vandenberghe. *Convex Optimization*. Berichte über verteilte messysteme. Cambridge University Press, 2004.

[32] K. Chakraborty, S. Das, O. Dural, K. Rajamani, and S. S. Soliman. Compression schemes for the feedback channel in multiband-OFDM UWB systems. In *IEEE International Conference on Ultra-Wideband, 2009. ICUWB 2009.*, pages 443–448, 2009.

[33] P. Cheng and Z. Chen. Multidimensional Compressive Sensing Based Analog CSI Feedback for Massive MIMO-OFDM Systems. In *2014 IEEE 80th Vehicular Technology Conference (VTC2014-Fall)*, pages 1–6, Sept 2014.

[34] Y. S. Cho, J. Kim, W. Y. Yang, and C. G. Kang. *MIMO-OFDM Wireless Communications with MATLAB*. Wiley, 2010.

[35] J. Choi and R. W. Heath. Interpolation based transmit beamforming for MIMO-OFDM with limited feedback. *IEEE Transactions on Signal Processing*, 53(11):4125–4135, 2005.

[36] Rajesh Chundury. Mobile broadband backhaul: Addressing the challenge. *Ericsson Review*, 2008.

[37] B. Clerckx, G. Kim, J. Choi, and Y. J. Hong. Explicit vs. Implicit Feedback for SU and MU-MIMO. In *2010 IEEE Global Telecommunications Conference GLOBECOM 2010*, pages 1–5, Dec 2010.

[38] Qimei Cui, Haiyan Wang, Pengxiang Hu, Xiaofeng Tao, Ping Zhang, Jyri Hamalainen, and Liang Xia. Evolution of Limited-Feedback CoMP Systems from 4G to 5G: CoMP Features and Limited-Feedback Approaches. 9:94–103, 09 2014.

[39] ARTIST4G D1.4. Interference avoidance techniques and system design. ARTIST4G deliverable, Jul. 2012. [Online]. Available: https://ict-artist4g.eu/projet/deliverables, [Accessed: Feb. 2014].

[40] A Dutta and G Fettweis. IEEE 5G and beyond initiative - A perspective. 17, 02 2018.

[41] M. E. Eltayeb, K. Elkhalil, H. R. Bahrami, and T. Y. Al-Naffouri. Opportunistic Relay Selection With Limited Feedback. *IEEE Transactions on Communications*, 63(8):2885–2898, Aug 2015.

[42] V. Erceg, L. J. Greenstein, S. Y. Tjandra, S. R. Parkoff, A. Gupta, B. Kulic, A. A. Julius, and R. Bianchi. An empirically based path loss model for wireless channels in suburban environments. *IEEE Journal on Selected Areas in Communications*, 17(7):1205–1211, 1999.

[43] Minghai Feng, Xiaoming She, Lan Chen, and Y. Kishiyama. Enhanced dynamic cell selection with muting scheme for DL CoMP in LTE-A. In *2010 IEEE 71st Vehicular Technology Conference (VTC 2010-Spring)*, pages 1–5, May 2010.

[44] G. Fodor, N. Rajatheva, W. Zirwas, L. Thiele, M. Kurras, K. Guo, A. Tolli, J. H. Sorensen, and E. d. Carvalho. An Overview of Massive MIMO Technology Components in METIS. *IEEE Communications Magazine*, 55(6):155–161, 2017.

[45] R. S. Garfinkel and G. L. Nemhauser. The set-partitioning problem: Set covering with equality constraints. *Operations Research*, 17(5):848–856, 1969.

[46] X. Ge, H. Cheng, M. Guizani, and T. Han. 5G wireless backhaul networks: challenges and research advances. *IEEE Network*, 28(6):6–11, Nov 2014.

[47] A. Gersho and R. M. Gray. *Vector Quantization and Signal Compression*. Kluwer Academic Publishers, Norwell, MA, USA, 1991.

[48] D. Gesbert, S. Hanly, H. Huang, S. Shamai Shitz, O. Simeone, and W. Yu. Multi-cell MIMO cooperative networks: a new look at interference. *IEEE Journal on Selected Areas in Communications*, 28(9):1380–1408, 2010.

[49] D. Gesbert, M. Kountouris, R. W. Heath, Chan-Byoung Chae, and T. Salzer. Shifting the MIMO paradigm. *IEEE Signal Processing Magazine*, 24(5):36–46, Sept. 2007.

[50] A. Goldsmith. *Wireless Communications*. Cambridge University Press, 2005.

[51] Guy Grebla, Berk Birand, Peter M. van de Ven, and Gil Zussman. Joint transmission in cellular networks with CoMP - stability and scheduling algorithms. *Perform. Eval.*, 91:38–55, 2015.

[52] Y. Han, W. Shin, and J. Lee. Projection based feedback compression for FDD massive MIMO systems. In *2014 IEEE Globecom Workshops (GC Wkshps)*, pages 364–369, Dec 2014.

[53] M. Hata. Empirical formula for propagation loss in land mobile radio services. *IEEE Transactions on Vehicular Technology*, 29(3):317–325, 1980.

[54] C. He, P. Zhu, B. Sheng, and X. You. Two novel interpolation algorithms for MIMO-OFDM systems with limited feedback. In *2011 IEEE Vehicular Technology Conference (VTC Fall)*, pages 1–5, 2011.

[55] X. Hou and C. Yang. Feedback overhead analysis for base station cooperative transmission. *IEEE Transactions on Wireless Communications*, PP(99):1–14, 2013.

[56] J. Huang, J. Zhang, Z. Liu, J. Li, and X. Li. Transmit beamforming for MIMO-OFDM systems with limited feedback. In *IEEE 68th Vehicular Technology Conference, 2008. VTC 2008-Fall.*, pages 1–5, 2008.

[57] K. Huang, R. W. Heath, and J. G. Andrews. Limited feedback beamforming over temporally-correlated channels. *IEEE Transactions on Signal Processing*, 57(5):1959–1975, 2009.

[58] K. Huang, B. Mondal, R. W. Heath, and J. G. Andrews. Markov models for limited feedback MIMO systems. In *2006 IEEE International Conference on Acoustics, Speech and Signal Processing, 2006. ICASSP 2006 Proceedings.*, volume 4, pages IV–9 – IV–12, 2006.

[59] K. Huang, B. Mondal, R. W. Heath, and J. G. Andrews. Multi-antenna limited feedback for temporally-correlated channels: feedback compression. In *IEEE Global Telecommunications Conference, 2006. GLOBECOM '06.*, pages 1–5, 2006.

[60] T. Inoue and R. W. Heath. Geodesic prediction for limited feedback multiuser MIMO systems in temporally correlated channels. In *IEEE Radio and Wireless Symposium, 2009. RWS '09.*, pages 167–170, 2009.

[61] R. Irmer, H. Droste, P. Marsch, M. Grieger, G. Fettweis, S. Brueck, H. P Mayer, L. Thiele, and V. Jungnickel. Coordinated multipoint: concepts, performance, and field trial results. *IEEE Communications Magazine*, 49(2):102–111, February 2011.

[62] M. Jaber, M. A. Imran, R. Tafazolli, and A. Tukmanov. 5G Backhaul Challenges and Emerging Research Directions: A Survey. *IEEE Access*, 4:1743–1766, 2016.

[63] Raj Jain, Dah-Ming Chiu, and W. Hawe. A quantitative measure of fairness and discrimination for resource allocation in shared computer systems. *CoRR*, cs.NI/9809099, 1998.

[64] S. Jain, S. J. Kim, and G. B. Giannakis. Backhaul-constrained multicell cooperation leveraging sparsity and spectral clustering. *IEEE Transactions on Wireless Communications*, 15(2):899–912, Feb 2016.

[65] N. Jindal. MIMO broadcast channels with finite-rate feedback. *IEEE Transactions on Information Theory*, 52(11):5045–5060, Nov. 2006.

[66] N. Jindal, J. G. Andrews, and S. Weber. Rethinking MIMO for Wireless Networks: Linear Throughput Increases with Multiple Receive Antennas. In *2009 IEEE International Conference on Communications*, pages 1–6, June 2009.

[67] Jarkko Kaleva, Antti Tölli, Markku J. Juntti, Randall Berry, and Michael L. Honig. Joint transmission with limited backhaul connectivity. *CoRR*, abs/1705.05252, 2017.

[68] T. Kim, D. J. Love, and B. Clerckx. A feedback update control scheme for limited feedback multiple antennas systems. In *2010 IEEE Global Telecommunications Conference (GLOBECOM 2010)*, pages 1–5, 2010.

[69] T. Kim, D. J. Love, and B. Clerckx. Leveraging temporal correlation for limited feedback multiple antennas systems. In *2010 IEEE International Conference on Acoustics Speech and Signal Processing (ICASSP)*, pages 3422–3425, 2010.

[70] T. Kim, D. J. Love, and B. Clerckx. Does frequent low resolution feedback outperform infrequent high resolution feedback for multiple antenna beamforming systems? *IEEE Transactions on Signal Processing*, 59(4):1654–1669, 2011.

[71] V. K. N. Lau and T. Wu. Optimal transmission and limited feedback design for OFDM/MIMO systems in frequency selective block fading channels. *IEEE Transactions on Wireless Communications*, 6(5):1569–1573, 2007.

[72] Daewon Lee, Hanbyul Seo, B. Clerckx, E. Hardouin, D. Mazzarese, S. Nagata, and K. Sayana. Coordinated multipoint transmission and reception in LTE-advanced: deployment scenarios and operational challenges. *IEEE Communications Magazine*, 50(2):148–155, February 2012.

[73] Namyoon Lee and Wonjae Shin. Adaptive feedback scheme on K-cell MISO interfering broadcast channel with limited feedback. *IEEE Transactions on Wireless Communications*, 10(2):401–406, February 2011.

[74] W. C. Lee. *Mobile Cellular Telecommunications Systems*. Electronic engineering series. McGraw-Hill, 1989.

[75] Q. Li and X. E. Lin. Compact feedback for MIMO-OFDM systems over frequency selective channels. In *2005 IEEE 61st Vehicular Technology Conference, 2005. VTC 2005-Spring*, volume 1, pages 187–191, 2005.

[76] D. J. Love and R. W. Heath. Limited feedback power loading for OFDM. In *2004 IEEE Military Communications Conference, 2004. MILCOM 2004.*, volume 1, pages 71–77, 2004.

[77] D. J. Love, R. W. Heath, V. K. N. Lau, D. Gesbert, B. D. Rao, and M. Andrews. An overview of limited feedback in wireless communication systems. *IEEE Journal on Selected Areas in Communications*, 26(8):1341–1365, October 2008.

[78] D. J. Love, R. W. Heath, and T. Strohmer. Grassmannian beamforming for multiple-input multiple-output wireless systems. *IEEE Transactions on Information Theory*, 49(10):2735–2747, Oct. 2003.

[79] Helka-Liina Määttänen, Kari Hämäläinen, Juha Venäläinen, Karol Schober, Mihai Enescu, and Mikko Valkama. System-level performance of LTE-advanced with joint transmission and dynamic point selection schemes. *EURASIP J. Adv. Sig. Proc.*, 2012:247, 2012.

[80] P. Marsch and G. P. Fettweis. *Coordinated Multi-Point in Mobile Communications: From Theory to Practice.* Cambridge University Press, 2011.

[81] Patrick Marsch. *Coordinated Multi-Point under a Constrained Backhaul and Imperfect Channel Knowledge.* PhD thesis, Dresden University of Technology, 2010.

[82] Roy E. Marsten. An algorithm for large set partitioning problems. *Management Science*, 20(5):774–787, 1974.

[83] J. Medbo and P. Schramm. Channel models for HIPERLAN/2 in different indoor scenarios. *ETSI/BRAN 3ERI085B*, 1998.

[84] B. Mondal and R. W. Heath. Algorithms for quantized precoding for MIMO OFDM beamforming systems. In *Proc. of Third SPIE Int. Symp. on Fluctuations and Noise*, 2005.

[85] António Morgado, Kazi Mohammed Saidul Huq, Shahid Mumtaz, and Jonathan Rodriguez. A survey of 5G technologies: regulatory, standardization and industrial perspectives. *Digital Communications and Networks*, 4(2):87 – 97, 2018.

[86] S. M. Moser. Some expectations of a non-central chi-square distribution with an even number of degrees of freedom. In *TENCON 2007 - 2007 IEEE Region 10 Conference*, pages 1–4, Oct. 2007.

[87] G. Nardini, A. Virdis, and G. Stea. Modeling X2 backhauling for LTE-advanced and assessing its effect on CoMP coordinated scheduling. In *2016 1st International Workshop on Link- and System Level Simulations (IWSLS)*, pages 1–6, July 2016.

[88] G. Nigam, P. Minero, and M. Haenggi. Coordinated multipoint joint transmission in heterogeneous networks. *IEEE Transactions on Communications*, 62(11):4134–4146, Nov 2014.

[89] Y. Okumura, E. Ohmori, T. Kawano, and K. Fukuda. Field strength variability in VHF and UHF land mobile service. *Review Electronic Communication Laboratories*, pages 825–873, 1968.

[90] A. Papadogiannis and G. C. Alexandropoulos. The value of dynamic clustering of base stations for future wireless networks. In *2010 IEEE International Conference on Fuzzy Systems (FUZZ)*, pages 1–6, July 2010.

[91] A. Papadogiannis, H. J. Bang, D. Gesbert, and E. Hardouin. Efficient selective feedback design for multicell cooperative networks. *IEEE Transactions on Vehicular Technology*, 60(1):196–205, Jan. 2011.

[92] A. Papadogiannis, D. Gesbert, and E. Hardouin. A dynamic clustering approach in wireless networks with multi-cell cooperative processing. In *IEEE International Conference on Communications, 2008. ICC '08.*, pages 4033–4037, May 2008.

[93] Agisilaos Papadogiannis. *Systems and techniques for multicell-MIMO and cooperative relaying in wireless networks*. PhD thesis, Thesis, 12 2009.

[94] J. D. Parsons. *The Mobile Radio Propagation Channel*. Wiley, 2000.

[95] C. B. Peel, B. M. Hochwald, and A. L. Swindlehurst. A vector-perturbation technique for near-capacity multiantenna multiuser communication-part I: channel inversion and regularization. *IEEE Transactions on Communications*, 53(1):195–202, Jan. 2005.

[96] 3GPP R1-090140. Clustering for CoMP transmission. 2009.

[97] 3GPP R1-090657. Dynamic cell clustering for CoMP. 2009.

[98] 3GPP R1-100172. Consideration on feedback for adaptive cell clustering. 2010.

[99] 3GPP R1-111174. Backhaul modelling for CoMP. 2011.

[100] T. Rappaport. *Wireless Communications: Principles and Practice*. Prentice Hall PTR, Upper Saddle River, NJ, USA, 2nd edition, 2001.

[101] J. C. Roh and B. D. Rao. Transmit beamforming in multiple-antenna systems with finite rate feedback: a VQ-based approach. *IEEE Transactions on Information Theory*, 52(3):1101–1112, March 2006.

[102] Wiroonsak Santipach and M. L. Honig. Signature optimization for DS-CDMA with limited feedback. In *2002 IEEE Seventh International Symposium on Spread Spectrum Techniques and Applications*, volume 1, pages 180–184 vol.1, 2002.

[103] Wiroonsak Santipach and M. L. Honig. Asymptotic performance of MIMO wireless channels with limited feedback. In *2003 IEEE Military Communications Conference, 2003. MILCOM '03.*, volume 1, pages 141–146 Vol.1, Oct. 2003.

[104] N. Saquib, E. Hossain, and Dong In Kim. Fractional frequency reuse for interference management in LTE-advanced HetNets. *IEEE Wireless Communications*, 20(2):113–122, 2013.

[105] M. Sawahashi, Y. Kishiyama, A. Morimoto, D. Nishikawa, and M. Tanno. Coordinated multipoint transmission/reception techniques for LTE-advanced [coordinated and distributed MIMO]. *IEEE Wireless Communications*, 17(3):26–34, June 2010.

[106] H. Schulze and C. Lueders. *Theory and Applications of OFDM and CDMA: Wideband Wireless Communications*. Wiley, 2005.

[107] M. S. Sim, J. Park, C. Chae, and R. W. Heath. Compressed channel feedback for correlated massive MIMO systems. *Journal of Communications and Networks*, 18(1):95–104, Feb 2016.

[108] C. Simon and G. Leus. Feedback reduction for spatial multiplexing with linear precoding. In *IEEE International Conference on Acoustics, Speech and Signal Processing, 2007. ICASSP 2007.*, volume 3, pages III–33–III–36, 2007.

[109] M. Simsek, T. Akbudak, B. Zhao, and A. Czylwik. An LTE-femtocell dynamic system level simulator. In *2010 International ITG Workshop on Smart Antennas (WSA)*, pages 66–71, Feb 2010.

[110] M. Simsek, H. Wu, B. Zhao, T. Akbudak, and A. Czylwik. Performance of different cell selection modes in 3GPP-LTE macro-/femtocell scenarios. In *2011 Wireless Advanced*, pages 126–131, June 2011.

[111] O. Somekh, O. Simeone, Y. Bar-Ness, and A. M. Haimovich. CTH11-2: Distributed multi-cell zero-forcing beamforming in cellular downlink channels. In *IEEE Global Telecommunications Conference, 2006. GLOBECOM '06*, pages 1–6, Nov. 2006.

[112] Di Su, Xueying Hou, and Chenyang Yang. Quantization based on per-cell codebook in cooperative multi-cell systems. In *2011 IEEE Wireless Communications and Networking Conference (WCNC)*, pages 1753–1758, March 2011.

[113] Huan Sun, Xiaobo Zhang, and Wei Fang. Dynamic cell clustering design for realistic coordinated multipoint downlink transmission. In *2011 IEEE 22nd International Symposium on Personal Indoor and Mobile Radio Communications (PIMRC)*, pages 1331–1335, Sept. 2011.

[114] T. Tao, B. Zhao, and A. Czylwik. Beamforming design for a cooperative relay system with limited feedback. In *2013 IEEE 24th Annual International Symposium on Personal, Indoor, and Mobile Radio Communications (PIMRC)*, pages 2616–2620, Sept 2013.

[115] I. Emre Telatar. Capacity of multi-antenna Gaussian channels. *EUROPEAN TRANSACTIONS ON TELECOMMUNICATIONS*, 10:585–595, 1999.

[116] R. van Nee and R. Prasad. *OFDM for Wireless Multimedia Communications*. Artech House universal personal communications series. Artech House, 2000.

[117] R. Vaughan and J. B. Andersen. *Channels, Propagation and Antennas for Mobile Communications*. IEE electromagnetic waves series. The Institution of Electrical Engineers, 2003.

[118] H. Wang, W. Wang, V. K. N. Lau, and Z. Zhang. Hybrid Limited Feedback in 5G Cellular Systems With Massive MIMO. *IEEE Systems Journal*, 11(1):50–61, March 2017.

[119] R. Weber, A. Garavaglia, M. Schulist, S. Brueck, and A. Dekorsy. Self-organizing adaptive clustering for cooperative multipoint transmission. In *2011 IEEE 73rd Vehicular Technology Conference (VTC Spring)*, pages 1–5, May 2011.

[120] M. Wu, S. Chao, and Z. Qiu. Feedback reduction based on clustering in MIMO-OFDM beamforming systems. In *5th International Conference on Wireless Communications, Networking and Mobile Computing, 2009. WiCom '09.*, pages 1–4, 2009.

[121] Y. Wu, H. Luo, M. Ding, J. Zou, and X. Li. Efficient Limited Feedback for MIMO-Relay Systems. *IEEE Communications Letters*, 15(2):181–183, February 2011.

[122] W. Xia, J. Zhang, S. Jin, C. K. Wen, F. Gao, and H. Zhu. Large System Analysis of Resource Allocation in Heterogeneous Networks With Wireless Backhaul. *IEEE Transactions on Communications*, 65(11):5040–5053, Nov 2017.

[123] M. Xiao, S. Mumtaz, Y. Huang, L. Dai, Y. Li, M. Matthaiou, G. K. Karagiannidis, E. Björnson, K. Yang, I. Chih-Lin, and A. Ghosh. Millimeter Wave Communications for Future Mobile Networks (Guest Editorial), Part I. *IEEE Journal on Selected Areas in Communications*, 35(7):1425–1431, July 2017.

[124] C. Yang, S. Han, X. Hou, and A. F. Molisch. How do we design CoMP to achieve its promised potential? *IEEE Wireless Communications*, 20(1):67–74, February 2013.

[125] Taesang Yoo, N. Jindal, and A. Goldsmith. Multi-antenna downlink channels with limited feedback and user selection. *IEEE Journal on Selected Areas in Communications*, 25(7):1478–1491, September 2007.

[126] S. Yu, H. Kong, Y. Kim, S. Park, and I. Lee. Novel Feedback Bit Allocation Methods for Multi-Cell Joint Processing Systems. *IEEE Transactions on Wireless Communications*, 11(9):3030–3036, September 2012.

[127] J. Y. Yun, S. Y. Chung, J. Choi, Y. U. Jang, and Y. H. Lee. Predictive transmit beamforming for MIMO-OFDM in time-varying channels with limited feedback. In *Proceedings of the 2007 International Conference on Wireless Communications and Mobile Computing*, IWCMC '07, pages 1–5, New York, NY, USA, 2007. ACM.

[128] H. Zhang and H. Dai. Cochannel interference mitigation and cooperative processing in downlink multicell multiuser MIMO networks. *EURASIP J. Wirel. Commun. Netw.*, 2004(2):222–235, December 2004.

[129] H. Zhang, Y. Li, V. Stolpman, and N. van Waes. A reduced CSI feedback approach for precoded MIMO-OFDM systems. *IEEE Transactions on Wireless Communications*, 6(1):55–58, 2007.

[130] Jun Zhang and J. G. Andrews. Adaptive spatial intercell interference cancellation in multicell wireless networks. *IEEE Journal on Selected Areas in Communications*, 28(9):1455–1468, December 2010.

[131] Tiankui Zhang, Anmeng Ge, Norman C. Beaulieu, Zhirui Hu, and Jonathan Loo. A limited feedback scheme for massive MIMO systems based on principal component analysis. *EURASIP Journal on Advances in Signal Processing*, 2016(1):64, May 2016.

[132] B. Zhao, T. Akbudak, M. Simsek, A. Czylwik, and H. Xu. Limited feedback for MISO-OFDM systems. In *Proceedings of 17th International OFDM Workshop 2012 (InOWo'12)*, pages 1–4, 2012.

[133] Bo Zhao and A. Czylwik. Cooperative beamforming for a two-cell system with limited feedback. In *2013 IEEE 77th Vehicular Technology Conference (VTC Spring)*, pages 1–5, June 2013.

[134] J. Zhao, T. Q. S. Quek, and Z. Lei. Coordinated multipoint transmission with limited backhaul data transfer. *IEEE Transactions on Wireless Communications*, 12(6):2762–2775, June 2013.

[135] L. Zhou and W. Yu. Uplink multicell processing with limited backhaul via per-base-station successive interference cancellation. *IEEE Journal on Selected Areas in Communications*, 31(10):1981–1993, October 2013.

[136] S. Zhou and B. Li. BER criterion and codebook construction for finite-rate precoded spatial multiplexing with linear receivers. *IEEE Transactions on Signal Processing*, 54(5):1653–1665, 2006.

[137] S. Zhou, B. Li, and P. Willett. Recursive and trellis-based feedback reduction for MIMO-OFDM with rate-limited feedback. *IEEE Transactions on Wireless Communications*, 5(12):3400–3405, 2006.

[138] F. Zhuang and V. K. N. Lau. Backhaul limited asymmetric cooperation for MIMO cellular networks via semidefinite relaxation. *IEEE Transactions on Signal Processing*, 62(3):684–693, Feb 2014.

[139] W. Zirwas, M. Sternad, and R. Apelfröjd. Key solutions for a massive MIMO FDD system. In *2017 IEEE 28th Annual International Symposium on Personal, Indoor, and Mobile Radio Communications (PIMRC)*, pages 1–7, Oct 2017.

DuEPublico

Duisburg-Essen Publications online